2017

The Role of CIC in Neural Progenitors.

Rogers, Alexandra

UNIVERSITY OF CALGARY

The Role of CIC in Neural Progenitors

by

Alexandra Rogers

A THESIS

SUBMITTED TO THE FACULTY OF GRADUATE STUDIES

IN PARTIAL FULFILMENT OF THE REQUIREMENTS FOR THE

DEGREE OF MASTER OF SCIENCE

GRADUATE PROGRAM IN NEUROSCIENCE

CALGARY, ALBERTA

APRIL, 2017

Abstract

Oligodendrogliomas (ODG) are brain tumours with distinct genetic hallmarks, including 1p/19q chromosomal co-deletion and IDH1/2 mutation. The gene encoding Capicua (CIC), on chr19q13.2, has been identified as mutated in ODGs with 1p/19q loss and IDH1/2 mutation, a rare genetic signature. Mutation of the retained 19q CIC allele is likely functionally important, but its contribution to ODG biology is unknown. To characterize the temporal and spatial expression of CIC in the normal mouse cerebrum, I examined CIC expression throughout development. CIC is expressed at a time and place in development in which it may influence cortical progenitors. To determine if CIC loss affects proliferation or differentiation of neural progenitors, CIC biologic functions were examined using loss-of-function approaches *in vitro* and *in vivo*. CIC loss was increased proliferation and cell growth, and effected progenitor differentiation and migration. Thus, my data supports a role for CIC in regulating processes in neural progenitors that are relevant to cancer.

Preface

Contributions to thesis work:

Alexandra Rogers performed, analyzed, and interpreted the majority of the experiments with the support of her supervisors **Dr. Gregory Cairncross and Dr. Jennifer Chan**. **Dr. Rajiv Dixit** performed all *in utero* electroporation techniques for this work. **Dr. Samuel Lawn** performed the preliminary CIC shRNA knockdown experiments using p53 -/- mouse neural stem cells.

Acknowledgements

To begin, I have to thank the Alberta Cancer Foundation and all of their donors for investing in my research, and providing me with the funding necessary to get this project off the ground.

I would like to thank my supervisor Dr. Gregory Cairncross for providing me with the opportunity to pursue this research, and for trusting a student with no previous training, who came out of nowhere at a brain cancer awareness day event to talk about your work, with such an interesting and novel project. If you had not offered me a volunteer position in your lab that fateful day in 2010, my life would be completely different.

A massive thank you goes out to my supervisor Dr. Jennifer Chan, who spent countless hours working with me on this project; answering my (ridiculous) questions about all things science, helping me troubleshoot all of the experiments I couldn't figure out on my own, infecting me with your excitement over good results, being proud of my achievements, and just generally pushing me to work harder, ask bigger questions, and strive for greater successes. It was a long road to get to this point, but we made it!

Thank you to my committee members, Dr. Savraj Grewal and Dr. Carol Schuurmans, for being excited about my work, and for guiding my research and constantly providing excellent suggestions and input on everything I had to show you.

I could not have done all this work without the help and instruction of all of my fantastic lab mates in the Chan/Cross lab emporium. Shout outs and thank yous to: Christian (aka Sunshine), for putting up with all of my annoying questions and for always having just the right answer; Rajiv, for being an absolute superstar, and my rock in the last few months of frantic data collection and thesis writing; Sam, for being a font of knowledge for all thing cloning, and for

always eating any food I brought in for the lab, no matter what; Lori, Jessica, and Karol, for listening to my complaints at morning coffee, and always being exceptionally positive and supportive towards me; and to Mike, for keeping me sane and grounded throughout this crazy process. As well, a shout out to previous lab mates and past and present summer students for all of your help and for teaching me how to teach (Western Blots, at least.)

A big thank you to my class of 2017 Leaders in Medicine crew for spending time with me in the library, editing my thesis (I'm looking at you Jason!), and generally being a ridiculously supportive group of amazing cheerleaders and friends. I can't wait to spend the next three years getting into all sorts of trouble with you crazy kids!

To Kyle: thank you for not saying 'I told you so' (even though I know you wanted to so bad!) Thank you for listening to my nonsense and actually caring about it even if it was ridiculous. Thank you for keeping me fed post working in the lab all weekend, for never being mad when I had to put science over you, and for being truly understanding and supportive of my dreams.

Last but not least, thank you to the people I wouldn't be here without: my family. I literally could not have done this without your constant, unwavering belief in my ability to succeed at anything I truly put my mind to. Thank you for instilling in me a love of learning, the confidence to set my sights on a goal, and the work ethic to persist until I achieve it. I can't even articulate how much your love and support means to me, except to repeat what I said above: I literally could not have done this without Heather, Floyd, and Ian Rogers. You guys are amazing, thank you for everything!

Dedication

I dedicate this thesis to everyone who has believed in me and supported me over the years, most especially my parents, Heather and Floyd Rogers.

Table of Contents

List of Tables

List of Figures and Illustrations

List of Symbols, Abbreviations and Nomenclature

Symbol	Definition
aa	amino acid
aos	*argos*
ascl1	achaete-scute homolog 1
ATXN1	ataxin 1
BAC	bacterial artificial chromosome
bHLH	basic helix-loop-helix
BrdU	bromodeoxyuridine
CC	corpus callosum
CIC	Capicua
CIC-L	CIC long form
CIC-S	CIC short form
CKO	conditional knockout
CNS	central nervous system
CNTF	ciliary neurotrophic factor
CP	cortical plate
DAPI	4',6-diamidino-2-phenylindole, dihydrochloride
DG	dentate gyrus
DNA	deoxyribonucleic acid
dpp	*decapentaplegic*
DTT	dithiothreitol
DUX4	double homeobox 4
E	embryonic day
EGF	epidermal growth factor
EGFR	epidermal growth factor receptor
ERK	extracellular signal-related kinase
ETS	E26 transformation-specific transcription factors
ETV1/4/5	ETS translocation variant 1/4/5
FGF	fibroblast growth factor
FIU	fluorescence intensity units
fl/fl	floxed/floxed
FUBP1	far upstream binding protein 1
GCL	granule cell layer
GFAP	glial fibrillary acidic protein
GFP	green fluorescent protein
GRO	groucho
GRO-L	groucho-like
HBSS	Hank’s balanced salt solution
HMG	high-mobility group
hkb	*huckebein*
IDH	isocitrate dehydrogenase
IL-6	interleukin 6
ind	*intermediate neuroblasts defective*

IRES	internal ribosome entry site
IZ	intermediate zone
JAK/STAT pathway	janus kinase/signal transducer activator of transcription pathway
KO	knockout
LIF	leukemia inhibitory factor
LOF	loss of function
MAPK	mitogen-activated protein kinase
MZ	marginal zone
MEK	mitogen activated protein kinase kinase
MGE	medial ganglionic eminence
MNSC	mouse neural stem cells
NeuN	neuronal nuclear antigen
Neurog2	neurogenin-2
NF1	neurofibromin 1
NGS	normal goat serum
NG2	neuroglial chondroitin sulfate proteoglycan 4
NLS	nuclear localization sequence
NSC	neural stem cell
ODG	oligodendroglioma
Olig1/2	oligodendrocyte transcription factor ½
OPC	oligodendrocyte precursor cell
P	postnatal day
PBS	phosphate buffered saline
PBST	PBS with triton X-100
PDGF	platelet-derived growth factor
PDGFR	platelet-derived growth factor receptor
PDGFRα	platelet-derived growth factor receptor alpha
PFA	paraformaldehyde
qRT-PCR	quantitative real-time polymerase chain reaction
RGC	radial glial cell
RIPA buffer	radioimmunoprecipitation assay buffer
RMS	rostral migratory stream
RNA	ribonucleic acid
ROS	reactive oxygen species
RT	room temperature
RTK	receptor tyrosine kinase
RT-PCR	reverse transcription polymerase chain reaction
SDS-PAGE	SDS polyacrylamide gel electrophoresis
SGZ	subgranular zone
STAT3	signal transducer and activator of transcription 3
STR	striatum
SVZ	subventricular zone
tll	*tailless*
TBS	tris buffered saline
TBST	TBS with triton X-100

tor-RE	torso response element
Tuj1	neuron-specific class III beta-tubulin
wt	wild type
V	ventricle
vvl	*ventral veinless*
VZ	ventricular zone
zen	*zerknullt*

CHAPTER 1: INTRODUCTION

Cancer is a disease of dysregulated cell proliferation and aberrant differentiation. In the brain, the most commonly found cancer is glioma, a primary tumor composed of abnormal glial cells or their precursors (Kleihues et al., 1995). Under the broad umbrella of glioma is a clinically and genetically distinctive subtype of tumour called oligodendroglioma (ODG), a cancer composed of cells resembling oligodendrocytes (Figure 1.1A, B).

Recently, we and others found that the gene Capicua (CIC) located at chr19q13.2 is mutated in over 70% of ODGs (Bettegowda et al., 2011; Yip et al., 2012). Furthermore, CIC mutations occur nearly exclusively in the context of 1p/19q co-deletion, and it is thought that the CIC mutation on the remaining 19q allele is integral to the disease pathogenesis. How CIC alterations act to initiate ODG tumorigenesis, however, is unknown – which is not surprising, given that little is known about the normal functions of CIC in the brain.

In order to gain insight into the mechanisms of ODG formation, it is essential to understand the functions of the genes that are altered in this disease. To this end, the goal of my research has been to characterize the temporal and spatial expression of CIC in mammalian brain development and to begin to define its functional roles in cortical neural progenitor cells.

1.1 Cortical Organization and Development

Before discussing CIC and its potential roles in cortical development, the cellular constituents and events that are involved in the development of the cerebral cortex will be reviewed.

1.1.1 Cortical cell types and structure

The major cell types in the cerebrum include neurons, astrocytes and oligodendrocytes. Neurons are the excitable cells that transmit information electrically and chemically. There are two principle types of neurons found in the cortex – excitatory glutamatergic pyramidal cells which function as projection neurons, and non-pyramidal GABAergic inhibitory interneurons. Markers of neuronal identity include beta-III-Tubulin (Tuj1) (Menezes and Luskin, 1994), an early neuronal marker, and neuronal nuclear antigen (NeuN) (Sarnat et al., 1998), a transcription factor that is present in mature neurons. In addition to neurons, other main constituents present are glial cells – astrocytes and oligodendrocytes. Astrocytes are the star-like shaped support cells in the brain that provide nutrients to nervous tissue and assist in repair processes in the brain. Oligodendrocytes support axons throughout the central nervous system and elaborate the myelin sheaths that increase impulse speed. Sox9 is a general marker for glial cell fate (Stolt et al., 2003). More specifically, S100B (Ghandour et al., 1981) and glial fibrillary acidic protein (GFAP) (Bignami et al., 1972) are considered to be astrocyte markers, while platelet derived growth factor receptor alpha (PDGFRa) (Ellison and de Vellis, 1994) and the basic helix-loop-helix (bHLH) oligodendrocyte transcription factor (Olig2) (Zhou et al., 2001) are both markers of oligodendrocytic lineage. Other cell types found in the brain include microglia, which participate in the immune response and homeostasis maintenance (Kreutzberg, 1996), and the endothelial cells and pericytes of the vasculature.

In the mature mammalian cerebrum, these distinct cell types are arranged in defined structures, comprised of the cerebral cortex, underlying white matter, and deep gray matter nuclei (Mancall and Brock, 2011). At the surface is the cerebral cortex, a six-layered laminar structure containing neurons of different morphologies (Shatz, 1992). Laminae are representative

of cells with common connections. Afferents to cortical regions stop in layers I, IV and VI. Layers II and III give rise to ipsilateral and contralateral pathways between cortical areas, and Layer V produces connections between cortical and subcortical areas (Mancall and Brock, 2011). The majority of excitatory pyramidal cells reside in Layers III, V, and VI of the cortex, while non-pyramidal cells tend to aggregate in Layers I, II, and IV (Mancall and Brock, 2011). In general, the major input to an area of the cortex tends to terminate in layer IV, although some projections terminate in Layers II, III, and V (Mancall and Brock, 2011). The rodent cortex includes several deviations from that of the primate; layers II/III are fused in rodents and they have a decreased number of neurons in these layers. The expansion of the primate proliferative 'outer subventricular zone' produces a larger pool of progenitors that allow for an increased number of superficial layer neurons when compared to the rodent cortex (Smart et al., 2002).

Neuron cell bodies, astrocytes, and oligodendrocytes are found throughout the gray matter of the cortex. The white matter contains axons (but not cell bodies) of neurons as well large numbers of astrocytes and oligodendrocytes (Mancall and Brock, 2011). In this project, my focus is on cells and developmental events in the cortex, as oligodendrogliomas are often formed here (Mork et al., 1985).

1.1.2 Events in forming the Neocortex

Formation of the human cortex is an intricate and tightly regulated process. During early development, the neural tube is formed from the ectoderm germ layer, which is specified into distinct domains. The forebrain is created out of the prosencephalon, which gives rise to the cerebral cortex, including the neocortex and hippocampus (Figure 1.2A, B). However, none of the neurons found in the cortex are generated in their final locations. Instead, they arise in

specialized proliferative areas such as the ventricular (VZ) and subventricular (SVZ) zones (Rakic, 1988).

The first step of cortical formation involves producing an expansive pool of progenitor cells through symmetric proliferative cell division in the VZ (Fig 2). The walls of the neural tube consist of the densely cellular and highly proliferative VZ, which contains neuroepithelial cells that proliferate through symmetric cell division - each neuroepithelial cell dividing into two identical neuroepithelial cells (Alvarez-Buylla et al., 2001; Fishell and Kriegstein, 2003). Next, the neuroepithelial cells are transformed into elongated multipotent radial glial cells (RGC) which have radial fibers stretching towards the pial surface while cell bodies remaining in the VZ. Like neuroepithelial cells, radial glia are also functionally neural stem cells (NSC). Radial glia, however, then undergo asymmetric division, giving rise to two different cell types, one that remains divisible, while the other leaves the cell cycle to become an immature neuron or a basal/intermediate progenitor with limited proliferative potential (Malatesta et al., 2000; Miyata et al., 2001). Sox2 (Graham et al., 2003) and Pax6 (Ericson et al., 1997) are considered markers of stem/progenitor cells in these regions. After progenitor cells are born in these regions, they migrate radially and tangentially to their final positions in the brain (Rakic, 1990). This step of cortex formation is referred to as the neurogenic phase (Figure 1.3) (Shimojo et al., 2011). In the next phase of development, the gliogenic phase (Figure 1.3), cell production switches from generation of neurons to generation of astrocytes, and then to generation of oligodendrocytes. Although these basic phases might suggest uniformity to the process, superimposed on these developmental phases are spatial and temporal constraints that are linked to the types of cells generated and where they eventually reside in the mature brain.

The development of cortical layers begins with a transient structure called the preplate, which is formed by the earliest born neurons. The preplate later divides into the subplate and the marginal zone (MZ); the cortical plate (CP) develops between these two sections as immature neurons migrate from the VZ using radial fibers (Molyneaux et al., 2007). Cajal-Retzius cells in the marginal zone assist with the radial migration of neurons through secretion of the protein reelin (Molyneaux et al., 2007). During this process, some progenitors migrate into the SVZ where they remain cycling and give rise to more neurons (Rakic, 1990). The layers, or laminae, of the cortex are formed in an inside-out manner, and are labelled as I – VI, with layer I arising from the marginal zone, and located closest to the pial surface. Thus, the latest born neurons are destined to form layer II of the cortex (Angevine and Sidman, 1961).

In contrast to the excitatory pyramidal cells described above, inhibitory non-pyramidal GABAergic neurons are produced in separate proliferative areas more ventrally, migrating in a tangential fashion from the medial ganglionic eminence (MGE) and the lateral ganglionic eminence (LGE) of the ventral telencephalon to populate the various cortical layers (Colasante and Sessa, 2010; Parnavelas, 2000).

Astrocyte production occurs both in the dorsal and ventral proliferative zones. Oligodendrocyte precursor cells (OPCs) are also produced dorsally and ventrally (Tekki-Kessaris et al., 2001; Vallstedt et al., 2005). In the mouse, however, most OPC generation is from the MGE during embryonic life, whereas postnatally, oligodendrocytes are produced dorsally in the cortex from radial glial cell progenitors (Richardson et al., 2006), after astrocyte generation.

1.1.3 Timing of cerebral cortical development

Rodent and primate cortical development follow a similar sequence, although there are some differences in the cortical structures, as well as a prolonged period for primate neurodevelopment. In the mouse, neurogenesis extends from approximately embryonic day (E) 10 to E17, followed by gliogenesis. During gliogenesis, astrocyte production begins first at approximately E17, and peaks around birth. Oligodendrocyte production begins around birth and proceeds postnatally, peaking at approximately postnatal day (P) 6 (Miller and Gauthier, 2007) (Figure 1.4). Human cortical development follows a similar course, with neurogenesis beginning around 4 weeks, then a transition to gliogenesis in the second and third trimester, with completion in postnatal life (Figure 1.4).

Once development is complete, progenitor cells remain in specialized zones of adult neurogenesis and gliogenesis. These areas, the subependymal zone (SEZ) (also known as the adult SVZ) (Lois and Alvarez-Buylla, 1993) and the dentate gyrus (DG) of the hippocampus (Eriksson et al., 1998), are rich in stem cells and remain proliferatively active at a low rate. The SVZ is the largest site of adult neurogenesis. In this zone, stem cells produce GABAergic, dopaminergic and glutamatergic interneurons (Brill et al., 2009; Scheffler et al., 2005), that migrate through the rostral migratory stream (RMS) to integrate in the olfactory bulb (Doetsch et al., 1997). A small number of oligodendrocytes are also produced by stem cells in the SEZ (Menn et al., 2006). In the subgranular zone (SGZ) of the DG, precursor cells differentiate into granule neurons, which go on to receive glutamatergic inputs (Cameron et al., 1993).

1.2 Regulators of cell fate

The fates of progenitors generated during cortical development and in adult neurogenesis are controlled through extrinsic and intrinsic factors. Extrinsic cues are factors present in the cellular environment that can influence neighboring cells to differentiate in a certain manner; these may be elements of extracellular matrix, cell-cell interactions, or growth factors secreted by neighboring cells. In contrast, intrinsic cues are expressed within the cells, and are often genes such as transcription factors. These transcription factors influence the phenotype of a cell by mediating the effects of signalling and/or priming it to respond to extrinsic factors. Extrinsic and intrinsic cues work together to specify precursor cell fate (Fishell, 1995; Li et al., 2014; Shen et al., 2006). In rodents, cell fate is determined prior to migration, and the extrinsic factors present during the final mitoses may influence these fates (Krushel et al., 1993; McConnell and Kaznowski, 1991).

1.2.1 Extrinsic controls

Extrinsically, cell fate specification, proliferation, and differentiation are controlled by signalling through several major signalling axes that are activated upon binding of extracellular molecules to their receptors on the progenitor cells. Among the key extrinsic controls in the progenitor cell's environment are Notch ligands (which activate Notch signaling) epidermal growth factor (EGF), fibroblast growth factor (FGF), and platelet-derived growth factor (PDGF) (which activate receptor tyrosine kinase (RTK) signaling to Ras and AKT pathways), and leukemia inhibitory factor (LIF), ciliary neurotrophic factor (CNTF), and interleukin 6 (IL-6) (which activate janus kinase/signal transducer activator of transcription (JAK/STAT) signaling). The Notch pathway laterally inhibits neuronal differentiation by controlling cell-cell signalling;

Notch antagonizes proneural genes such as achaete-scute homolog 1 (*Ascl1*), blocking early neuronal gene expression, and maintaining progenitors in a proliferative state (Yoon and Gaiano, 2005). Members of the delta-like and jagged families act as ligands for the Notch receptor (Kopan and Ilagan, 2009). Upon binding, the intracellular domain of the Notch receptor translocates to the nucleus, where it activates target genes (Kopan and Ilagan, 2009) STAT proteins, downstream of cytokine signaling by LIF, CNTF, and Il-6, play a role in differentiation and proliferation throughout development (Levy and Darnell, 2002), and are key mediators regulating gliogenesis through transcriptional regulation of GFAP and other targets (Bonni et al., 1997; Nakashima et al., 1999; Taga and Fukuda, 2005). The Ras/mitogen-activated protein kinase (MAPK) pathway, activated downstream of RTKs, is similarly important. We will discuss this pathway in more detail, as it is known to regulate OPC specification and proliferation, and can regulate CIC function in diverse systems (Astigarraga et al., 2007; Li et al., 2014; Tseng et al., 2007).

The Ras/Raf/MAPK pathway is a signal transduction pathway which functions by transducing extracellular signals into the nucleus in order to activate genes for cell growth, proliferation and differentiation (Molina and Adjei, 2006). Signalling in this pathway begins at the cell membrane when extracellular growth factors (e.g. EGF, FGF, PDGF) binding to their respective RTKs (e.g. EGFR, FGFR, PDGFR), resulting in activation of the kinase activity of the receptor's intracellular catalytic domain that results in both receptor auto-phosphorylation and phosphorylation of tyrosine phosphorylation of its substrates. The activated RTK then interacts with adapter proteins such as Grb and Sos to engage binding and conversion of the GTP-binding switch protein Ras from an inactive GDP-bound form to activated Ras-GTP. This conversion to activated Ras-GTP is facilitated by guanine nucleotide exchange factors (GEFs), while

subsequent deactivation to Ras-GDP form is facilitated by the activity of a GTPase activating protein (Ras-GAP). Activation of Ras leads to a cascade of phosphorylation and activation of signalling proteins starting with Raf. Phosphorylated activated Raf then phosphorylates mitogen activated protein kinase kinase (MEK), which in turn phosphorylates extracellular signal-regulated kinase (ERK). Phosphorylated activated ERK then can phosphorylate and activate cytoplasmic and nuclear proteins, including a variety of transcription factors.

The role of Ras/ERK signalling in the developing embryo depends on context; the growth factors that activate the pathway can promote either progenitor cell differentiation or proliferation (Lukaszewicz et al., 2002). PDGFR in particular contributes to the production of oligodendrocytes in normal brain development (Baumann and Pham-Dinh, 2001). Ras pathways are directly linked to oligodendrocyte specification; ERK1 and 2, downstream effectors of the Ras/Raf/Mek pathway, regulate the transition of OPCs to immature oligodendrocytes (Guardiola-Diaz et al., 2012). As well, the Ras-GAP protein neurofibromin 1 (NF1), is a tumor suppressor that also influences OPC production. Knocking down NF1 orthologs in zebrafish results in an increased number of OPCs in the ventral spinal cord due to over proliferation (Lee et al., 2010). Similar results have been found in NF1 knockout mice (Bennett et al., 2003). Interestingly, recent work from our lab in collaboration with Carol Schuurmans' lab has found that the level of Ras/ERK can influence cell fate via its regulation of the expression and function of proneural transcription factors (Li et al., 2014). When Ras/ERK signalling is low, excitatory pyramidal neuronal differentiation is promoted. When Ras/ERK signalling increases to a moderate level, cortical interneurons are produced. Under high levels of RAS/ERK signalling, glioblast differentiation is promoted (Li et al., 2014). The Ras/MAPK pathway has been closely

linked to oligodendrocyte specification/proliferation, and directly regulates the activity of the oligodendroglioma-associated gene-of-interest, Capicua.

RTKs are well conserved throughout species, particularly in the tyrosine kinase domain (Livneh et al., 1985; Sprenger et al., 1989). In *Drosophila*, where Capicua was first discovered, the Torso (Tor) RTK pathway is important for regulating development. The tor gene encodes a RTK in which the catalytic domain is similar to the PDGFR class of RTK (Sprenger et al., 1989), and is required for appropriate patterning of the *Drosophila* embryo. Tor signalling activates a ras/raf/MAPK pathway, which regulates *tailless (tll)* and *huckebein (hkb)* expression. *tll* and *hkb* are terminal genes that encode transcription factors in order to differentiate the structures of the *Drosophila* head and tail regions (Duffy and Perrimon, 1994). Another important RTK pathway in *Drosophila* development is EGFR, which is similar to the human homolog (Livneh et al., 1985). EGFR signalling initiates dorsoventral patterning in the *Drosophila* embryo (Ray and Schüpbach, 1996).

1.2.2 Intrinsic controls

Intrinsically, cell type specification and differentiation are controlled by proneural transcription factors which are strictly regulated and promote neuronal differentiation in a context dependent manner (Bertrand et al., 2002). Many of these factors are part of the basic helix-loop-helix (bHLH) motif family, named for the structure that controls DNA binding and dimerization functions (Murre et al., 1989). *Neurogenin-2 (Neurog2)* is expressed in the dorsal telencephalon during the neurogenic period, but only promotes glutamatergic projection neuron differentiation at early stages (Li et al., 2012; Schuurmans et al., 2004). It does so by repressing

another proneural gene, *Ascl1*, which controls differentiation in the ventral telencephalon. *Ascl1* has three roles in ventral telencephalic progenitors which are distinct temporally and spatially. First, it encourages proliferation of progenitor cells through Notch signalling (Castro et al., 2011). Second, *Ascl1* targets GABAergic neuronal differentiation genes (Casarosa et al., 1999), and finally, it promotes an OPC fate (Parras et al., 2007).

Other key bHLH transcription factors include Olig1 and Olig2. Olig1/2 have been determined to regulate specification of oligodendrocytes and are found in oligodendrocyte precursors in the telencephalon and spinal cord (Tekki-Kessaris et al., 2001; Zhou et al., 2000). In the embryonic brain, Olig2 expression is seen in neuronal progenitors in the VZ and SVZ (Takebayashi et al., 2000). Expression of these TFs is maintained throughout development as well as in the differentiated oligodendrocyte (Lu et al., 2002). Removing Olig1 and Olig2 expression is sufficient to inhibit oligodendrocyte production throughout the central nervous system (Zhou and Anderson, 2002). In the spinal cord, V2 interneurons are generated instead of motor neurons with Olig loss. Olig 1/2 double mutant mice produce interneurons first and astrocytes second, compared to motor neurons and then oligodendrocytes in normal mice; thus Olig genes link specification of a neuronal subtype to a glial subtype without influencing the fate decision between neurons and glia (Zhou and Anderson, 2002). This action is independent of the decision to produce neuronal or glial fates. When proneural and Olig genes are both active, motor neurons are produced. However, when only Olig genes are functioning, oligodendrocyte cells are formed (Zhou and Anderson, 2002). This occurs as Olig2 derepresses Neurogenin2 to promote motor neuron progenitor differentiation (Novitch et al., 2001). Olig2 has also been seen to inhibit astrocyte production by interfering with the production of the signal transducer and

activator of transcription 3 (STAT3) - p300 complex necessary for astrocyte differentiation (Fukuda et al., 2004). In my studies, I will use Olig2 as a marker of oligodendrocyte lineage.

Our gene of interest, CIC, may also be an intrinsic regulator of neural development that mediates or influences stem/progenitor cell responses to RAS/MAPK signaling. It is a transcriptional regulator that, in *Drosophila*, is integral to regulating rostral-caudal and dorsal-ventral patterning in the developing embryo downstream of MAPK pathway signalling (Jimenez et al., 2000). Mutant CIC embryos lack trunk segmentation, due to ectopic expression of genes which differentiate tail and head structure (Jimenez et al., 2000). As well, there is evidence that CIC represses expression of vein specific genes in specific regions of the developing *Drosophila* wing pouch. This restricts vein tissue development to areas where CIC expression is low (Roch et al., 2002). These functions of CIC will be discussed in more depth below.

1.3 Capicua (CIC)

1.3.1 CIC structure

CIC is a 20 exon gene encoded on 19q13.2 of the human genome. The structure contains a novel high mobility group (HMG)-box DNA binding motif composed of 3 α-helices separated by loops. The HMG-box is found in the 200-268 amino acid (aa) region, encoded in exon 5. Other important regions include 28-46aa, where CIC interacts with Ataxin 1 (ATXN1), and the C-terminus region, approximately 1556-1608aa, which corresponds with Exon 20 – the Groucho-like (GRO-L) protein-protein interaction domain. ATXN1 is a protein involved in spinocerebellar ataxia type 1, an inherited neurodegenerative disease with progressive loss of cerebellar neurons, while GRO is a co-repressor which functions in embryonic patterning in

Drosophila. A nuclear localization sequence (NLS), which is located near the C-terminus, is not conserved in *Drosophila* (Jimenez et al., 2012) (Figure 1.5). Mutating the HMG box of CIC in *Drosophila* results in localization of the protein to the cytoplasm instead of the nucleus and is insensitive to Tor regulation. This suggests that this region contains NLSs necessary for proper function (Astigarraga et al., 2007). Mutating C-terminus motifs results in repression of CIC at the poles by Tor, or in premature mortality. Therefore, the C-terminus is required for downregulation by Tor, as *Drosophila* embryos with this mutation show CIC accumulation solely in nuclei at the embryonic poles (Astigarraga et al., 2007). In addition to these domains, other important features are consensus ERK phosphorylation motifs that are important for CIC regulation, as discussed below (Astigarraga et al., 2007; Lee et al., 2002).

In mammals, CIC has two major isoforms – a 1608aa, 160kD short form (CIC-S), and a 2517aa, 260 kD long form (CIC-L) (Lam et al., 2006). The two isoforms differ in their N-terminal regions; CIC-L includes a large exon at the beginning of the gene (Exon 0), and does not include Exon 1. Instead, Exon 0 is spliced to Exon 2 (Lam et al., 2006; Yip et al., 2012). In the normal brain and in oligodendrogliomas both CIC-L and CIC-S are expressed, however CIC-L is the predominant form (Lam et al., 2006; Yip et al., 2012).

There is a high level of homology between human, mouse and *Drosophila* CIC genes (Lee et al., 2002), especially in the HMG box, which is necessary for CIC function (Astigarraga et al., 2007). Homology between human and mouse CIC genes is 92%, with 100% identity shown between the two at the HMG box.

1.3.2 CIC interactions and regulation

Consistent with its structural elements, major properties of CIC are its ability to bind DNA, ability to interact with other proteins, and ability to be regulated by ERK phosphorylation. CIC preferentially binds to TGAATGAA or TGAATGGA octomeric sequences and acts as a transcriptional repressor, providing a mechanism by which RTK pathway signaling can control downstream gene expression. In *Drosophila*, a regulatory motif found in *tll,* the torso response element (tor-RE) which restricts *tll* to the embryonic poles is also the binding region for CIC. The same CIC-binding motifs are also found on *hkb*, and are required to recruit Groucho (Gro) as a co-repressor of terminal specific genes in the embryonic poles (Astigarraga et al., 2007). The gene *intermediate neuroblasts defective* (*ind*) which is downstream of the EGFR RTK pathway, was found to express an octomeric CIC binding site, implying that these CIC binding sites function downstream of several RTK pathways. CIC binding to target sites are sufficient to convert RTK signals into transcriptional responses in embryonic tissues, making them general response elements for RTK signalling during *Drosophila* development (Astigarraga et al., 2007).

CIC is post-transcriptionally repressed by the RTK pathways Tor and EGFR, and is directly regulated by these pathways. The involvement of a MAPK docking site on the CIC protein is critical to this process. These motifs can also interact with the human MAPK Erk2 (Astigarraga et al., 2007). The human protein has nine MAPK consensus phosphorylation sites, suggesting it may function in a similar fashion during human development (Lee et al., 2002). Following phosphorylation, the repression of CIC by RTK signalling includes mechanisms of nuclear export and protein degradation (Furriols and Casanova, 2003; Grimm et al., 2012; Lim et al., 2013). In *Drosophila,* Tor signalling induces phosphorylation of ERK, which reduces the level of CIC expressed at the embryonic poles (Furriols and Casanova, 2003). In the central

embryo, CIC levels decrease during mitosis, as the protein is exported to the cytoplasm. Nuclear levels recover during interphase. However, at high levels of Tor, CIC is degraded twice as quickly than when Tor is inactive. Tor levels are high at the embryonic poles, causing CIC to spend less time in the nucleus where it is protected. This in turn increases CIC degradation (Grimm et al., 2012). Further research on RTK control of CIC expression promotes a two-tiered model of gene repression. The first tier involves phosphorylation of CIC by EGFR-mediated activation of ERK, in order to quickly relieve its transcriptional repressor function. This primary derepression is then followed by the second tier, where inactive CIC is shuttled to the cytoplasm to be degraded (Lim et al., 2013). Thus, CIC repressor activity is directly downregulated by RAS–MAPK through a variety of mechanisms.

Downstream of CIC, E26 transformation-specific (ETS) -family transcription factors have CIC consensus binding motifs in their promoters and are some of the known CIC target genes. In human melanoma cell lines, EGFR activation leads to phosphorylation of CIC at multiple sites by MAPK and ribosomal protein p90RSK (Dissanayake et al., 2011). Of note, MAPK-dependent phosphorylation prevents CIC binding to importin-α4, a nuclear import adaptor, but the biological importance of this function remains unclear (Dissanayake et al., 2011). p90RSK phosphorylation of CIC occurs close to the HMG box, and allows CIC to bind to 14-3-3 regulatory proteins (Dissanayake et al., 2011). This interaction correlates with transcriptional upregulation of CIC targets, including ETS transcription factors such as ETS translocation variant 5 (ETV5). Human CIC can repress the expression of ETS transcription factors ETV1, ETV4 and ETV5, while the ERK cascade promotes expression of these genes (Dissanayake et al., 2011) by relieving CIC repression. Other targets of CIC include *tll* and *hkb*

(Jimenez et al., 2000), vein-specific genes (Roch et al., 2002), and microRNAs (Herranz et al., 2012) in *Drosophila.*

1.3.3 CIC biologic functions – Lessons from Drosophila

The functional consequences of CIC repressor activity are diverse and are dependent on the developmental stage and specific tissue within the organism. One such finding is shown in embryonic patterning, which establishes the basic *Drosophila* body plan. As detailed above, CIC acts as a repressor of *tll* and *hkb*, terminal genes which encode transcription factors that begin developmental programs leading to the differentiation of head and tail structures of the embryo (Jimenez et al., 2000). CIC loss-of-function (LOF) mutations in *Drosophila* cause Tor signalling in all regions of the embryo, resulting in ectopic expression of *tll* and *hkb* and lack of trunk segmentation in the mutant. In addition to rostral-caudal patterning, CIC was plays a role in dorsal-ventral patterning, repressing dorsal-specific gene *zerknullt (zen)* in follicle cells during normal *Drosophila* development (Jimenez et al., 2000). A de-repression mechanism similar to terminal embryo patterning is seen here as well, although it is under control of the EGFR RTK pathway instead of Tor.

Patterning and differentiation functions of CIC are also active in follicle cells of the *Drosophila* embryo. Here, CIC plays a role in repressing appendage-producing fates in ventral and lateral follicle cells at early stages of *Drosophila* development. Loss of function mutant CIC clones produced ectopic appendage material in the embryo when compared to wild type (wt) controls (Atkey et al., 2006). Similar results were found in the developing wing, where vein tissue formation is a complex process that requires EGFR signaling. EGFR decreases CIC protein levels in vein nuclei, antagonising CIC repressor activity and allowing for expression of

vein specific genes *argos (aos), decapentaplegic (dpp)* and *ventral veinless (vvl)* in assumptive veins (Roch et al., 2002). In contrast, in the intervein regions, high levels of CIC are maintained in nuclei throughout development. Therefore, the normal function of CIC during wing vein specification is to repress vein specific genes. *Drosophila* embryos with complete CIC loss of function develop abnormal wings, presenting with decreased wing size as well as ectopic and abundant vein tissue (Roch et al., 2002). Thus, these results also indirectly show that CIC influences growth and proliferation in the developing wing pouch.

A role for CIC in regulating proliferation is highlighted in studies using the developing eye. Flies with LOF mutations in eye disc cells show an increased representation of mutant tissue clones over normal tissue and contain more ommatidia, resulting in a slightly larger eye (Tseng et al., 2007). The mutant cells have an increased rate of proliferation with an accelerated cell cycle. Furthermore, this proliferative function of CIC in the eye is under control of the Ras/MAPK pathway, as loss of function clones of Ras and EGFR show increased CIC protein levels (Tseng et al., 2007). Interestingly, cell fate, differentiation, and tissue organization in the eye remain unaffected. Thus, while inhibition of proliferation and growth seems to be a general function of CIC, the ability to regulate cell fate and differentiation may be tissue specific. More recent work has found that CIC interacts with RBF1 (a homolog of the retinoblastoma tumor supressing gene RB) in Drosophila eye development to restrict proliferation. CIC and RBF1 promote G1 cell cycle arrest in dividing precursor cells by repressing Cyclin E expression (Krivy et al., 2013). Loss-of-function mutations of CIC in this model promote survival of rbf1 mutant cells. Here CIC modulates the sensitivity of rbf1 mutant cells to cell death by decreasing the levels of reactive oxygen species (ROS) in the developing eye disc (Krivy et al., 2013). Other

effects of CIC in flies include modulating growth by coordinated regulation of EGFR/MAPK and Hippo pathways via interactions with *bantam* miRNA (Herranz et al., 2012).

1.3.4 CIC in mice and humans

Compared to our knowledge of CIC in flies, little is known about CIC in mammalian systems. In the developing mouse brain, CIC is significantly expressed, at least at the transcriptional level, in the olfactory bulb at all ages and in the cerebellum postnatally (Lee et al., 2002). Using in situ hybridization (ISH) and reverse transcription polymerase chain reaction (RT-PCR), CIC expression was detectable postnatally at the RNA level in cerebellar granule cells, hippocampus and olfactory bulb (Lee et al., 2002). Although this transcriptional expression data was interpreted to suggest that CIC expression relates to cerebellar granule cell differentiation, expression was not measured at the protein level, results were not shown for expression at embryonic stages, and functional studies were not performed.

More recently, CIC was found to bind to ATXN1, a protein involved in the neurodegenerative disease spinocerebellar ataxia type 1 (Fryer et al., 2011; Lam et al., 2006; Lee et al., 2011). This binding is a functional link, as it has been shown to enhance transcriptional repressor activity of CIC in the mouse (Crespo-Barreto et al., 2010). To study this interaction, a CIC long-form knockout mouse was developed using a gene-trap cassette. In this non-conditional knockout mouse, long form (CIC-L) expression is removed completely, although some short form (CIC-S) expression remains, approximately 15% (Lee et al., 2011). The majority of CIC-L -/- mice die postnatally before day 21 and those that survive show a smaller body size than normal. Lung alveolarization defects were noted in CIC-L -/- mice, however the phenotype, if any, in the brain was not reported (Lee et al., 2011).

1.3.5 CIC as a cancer gene

Using next generation sequencing, our group and others have found recurrent mutations in CIC in ODGs (Bettegowda et al., 2011; Yip et al., 2012). These mutations occur throughout the CIC gene, and include missense mutations, truncation (premature stop)/nonsense mutations, insertions, deletions, and splice site mutations (Figure 1.1C). The majority of these mutations are clustered within Exon 5, the HMG DNA binding domain as well as Exon 20, the GRO-L protein-protein interaction domain (Yip et al., 2012), supporting the notion that these two structural domains are critical for CIC function.

Gliomas with a genetic constellation of wild-type CIC expression, far upstream element binding protein 1 (FUBP1) mutation, and isocitrate dehydrogenase (IDH) mutation, as well as 1p/19q loss have a longer median survival rate than gliomas without those genetic changes (Jiao et al., 2012). Although this finding may be a reflection of comparing oligodendrogliomas and astrocytomas, survival data has shown that within oligodendrogliomas, tumors lacking in CIC expression have a shorter progression-free and overall survival than CIC expressing tumors (Chan et al., 2014).. These findings are even more significant in tumors with 1p/19q co-deletion; tumors with 1p/19q co-deletion that lack CIC expression show progression free survival times of 14 months, versus 81 months for those with CIC expression (Chan et al., 2014).

The observation that abnormalities in CIC are present not only in ODGs but also in other cancers supports that CIC may play a role in tumor initiation or progression. Fusions of CIC with the double homeodomain gene DUX4 are implicated in the pathogenesis of pediatric primitive round cell sarcomas (Graham et al., 2012; Yoshimoto et al., 2009) and Ewing-like sarcomas. In these tumors, a t(4;19)(q25;q13) translocation result in CIC exon 20 fused in-frame to exon 1 of DUX4, forming a chimera in which the majority of the CIC gene is preserved including the

HMG-box and Erk phosphorylation sites but in which there is loss of important DUX4 functional domains including the DNA-binding domains (Graham et al., 2012; Yoshimoto et al., 2009). The CIC-DUX4 chimera acts as an oncogene, enhancing transcriptional activation, and possibly disturbing the expression of targets downstream of CIC. In these tumors, CIC-DUX4 up-regulates several genes, including ETV5 and ETV1, members of the PEA3 ETS transcription factor family that play a role in development and cancer progression (Kawamura-Saito et al., 2006). As well, recent work in a *Drosophila* model of retinoblastoma has shown that CIC mutations promote survival of RBF1 mutant cells, by decreasing the levels of reactive oxygen species (Krivy et al., 2013).

1.4 Developmental aspects of oligodendrogliomas

Comprising 4 to 25% of brain tumors, and most frequently occurring in the frontal and temporal lobes, ODGs have relatively early disease onset and slow progression (Cairncross and Jenkins, 2008). Although they are slow growing, ODGs are diffusely infiltrative, progressive in malignancy and surgically incurable. Eventually they are fatal to most patients. New diagnoses of ODG peak in early to mid-adulthood, after which the rate declines (Lwin et al., 2009). Considering their known indolent growth, the somewhat younger age of patients, and the size of lesions at diagnosis, there may be a temporal window of susceptibility for ODG development. Furthermore, the initial transformative event(s) likely occur years before clinical presentation of the tumour mass and associated symptoms. Thus, tumours may arise during a time when progenitor pools are actively proliferating in development.

1.4.1 Links between oligodendrocyte precursor cells and oligodendrogliomas

The concept of ODG as a disease of aberrant developmental control is supported by parallels between ODG and oligodendrocyte precursor cells. In the human brain, postnatal oligodendrocytes arise from OPCs, which remain as a population of cycling cells in the SEZ, a stem cell rich region, as well as white matter areas (Geha et al., 2010; Menn et al., 2006). ODGs express PDGF, and the receptor for this factor (Ellison and de Vellis, 1994). Furthermore, *Ascl1* and Olig2 are strongly expressed in ODGs, suggesting that the intrinsic proneural transcription factors important in OPC specification during development may be active in these tumors (Casarosa et al., 1999). ODGs also express high levels of Neuroglial chondroitin sulfate proteoglycan 4 (NG2), a marker of oligodendrocyte cell fate (Shoshan et al., 1999), further highlighting the similarities between ODG cells and abnormal OPCs.

Indeed, in experimental settings, there is evidence that OPCs may be a cell-of-origin for ODG. A study using a transgenic mouse glioma model driven by EGFR activation and controlled by the human S100b promoter found that the tumors formed did so from NG2-expressing OPCs (Persson et al., 2010). NG2+ cells in both mouse and human ODG showed increased tumorigenicity compared to NG2 negative cells. Nevertheless, whether tumors arose from an expansion of existing OPCs or by transforming existing precursors into OPCs remains unknown (Persson et al., 2010). In addition to OPCs, NSCs and astrocytes have also been thought to be the potential cells-of-origin for at least some gliomas (Lindberg et al., 2009; Liu et al., 2011; Persson et al., 2010). That there are persistent proliferating pools of NSCs and OPCs resident within the adult brain, makes these attractive candidates for glioma cells-of-origin (Eriksson et al., 1998; Lois and Alvarez-Buylla, 1993).

In summary, CIC is a gene that is regulated by RTK signalling in normal development. In *Drosophila*, CIC has been found to function as a repressor of proliferation and/or differentiation in diverse regions of the developing embryo. However questions remain regarding its roles in normal mammalian brain development, and how it may contribute to the genesis or biology of ODGs. In this work, I will take a LOF approach to gain insight into CIC's potential roles in cortical progenitors. Ultimately, my studies may shed light on the pathogenesis of ODGs and point to new targets and approaches for future therapies.

1.5 Hypothesis & Aims

I hypothesize that CIC is critical to restricting oligodendrocyte precursor cell specification and proliferation to the correct time and place in neurodevelopment. Conversely, loss of CIC may bias progenitors to an OPC fate and/or de-repress proliferative controls, resulting in conditions that promote oligodendroglioma-genesis (Figure 1.6A, B). To test this, I will address the following specific aims:

Aim 1. Characterize the temporal and spatial expression of CIC in cerebral cortex.

1a. Which cell types in the cerebral cortex express CIC?

1b. Does expression and subcellular localization of CIC protein change over time?

Aim 2. Determine the biologic function of CIC in neural progenitors.

2a: Does CIC influence proliferation?

2b: Does CIC regulate developmental potential of progenitors?

1.6 Figures and Figure Legends

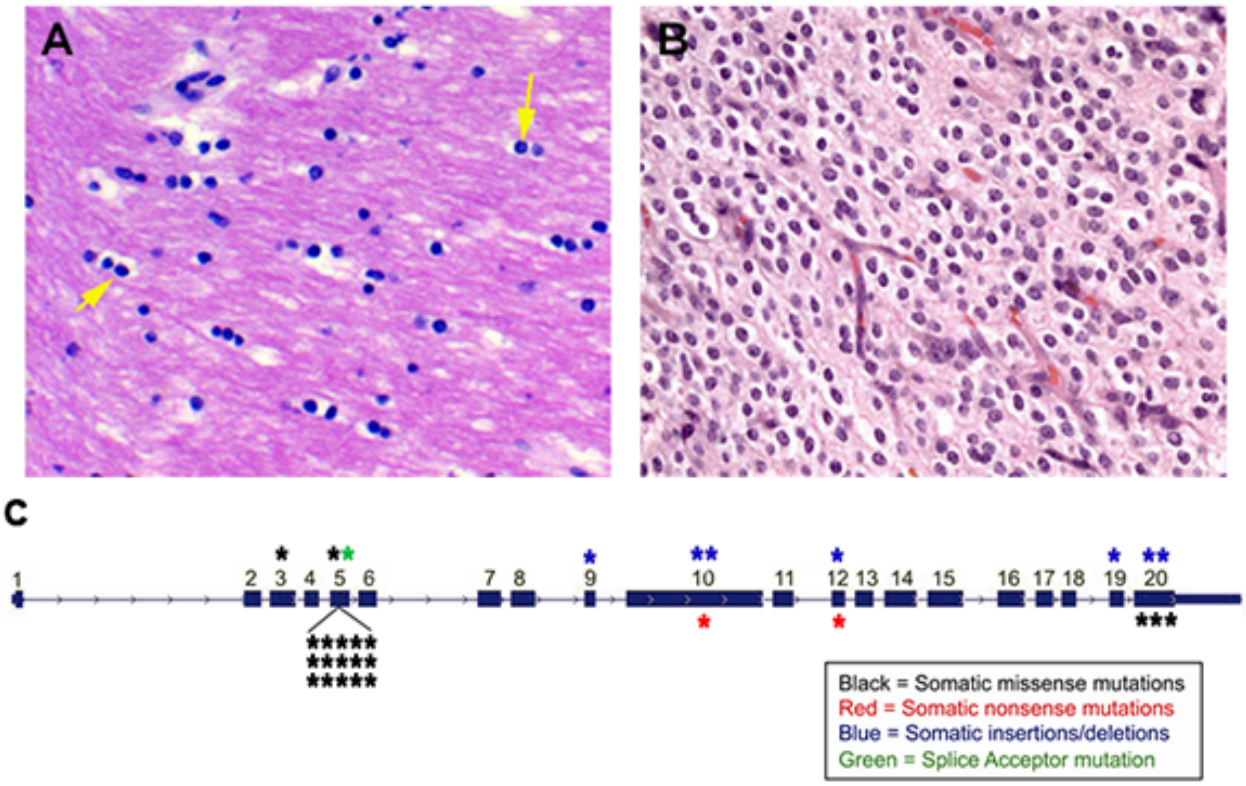

Figure 1.1. Histology of non-neoplastic brain and oligodendroglioma tissue.

A. Histology of normal cerebral white matter. Examples of oligodendrocytes are highlighted with yellow arrows. B. Histology of ODG shows round uniform cells similar to oligodendrocytes. C. Structure of the CIC gene with mutation type and location shown. (Adapted from Yip et al, 2011).

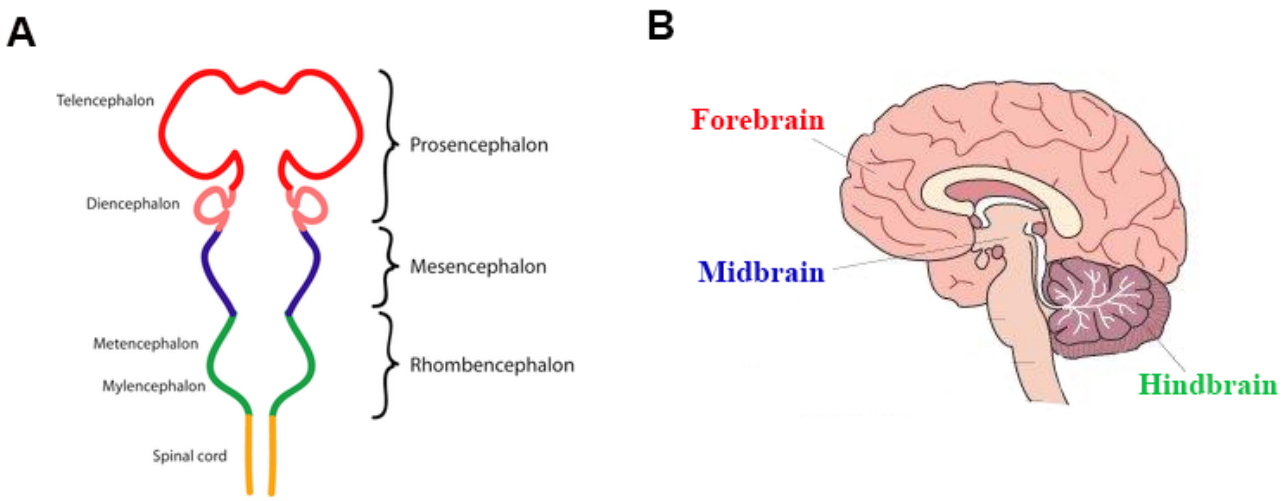

Figure 1.2. Diagram of developmental brain regions.

A. The prosencephalon, mesencephalon, and rhombencephalon are the main subdivisions of the embryonic brain. B. The forebrain arises from the prosencephalon, the midbrain from the mesencephalon, and the hindbrain from the rhombencephalon. (Adapted from public domain content).

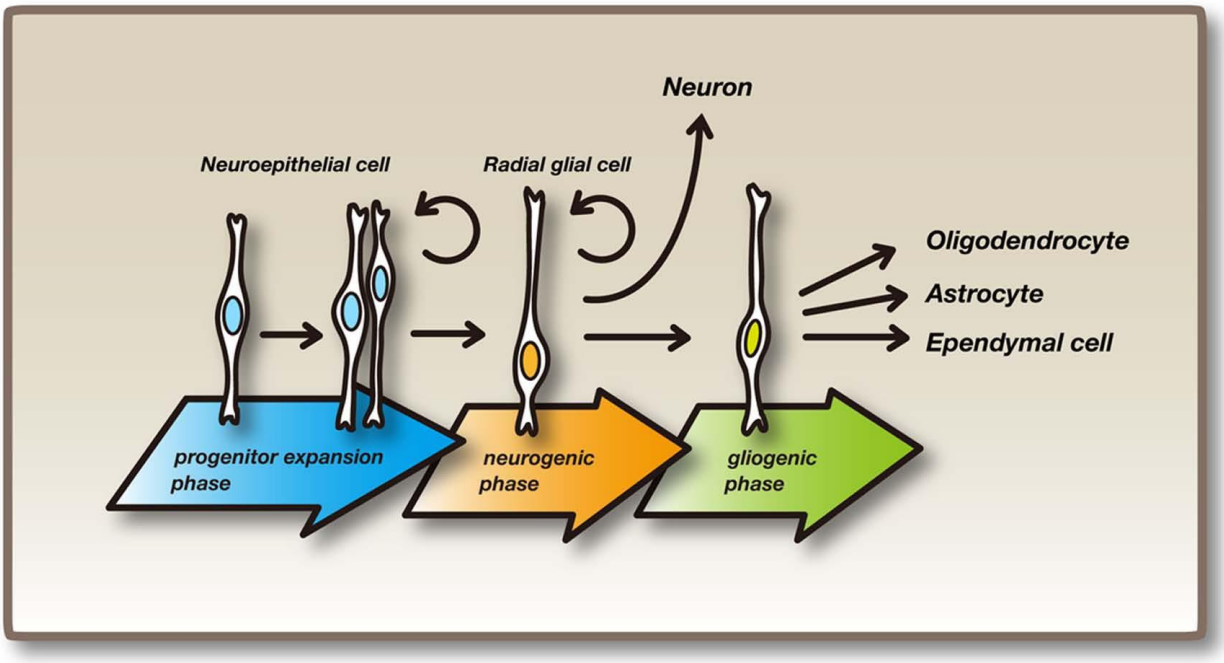

Figure 1.3. Phases of cortical development.

The phases include progenitor expansion, the neurogenic phase, during which neurons are formed, and the gliogenic phase, which produces oligodendrocytes, astrocytes and ependymal cells. (Adapted from Shimojo et al, 2007).

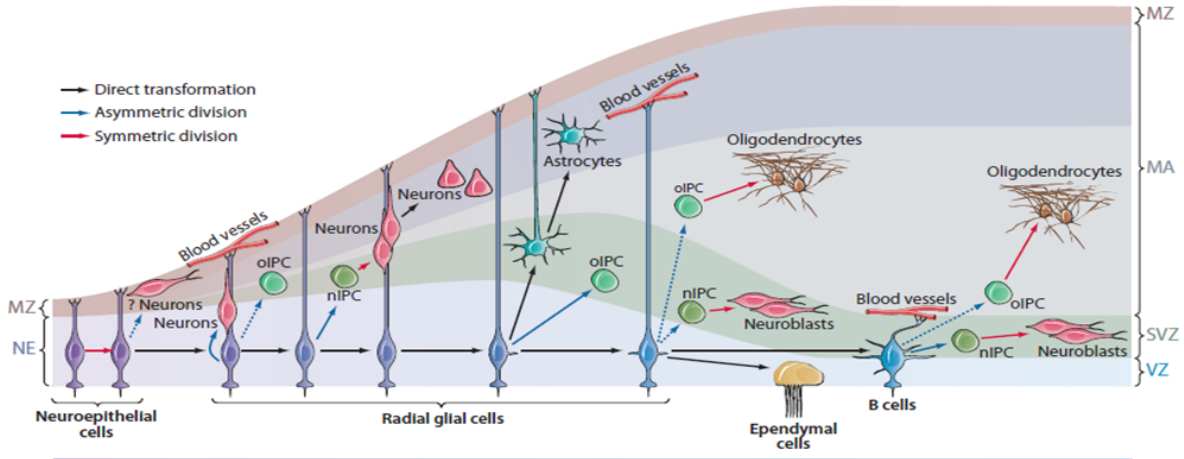

Mouse	E9.5	E12.5	E15.5	P0	P7	P0-P14
Human	~4 wks	~8 wks	~12-14 wks	2nd trimester	3rd trimester	6 mo gestation- to several yrs postnatal

Figure 1.4. Proliferation and cell fate specification in the developing brain.

Neurogenesis occurs from approximately E12.5 to E17.5 in mice, followed by a switch to gliogenesis. Generation of astrocytes occurs in late embryonic stages. Generation of oligodendrocytes begins at approximately P0, peaking around P7. Neuroepithelium (NE), Ventricular Zone (VZ), Subventricular zone (SVZ), Marginal zone (MZ), and Mantle (MA). (Adapted from Kriegstein and Alvarez-Buylla, 2009)

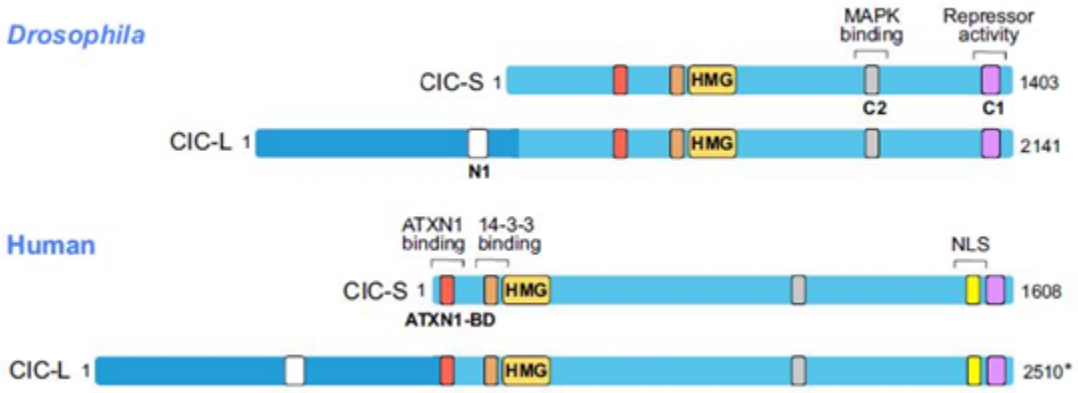

Figure 1.5. Comparison of *Drosophila* and human CIC proteins.

The two isoforms of CIC, CIC-S and CIC-L are shown. Important conserved regions are highlighted in the same color. The nuclear localization sequence is not conserved between human and *Drosophila* proteins; however other important domains such as the ATXN1, 14-3-3, and MAPK binding domains are conserved. (Adapted from Jiminez et al, 2012).

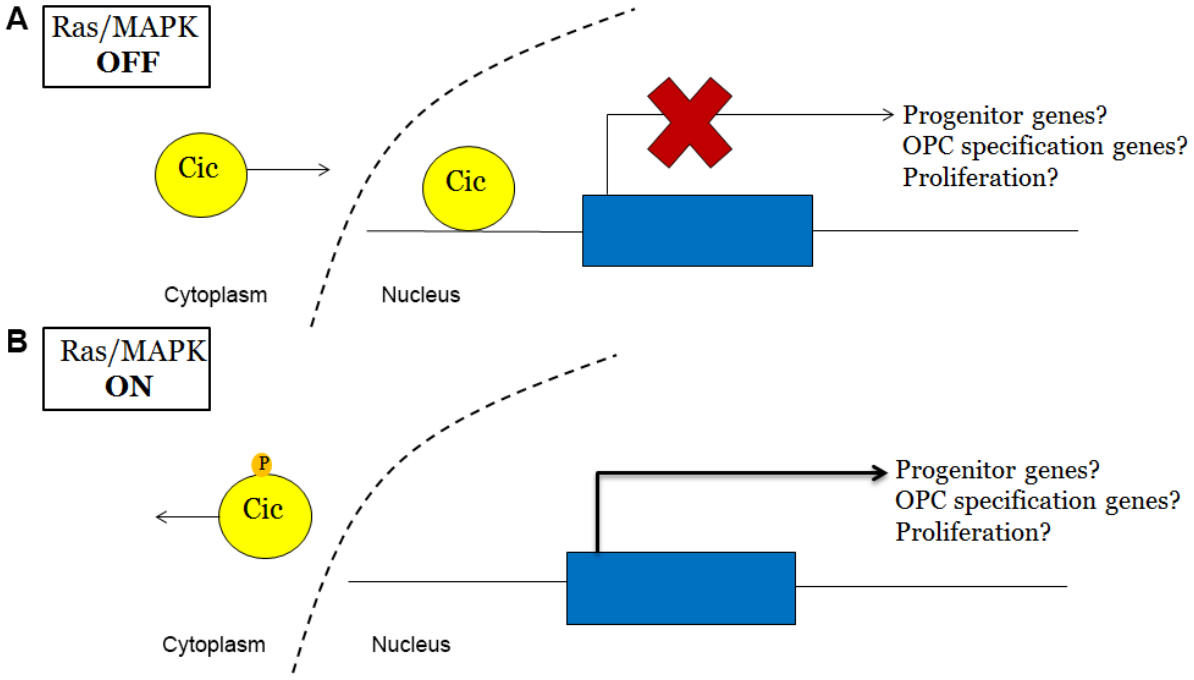

Figure 1.6. Hypothesis for the potential role of CIC in cortical development and gliomagenesis. A. CIC may act as a transcriptional repressor under the control of Ras/MAPK signalling. Turning off Ras/MAPK signalling allows nuclear CIC to enter the nucleus and bind to DNA, thus repressing transcription of downstream genes which may be important in regulating progenitor or OPC specification, or proliferation. B. Loss of CIC repression (due to mutational loss/inactivation, or its inappropriate removal from the nucleus as a result of oncogenic Ras/MAPK signalling), may bias progenitors to an OPC fate and de-repress proliferative controls, resulting in conditions that promote oligodendroglioma formation.

CHAPTER 2: MATERIALS AND METHODS

2.1 Animals

2.1.1 CD1 Mice

CD1 outbred mice from Charles River Laboratories were used for analysis of CIC expression in normal brain development, and for *in utero* electroporation studies. Animals were used for timed matings, and the morning of detection of the vaginal plug was considered E0.5.

2.1.2 CIC conditional knockout (CIC-CKO) mice

Our lab generated a CIC conditional knockout mouse line in which exons 2-11 of the CIC gene were flanked by loxP sites (size of floxed region approximately 5.5 kb). The floxed region contained all exons encoding the DNA binding domain (HMG box) of CIC. Briefly, the targeting vector was generated using bacterial artificial chromosome (BAC) clones from the C57BL/6J RPCIB-731 BAC library. The targeting vector consisted of a ~4.0 kb 5' flanking arm, a neomycin resistance cassette (flanked by FRT sites), the 5.5 kb lox-P flanked region, a puromycin resistance cassette (flanked by F3 sites), and a ~6.0 kb 3' flanking arm. After homologous recombination in C57BL/6N Tac ES cells, generation of chimeric animals, and confirmation of germline transmission, the NeoR and PuroR selection cassettes were removed via Flp recombination. The conditional KO allele thus carries two loxP sites (in introns 1 and 11) and single residual FRT and F3 sites. Expression of cre recombinase in the cells/tissues would thus yield the final CIC KO allele consisting of CIC exon 0 or exon 1, deletion of exons 2-11, and frameshifting of the remaining exons 12-20. The overall design and targeting strategy was performed and approved by the Chan lab, while technical work to generate the mouse line was performed commercially by

Taconic Artemis. In my thesis work, I used CIC knockout mouse and wild type embryos to generate CIC knockout and wild type cell lines as described below.

2.2 Plasmids

2.2.1 CIC shRNA

Five CIC shRNA pLKO.1 plasmids were purchased from Sigma-Aldrich. The sequence of each shRNA is shown below. CIC shRNA plasmids were cloned into bacteria and selected for ampicillin resistance. DNA was isolated from individual colonies and was sequenced to confirm successful ligation and correct shRNA sequences.

CIC shRNA #1 (Exon 4):

5’-CCGGCCAAGGAACGAGACTCATCTTCTCGAGAAGATGAGTCTCGTTCCTTGGTTTTTG-3’

CIC shRNA #2 (Exon 9):

5’- CCGGCCGACATTGATCTCAAGTGCACTCGAGTGCACTTGAGATCAATGTCGGTTTTTG-3’

CIC shRNA #3 (Exon 17):

5’- CCGGGTGGACTTTGAAGAGCGGTTTCTCGAGAAACCGCTCTTCAAAGTCCACTTTTTG-3’

CIC shRNA #4 (Exon 5):

5’-CCGGAGCGGGAGAAGGACCATATTCCTCGAGGAATATGGTCCTTCTCCCGCTTTTTTG-3’

CIC shRNA #5 (3’UTR):

5’- CCGGTCCAAGCTGGAGGGTAGTATGCTCGAGCATACTACCCTCCAGCTTGCATTTTTG-3’

Non-targeting (NT) shRNA:

5’- CCTAAGGTTAAGTCGCCCTCGCTCGAGCGAGGGCGACTTAACCTTAGG -3’

2.3 *In utero* electroporation

In utero electroporations were performed on CD1 mice (Figure 2.1) as previously described (Dixit et al, 2011). Briefly, 2-4 µg of plasmid DNA encoding shRNAs (either CIC shRNA#4 or NT control) was co-injected into the lateral ventricles of developing brain at E14 along with pCIG2 plasmid containing enhanced green fluorescent protein (eGFP) (Britz et al., 2006; Mattar et al., 2008) to allow for labelling and tracking of electroporated cells. The constructs were drawn into ventricular zone progenitor cells using 5 pulses of 50 V current from electrodes placed on the external surfaces of the uterus, flanking the region of the embryonic brain/skull. The pulse duration was 50 ms/pulse, with 780 ms between each pulse. Following electroporation, embryos were allowed to develop to E16 or E18 before sacrificing and processing. Bromodeoxyuridine (BrdU) labeling (Sigma, B5002) was performed by injecting 200 µl at 100-150 µg/gram into the pregnant dam in the final 30 minutes prior to sacrifice and embryo dissection.

2.4 Tissue preparation

Dissections were performed in ice cold 1X phosphate buffered saline (PBS). Isolated brains were fixed overnight at 4ºC in 4% PFA. Post-fixation, tissues were washed with 1X PBS and then cryoprotected overnight in 20% sucrose solution at 4ºC. Brains were washed in 1X PBS before embedding in Tissue-Tek OCT (Electron Microscopy Services, 4583) and sectioning using a Shandon Cryotome E cryostat (Thermo Scientific). 10 micron thick coronal sections were collected on Superfrost Plus slides (VWR, 48311-703) for histology and immunofluorescence studies. Fresh tissue from dissected the dorsal cortices were also used for preparation of protein lysates and for cell culture as described below.

2.5 Immunofluorescence staining

For all antibodies except anti-BrdU, slides were rehydrated in 1X PBS for 5 minutes, then permeabilized and blocked using blocking solution (200 nM Tris, 1.37 M NaCl, 0.3% Triton X-100, 3% normal goat serum (NGS)) for 1 hour at room temperature (RT). After blocking, slides were washed 3x10 minutes using TBST (200 mM Tris, 1.37 M NaCl, and 0.01% Triton X-100) and incubated in primary antibody in blocking solution (0.1% Triton X-100, 3% NGS in 1X TBS) for 1 hour at room temperature. A list of specifications for each antibody can be found in Table 2.1. Slides were washed 1x 5 minutes using TBST and incubated in secondary antibody in blocking solution for 1 hour at RT. Following the application of the secondary antibody, the slides were washed 3x10 minutes using TBST, and then stained with 4',6-Diamidino-2-Phenylindole, Dihydrochloride (DAPI) (Polysciences) diluted in 1XTBST (1/10,000) for 5 minutes. Coverslips were mounted to the slides using FluorSave Reagent (Calbiochem, 345789).

For BrdU/GFP double immunostaining, slides were rehydrated in 1X TBST and blocked in blocking solution for one hour at RT. After blocking, GFP antibody was added to each slide and incubated overnight at 4ºC. Slides were washed with PBT (1X PBS, 0.01% Triton X-100) and incubated for one hour at RT in secondary antibody in TBST. Following incubation, the slides were washed with PBT and post fixed with 4% PFA for 15 minutes at 4ºC. The slides were washed with PBT, and then re-blocked with blocking solution for 10 minutes. 2N HCl pre-incubated at 37ºC was added to the slides for 17 minutes, which were then washed in PBT. The slides were incubated overnight for 4ºC in an anti-BrdU antibody (AbD Serotec). Secondary antibody application, counterstaining, and coverslipping were performed as above.

Immunofluorescence images were either taken in color using an Olympus Virtual Slide System Macro Slide Scanner (VS120-5 Slide) or were taken in black and white then false-colorized using an Olympus IX70 fluorescence microscope. Quantitation of immunofluorescence

staining for percentage of cells positive (i.e. cell counting) was performed on at least 3 animals per condition, using 3 images per brain, representing at least 900 cells counted.

Quantitation of CIC nuclear staining intensity in Olig2+ and Olig2- nuclei was performed using Photoshop CS5 Extended by selecting nuclear areas based on Olig2 staining and DAPI staining, then measuring the average pixel density in the nucleus in the corresponding area of the CIC layer that had been previously gray-scaled. Quantitation of CIC staining intensity was performed on one brain, and representing ~100 cells counted of each type. Results are shown alongside sampling of background levels.

2.6 Immunoblotting

Whole cell lysates or fractionated lysates were used for western blotting. For whole cell lysates, protein was extracted from harvested tissue or cultured cells using radioimmunoprecipitation assay (RIPA) buffer (50 mM Tris pH 8.0, 1% NP-40, 0.5% Sodium deoxycholate, 0.1% SDS, 150 mM NaCl) supplemented with phosphatase inhibitors (Thermo Scientific #78420, 100X cocktail includes sodium fluoride, sodium orthovanadate, sodium pyrophosphate and beta-glycerophosphate) and protease inhibitors (Thermo Scientific #78415, 100X cocktail includes 100 mM AEBSF-HCl, 80µM aprotinin, 5 mM bestatin, 1.5 mM E-64, 2 mM leupeptin, and 1 mM pepstatin A). Samples were incubated with rotation at 4ºC for 1 hour, and then lysates were clarified by centrifugation at 16,000 x g for 10 minutes. The supernatant was removed and stored at -80ºC before use.

For preparation of nuclear and cytoplasmic fractions, protein was harvested from embryonic and postnatal mouse brains as previously discussed above. Fractionation was

conducted using the Qproteome Cell Compartment Kit (Qiagen, #37502) per manufacturer's instructions, to separate nuclear and cytoplasmic components for analysis.

Protein concentrations were determined using the BioRad Protein Assay kit (BioRad). Protein samples (50 µg/well) were prepared in NuPage Loading buffer and dithiothreitol (DTT) (Sigma, #43816) and denatured by incubating for 10 minutes at 70ºC prior to loading. Proteins up to 300kD were resolved on a 3-8% Tris-Acetate gel (Life Technologies EA03752) using SDS-polyacrylamide gel electrophoresis (SDS-PAGE) in 1X Tris-Acetate SDS running buffer (Life Technologies LA0041) at 200 V for 50 minutes at RT. Novex Sharp Pre-Stained Protein Standard (Life Technologies LC5800) was used for molecular weight estimates. Following resolution, proteins were transferred onto nitrocellulose membrane using NuPage Transfer Buffer (Life Technologies NP0006-1) at 30 V for 70 minutes at RT. Membranes were blocked in 5% skim milk powder in 1X PBST (1X PBS, 0.01% Tween-20) for an hour at RT, and then incubated with primary antibody overnight. A list of antibodies and the specifications used is in Table 2.2. Following incubation, membranes were washed for 3x 10 minutes with milk buffer, and then incubated in secondary antibody for one hour at RT. Immunoblots were washed 3 x10 minutes in 1X PBS, followed by a brief incubation in Western Lightning enhanced chemiluminescence reagent (ECL, PerkinElmer, NEL104001) and exposure to film (Amersham Hyperfilm ECL, GE Healthcare 28906835). Densitometry of western blotting bands to quantitate protein expression was conducted using ImageJ (NIH).

2.7 Tissue culture

2.7.1 Mouse neural stem cell (MNSC) cultures

Brains from E15.5 embryos were dissected and placed in ice-cold dissection media (Hanks balanced salt solution (HBSS) without Ca^{2+} or Mg^{2+}, supplemented with 5.6 g/L glucose, 15 mM HEPES pH 7.4). Dorsal cortical tissue including the regions of interest (VZ/SVZ) was transferred to 5mL of fresh dissection media for washing. Dissection media was removed, and 1 mL of 1X Accumax (StemCell Technologies, #07921) added. Tissue was incubated at 37ºC for 15 minutes, and then 4 mL of ice-cold mouse neural stem cell (MNSC) media (Neurocult mouse proliferation media, Stem Cell Technologies catalog #05702) was added. Samples were spun at 300 x g for 5 minutes, supernatant removed and 1mL of MNSC media added. Tissue was mechanically dissociated using a fire-polished Pasteur pipette, and passed through a 70 µm cell strainer. Cells were then placed in 5 mL of MNSC media in T25 tissue culture flasks at 8000 cells/mL and maintained at 37ºC in a 5% CO_2 incubator.

2.7.2 CIC knockout (KO) cell lines

To generate CIC knockout (CIC-KO) and control cell lines, mouse neural stem cells were cultured from E15.5 CIC conditional knockout embryos or wild-type embryos as above and subsequently transfected *ex vivo* with either Cre-encoding or control plasmids (Figure 2.2A,B). Cells from each culture ($CIC^{wt/wt}$ or $CIC^{fl/fl}$) were co-transfected with a piggyBAC helper plasmid (containing piggyBAC transposase, System Biosciences #PB210PA-1) and a piggyBAC donor plasmid (System Biosciences, #PB513B1) which carried either Cre-internal ribosome entry site (IRES)-GFP (henceforth referred to as Cre-GFP) or GFP only. Transfection was performed using Amaxa Mouse NSC Nucleofector Kit (Lonza). Cells were suspended at 3,000,000 per 100 µL of

Nucleofector Solution V with Supplement (Lonza, VCA1003) and 5 µg of DNA. The cells were nucleofected using the neural stem cell protocol A033 on the Amaxa Nucleofector machine, and then re-suspended in fresh mouse neural stem cell media. The nucleofected cells were selected with 2 µg/ml of Puromycin (Invitrogen, #A11138-03) three days later. This resulted in four cell lines where $CIC^{fl/fl}$ +Cre cells were CIC null, and $CIC^{wt/wt}$, $CIC^{wt/wt}$ +Cre, $CIC^{fl/fl}$ were control lines with intact CIC.

2.7.3 Maintenance of cells

Cells were grown in serum-free defined MNSC media supplemented with heparin (StemCell Technologies, #07980, 4 µg/mL), EGF (Peprotech, AF-100-15, 20 ng/mL), and FGF (R&D Systems, #233-FB-025/CF, 20 ng/mL) in low-adhesion flasks at 37ºC with 5% CO_2. Cells were passaged when neurospheres were approximately 200 µm in diameter, before their centers appeared optically dense. For passaging, the contents of flasks were transferred to 15 mL tubes and centrifuged for 5 minutes at 250 x g. Supernatant was removed and 150 µl of Accumax was added to each sample, which was then mechanically dissociated by triturating. Cells were incubated in Accumax for 6 minutes at 37ºC. After dissociation, 1 mL of fresh media was added, and cell counts were performed with the TC10 Automated Cell Counter (BioRad) using 0.2% Trypan Blue (BioWhittaker, #17-942E). Cultures were re-seeded at 500,000 cells per 12 mL in T75 flasks (Sarstedt, 83.1813.502).

2.8 Cell-based assays

2.8.1 Viability

10% Alamar Blue reagent (Life Technologies, DAL1100) was added to cells in 96-well plates and allowed to incubate at 37ºC for 6 hours. The fluorescence reading from each well was then assessed ($\lambda_{ex/em}$: 544 nm/590 nm) using a SpectraMax M2^{e} microplate reader (Molecular Devices). Viability of CIC$^{fl/fl}$+Cre cells was assessed relative to that of control CIC$^{wt/wt}$+Cre.

2.8.2 Clonogenic / sphere forming assay

To analyze self-renewal, cells were plated in 96-well plates at a density of 1000 cells/well in 100 µl of normal MNSC media. After 48 hours, bright field images were taken of each well at 10x magnification using the Zeiss Observer Z1 microscope. Analysis of sphere number was conducted by counting two images from each well, for a total of ten images. Sphere/cluster volume was calculated by measuring the diameter of presumed spheres/clusters in pixels, and using the equation $V=4/3\pi r^3$ to calculate volume in μm^3.

2.9 Gene expression analyses

RNA extraction was performed on tissue and cell samples using the RNeasy Plus Mini Kit (Qiagen, 74134) as per manufacturer's specifications. The GE Nanovue spectrophotometer was used to determine RNA concentration and purity.

2.9.1 qRT-PCR

RNA was reverse transcribed to cDNA using random primers and the Sensiscript RT Kit (Qiagen, 205211) as per manufacturer's specifications. qRT-PCR was performed using the

7900HT Fast Real-Time PCR System (Life Technologies) per standard protocol. Samples were plated onto 96-well reaction plates (Applied Biosystems, 4346900) with 1X TaqMan Universal PCR Master Mix (Applied Biosystems, 4364341) combined with CIC primers/probe for Exon 1/2 (Applied Biosystems, #Mm00459191_m1), Exon 6/7 (Applied Biosystems, #Mm01173219_m1) and Exon 11/12 (Applied Biosystems, #Mm01173212_m1), or mouse GAPDH (Applied Biosystems, #4352339E) as a control.

2.10 Analysis & Statistics

Data was analyzed for statistical significance using the Student's t-test. A p-value of <0.05 was considered significant.

2.11 Figures and figure legends

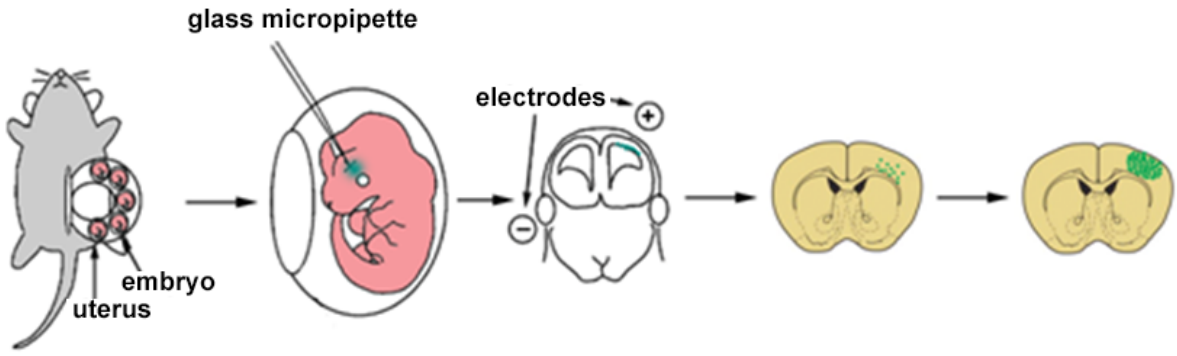

Figure 2.1. Schematic of *in utero* electroporation.

Plasmid DNA encoding either non-targeting shRNA or CIC shRNA is injected into the lateral ventricles of embryonic mice at E14. A pCIG2 plasmid containing enhanced green fluorescent protein (eGFP) is co-injected to label and track electroporated cells. The DNA is drawn into ventricular zone (VZ) progenitors using 5 pulses of 50 V current from electrodes placed externally on the uterus (Dixit et al., 2011). Post-electroporation, embryos are left to develop to the desired age and experiments measuring proliferation and cell fate specification can then be performed (E14-16 to assess proliferation, E14-18 to study specification and migration).

Table 2.1 – Antibodies used in immunoblotting studies

Antibody Target	Source	Catalog #	Host Animal	Working Dilution
Capicua (CIC)	Thermo Scientific	PA1-46018	Rabbit polyclonal	1:1000
Sox2	R&D Systems	MAB2018	Mouse monoclonal	1:1000
Pax6	Santa Cruz Biotech	Sc-81649	Mouse monoclonal	1:1000
Sox9	Millipore	AB5535	Rabbit polyclonal	1:1000
Tuj1	Millipore	CBL412	Mouse monoclonal	1:1000
PDGFRa	Cell Signaling	3164	Rabbit Polyclonal	1:1000
GFAP	Milipore	MAB360	Mouse monoclonal	1:1000
Olig2	Millipore	MABN50	Mouse monoclonal	1:1000
B-Actin	Cell Signaling	3700	Mouse monoclonal	1:2000

Table 2.2 – Antibodies used in immunofluorescence studies

Antibody Target	Source	Catalog #	Host Animal	Working Dilution
Capicua (CIC)	Thermo Scientific	PA1-46018	Rabbit polyclonal	1:500
Sox2	R&D Systems	MAB2018	Mouse monoclonal	1:200
Pax6	Santa Cruz Biotech	Sc-81649	Mouse monoclonal	1:200
Sox9	Millipore	AB5535	Rabbit polyclonal	1:500
NeuN	Millipore	MAB377	Mouse monoclonal	1:500
Olig2	Millipore	MABN50	Mouse monoclonal	1:200
S100B	Abcam	ab14849	Mouse monoclonal	1:200
PHH3	Cell Signaling	97065	Mouse polyclonal	1:100
BrdU	AbD Serotech	OBT00305	Rat monoclonal	1:20
GFP	Invitrogen	A11120	Mouse polyclonal	1:500
GFP	Invitrogen	A11122	Rabbit Polyclonal	1:500
Alexa Fluor 568	Life Technologies	A-11004	Goat anti-Mouse IgG	1:500
Alexa Fluor 568	Life Technologies	A-11011	Goat anti-Rabbit IgG	1:500
Alexa Fluor 488	Life Technologies	A-11001	Goat anti-Mouse IgG	1:500
Alexa Fluor 488	Life Technologies	A-11008	Goat anti-Rabbit IgG	1:500

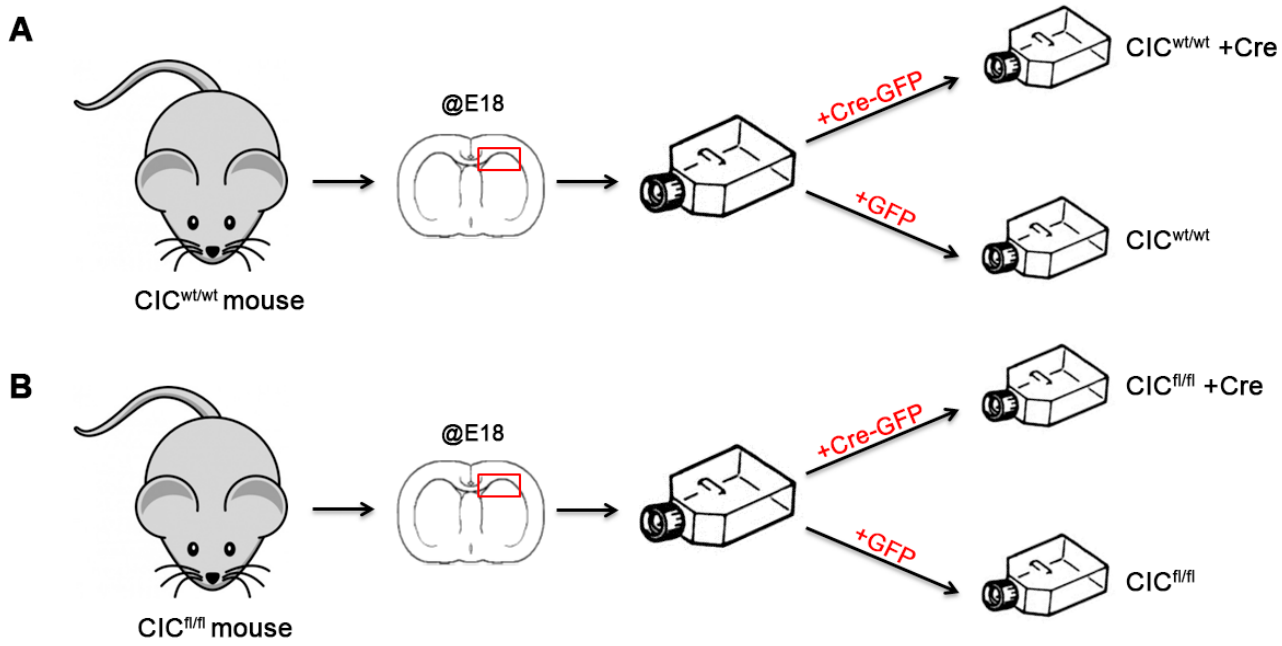

Figure 2.2. Schematic for creation of CIC knockout and control mouse neural stem cell lines. $CIC^{wt/wt}$ (A) and $CIC^{fl/fl}$ animals (B) are sacrificed at embryonic day 18. Cells are cultured from the SVZ/VZ into normal mouse neural stem cell media with the growth factors EGF and FGF. Cells from each background are nucleofected using a piggyBAC transposon carrying either Cre-IRES-GFP (+Cre-GFP) or GFP alone (+GFP). This results in the formation of four cell lines: $CIC^{wt/wt}$, $CIC^{wt/wt}$ +Cre, and $CIC^{fl/fl}$ are all predicted to be functionally wild-type and serve as controls, and $CIC^{fl/fl}$ +Cre, which is CIC null.

CHAPTER 3: CIC IS EXPRESSED AT AN APPROPRIATE TIME AND PLACE TO INFLUENCE CORTICAL DEVELOPMENT

3.1 Introduction

1p19q co-deletion was discovered as a genetic hallmark of ODG several decades ago (Cairncross et al., 1998; Reifenberger et al., 1994). However, causative genes on either 1p or 19q had yet to be identified until recently (Jiao et al., 2012; Yip et al., 2012). Next generation sequencing of a set of ODGs found that CIC was mutated in the majority of these tumors (Jiao et al., 2012; Yip et al., 2012). In ODG, these CIC mutations occur exclusively in the context of 19q loss (part of 1p19q codeletion) and IDH mutation. As one of the first ODG-specific mutations to be discovered, much remains to be learned about the role that CIC loss/mutation plays in tumorigenesis.

Currently, knowledge of CIC is largely restricted to studies in *Drosophila*, where the gene was first detected. In *Drosophila*, CIC plays a role in many developmental processes. Capicua is expressed at several time points in *Drosophila* development, during which it influences embryonic patterning (Jimenez et al., 2000), proliferation in the eye disc and wing pouch (Roch et al., 2002; Tseng et al., 2007), and differentiation of wing vein tissue (Roch et al., 2002). In the mouse, knowledge of CIC function is limited; the majority of work has focused on the role of CIC in extracellular matrix remodelling and lung alveolarization (Crespo-Barreto et al., 2010; Lee et al., 2011). In the brain, previous CIC studies have looked at the cerebellum, implicating CIC as having a role in granule cell development (Lee et al., 2002), although definitive functional studies were not performed.

As ODG is a tumour that most frequently presents as a large mass lesion in the frontal and temporal cerebral cortex of young adults, examining the cellular expression of CIC temporally and spatially over development might yield insight into the possible origins of ODG. In this Chapter, I describe my studies to characterize the expression of CIC in the developing mouse neocortex. Murine CIC shares 92% homology with its human counterpart, with 100% homology in critical regions such as the HMG-DNA binding domain (Lee et al., 2002). The mouse brain is a good model of the human brain, containing all the same cellular constituents. In addition, reagents such as commercial antibodies are readily available against CIC and many other developmental markers for murine study. Although there are recognized differences between rodent and primate corticogenesis (Richardson et al., 2006; Smart et al., 2002), the mouse is an economical and representative model for studying cortical development.

3.2 Validation of anti-CIC antibody

Because my temporal-spatial characterization of CIC expression would rely heavily on immunohistochemical / immunofluorescent localization, it was critical to identify and validate the performance of my CIC antibody in mouse cells and tissues. I used commercially available polyclonal anti-CIC antibody (Thermo Scientific) that was raised against an epitope at the c-terminus of CIC (amino acids 1500 to 1608 encoded by exon 20). Using western blotting of lysates from cultured mouse neural stem cells, I detected a strong and predominant band at 260kD, the predicted molecular weight of the long form of CIC (CIC-L) (Lam et al., 2006) (Figure 3.1A). A few bands of lower intensity were also detected at approximately 80 and 60 kD (Figure 3.1A). The latter could represent either non-specific binding to other proteins, CIC splice variants, or degradation products of full length CIC.

To further examine the specificity of the anti-CIC antibody, I tested the antibody by western blotting of CIC knockout and control mouse neural stem cell lines that I had created. The production of these cell lines took advantage of the Chan Lab's recent generation of a CIC conditional knockout mouse strain, wherein a 5.5 kb segment of CIC genomic DNA (including exons 2-11) is flanked by loxP sites. After dissecting E15.5 embryos and culturing neural stem cells from dorsal cortices of $CIC^{fl/fl}$ or $CIC^{wt/wt}$ mice, I transfected in plasmids carrying either Cre-IRES-GFP or GFP alone to generate 4 cell lines: $CIC^{wt/wt}$, $CIC^{fl/fl}$, $CIC^{wt/wt}$ +Cre which serve as controls, and $CIC^{fl/fl}$ +Cre which is CIC null (Figure 2.2). By western blotting, CIC expression was undetected in the CIC knockout cell line ($CIC^{fl/fl}$ +Cre), but was detected in the three control cell lines ($CIC^{wt/wt}$, $CIC^{wt/wt}$ +Cre, and $CIC^{fl/fl}$) (Figure 3.1B), thus validating my antibody for further use.

3.3 Temporal-spatial characterization of CIC expression in the dorsal cortex by immunohistochemistry

To begin characterizing neocortical CIC expression, I examined its expression at three developmental time points using immunofluorescence staining: 1) E15, the peak of neuron production in the murine brain at mid- to late- corticogenesis; 2) P0, the height of astrocyte production and beginning of oligodendrocyte production, and 3) P7, when oligodendrocyte generation is increased (Miller and Gauthier, 2007). Immunofluorescence staining of CIC and DAPI showed widespread expression of CIC at all three of these stages (Figures 3.2, 3.3, 3.4).

At E15, in the ventricular and subventricular zones (where undifferentiated stem/progenitor cells proliferate), CIC was expressed by most cells and was predominantly cytoplasmic in localization (Figure 3.2D-D''). At E15, CIC expression in the intermediate zone

(Figure 3.2C-C'') and the cortical plate (Figure3.2 B-B'') was diffuse, in both the cytoplasm and nuclei, with limited staining that was distinctly nuclear in cells of the cortical plate.

At P0, CIC expression was also both cytoplasmic and nuclear in the intermediate zone (Figure 3.3C', C''). In the cortical plate, somewhat more distinctly nuclear positivity in observed in subplate neurons (Figure 3.3B-B''). In contrast, CIC expression remained predominantly cytoplasmic in the subventricular and ventricular zones (Figure 3.3D-D'').

By P7, CIC expression was found to be predominantly nuclear in the cortical plate (Figure 3.4B-B''), the intermediate zone (Figure 3.4C', C''), and the subventricular zone (Figure 3.4D-D''). However, a subpopulation of SVZ cells have relatively weaker CIC nuclear expression (Figure 3.4D-D'' arrowheads).

Taken together, the immunostaining data show that CIC is widely expressed in proliferative and differentiative zones of the developing cortex, but the temporal and spatial pattern of expression is not uniform. At immature proliferative cell stages, there is relative absence or weakness of nuclear CIC whereas later stages are characterized by increasingly nuclear CIC localization. This suggests possible changes in CIC's capacity to function as a transcriptional regulator in cells over time.

3.3.1 Shift in CIC subcellular distribution over time detected by western blotting and immunofluorescence

In *Drosophila*, CIC is functional as a transcriptional repressor in the nucleus of cells, but is shuttled to the cytoplasm and degraded when RAS/MAPK signalling is activated (Grimm et al., 2012; Jimenez et al., 2012). To understand the importance of temporal localization of CIC expression in murine brain development, I performed immunofluorescence staining of CIC on

tissues from E15, P0 and P7 brains (Figure 3.5A-A''). CIC expression in the cortical region is largely found in the cytoplasm of cells at E15, although low-intensity nuclear expression is seen (Figure 3.5A). As the cells progress from early progenitors (E15) to differentiated cells (P0-P7), cytoplasmic CIC expression becomes increasingly nuclear (Figure 3.5A, A', A''). Thus, my results indicate that in normal murine brain development, CIC is expressed at a time (E15 to P7) and place (VZ and CP) where it may repress the activation of specific developmental genes.

To further explore the localization of CIC over time, protein fractionation was conducted using samples from E15, P0, and P7 mouse brains to separate cytoplasmic and nuclear proteins. CIC expression was measured using western blot analysis (Figure 3.5 B) and normalized to loading controls SMC1 (for nuclear fractions), and β-Tubulin (for cytoplasmic fractions) (Figure 3.5C, D). Western blot analysis revealed expression of two bands; CIC band #1 at 260kD, the predicted molecular weight of CIC, and CIC band #2, located just below at approximately 250kD. No significant increase in nuclear CIC expression was found in CIC Band #1 over time (Figure 3.5 C). However a significant change in nuclear localization was found with CIC band #2 between P0 and P7, consistent with my immunofluorescence findings (Figure 3.5D, n=3, p=0.0289). This band may result from post-translational modifications of CIC or another isoform of the gene, however more experiments are necessary to determine the nature of the band. Of note, the lysates used in these experiments were from bulk tissue (not sorted to enrich for specific cell types), and the fractionation technique also did not completely separate cytoplasmic contents from the nuclear fractions. Although less clear, the Western blotting data supports the immunohistochemical finding that CIC subcellular localization changes over time, shifting to increasingly nuclear localization at more mature stages.

3.4 CIC is expressed in cortical stem/progenitor cells in a predominantly cytoplasmic distribution

In the developing cortex, neural stem/progenitor cells are found in the VZ and can be identified by their expression of the transcription factor Sox2. To determine the expression of CIC in embryonic neural stem cells, I performed co-immunofluorescence staining on tissue from E15 with antibodies against Sox2 and CIC. In the VZ, I found that CIC is expressed predominantly in the cytoplasm of cells staining for Sox2 (Figure 3.6A-A'''), with absent or relatively weak nuclear co-expression.

Pools of stem/progenitor cells are not only found in the developing cortex but are also present in a few discrete regions in the adult brain. These regions include the dorsal and ventral subependymal zones (SEZ, also known as the adult SVZ) of the lateral ventricles and the subgranular layer (SGL) of the hippocampal dentate gyrus (DG). Stem cells in the SEZ are found adjacent to the ependymal cells lining the ventricle, and then move away from the ventricle to join the rostral migratory stream. In the DG, stem/progenitor cells proliferate in the SGL, and then move into the granule cell layer as they mature from stem cell to neuroblast to granule neuron. To examine CIC expression in these adult neural progenitor regions, I harvested adult mouse brain tissue and immunostained sections for CIC in the DG and SEZ. CIC was expressed in the SEZ (Figure 3.7B-B''), as well as in the DG (Figure 3.9B,C-C''). The presence of progenitor cells was confirmed in the SEZ by immunofluorescence co-expression of CIC and Sox2, a marker of progenitor fate (Figure 3.8B-B''). Similar to the pattern of expression observed in embryonic and earlier postnatal stages, CIC expression is absent or only weakly nuclear in cells in the SEZ and the SGL, in contrast to more strong and distinctly nuclear expression in adjacent areas composed of more mature cells (Figure 3.7B-B'', Figure 3.9C-C'').

Thus, in the embryonic, early postnatal, and adult brain, there is limited nuclear CIC present in uncommitted proliferative cells, at least as detected by immunohistochemical methods.

As CIC is thought to function as a repressor when expressed in the nucleus (Grimm et al., 2012; Lim et al., 2013), it may be that the low level of nuclear CIC allows for some basal derepression of either proliferation or stemness controlling genes in stem/progenitor cells.

3.5 Cortical cells of neuronal and astrocytic lineages, but not oligodendrocytic lineage, strongly express CIC in the nucleus.

As described above, at more mature developmental stages, CIC expression shifts to an increasingly nuclear localization. It is unknown, however, whether all mature cells express nuclear CIC or if strong nuclear CIC is restricted to specific cell types. To further characterize which cells express CIC, I performed immunofluorescence staining of P7 cortex with antibodies against CIC and markers of neurons, astrocytes, and oligodendrocytes.

CIC was strongly co-expressed in the nucleus of cells of two lineages; neurons and astrocytes (Figure 3.10A, B). Nearly all cells positive for the mature neuronal marker NeuN also showed nuclear CIC expression (Figure 3.10A-A’’’) (90.45±6.24% of NeuN cells are CIC+ vs 10.16±4.45% CIC-, n=3, p=0.0041). Similarly, nearly all cells positive for the astrocytic marker S100B expressed nuclear CIC (Figure 3.10B-B’’’) (86.72±2.97% of S100B cells are CIC+ vs 13.29±2.35% CIC-, n=3, p=0.0014). Therefore, CIC is strongly co-expressed in the nuclei of cells of neuronal and astrocytic lineages.

In contrast, examination of CIC co-expression with the bHLH transcription factor Olig2 revealed absent or weak nuclear CIC staining in oligodendrocytic lineage cells (Figure 3.10C-C’’’, D-D’, E). Olig2 is expressed throughout the entire oligodendrocyte lineage, from OPC to

mature oligodendrocyte. Quantification of the percentage of Olig2+ cells that are also CIC+ (Olig2+ CIC+/Olig2+) was performed (Figure 3.10C’’’, 26.21±12.46 % of Olig2+ cells are CIC+ vs 73.17±11.50% of Olig 2+ CIC–, n=3, p=0.0472). Furthermore, of the minority of Olig2+ cells that were scored as CIC+ positive, the intensity of CIC nuclear staining was generally weak; quantitation of the signal intensity for CIC was significantly lower in Olig2+ cells than in Olig2- cells (Figure 3.10D-D’’, E). Thus, it can be concluded that CIC is either not expressed, or expressed at very low levels in nuclei of oligodendrocyte lineage cells.

3.6 Conclusion

I have shown above that CIC is widely expressed in cortical tissue throughout development. However CIC expression is neither uniform across cell types nor is it static with respect to its subcellular localization over developmental stages of from stem cell to mature cells. In stem/progenitor populations in the embryonic, early postnatal, and mature neocortex, CIC expression is absent or relatively weakly expressed in the nucleus. As cells differentiate into oligodendrocytes, nuclear CIC expression remains low or absent. However differentiation into neuronal and astrocytic lineages is associated with strong nuclear CIC expression. Indeed, the presence of nuclear CIC in specific cell types and stages, and its absence in others, suggests that this gene might influence cell type specification or proliferation in neurodevelopment.

Previous work has found that that by E15, ERK activity is relatively high in the VZ presence, and that the intensity of ERK signalling regulates both proliferation and cell fate of neural progenitors (Li et al., 2014). My CIC expression data is consistent with this pattern of ERK activation, as CIC nuclear-to-cytoplasmic localization and CIC function is regulated by

ERK-mediated phosphorylation (Grimm et al., 2012; Jimenez et al., 2012; Lim et al., 2013), and as I observed predominantly cytoplasmic localization of CIC in the cells that are known to have high ERK activity. The expression pattern would fit with a model wherein nuclear CIC bound to target genes represses the expression of stem/progenitor- or OPC-promoting genes, whereas removal of CIC from the nucleus derepresses stemness or OPC-promoting programs. As gliomas are thought to arise from an OPC origin (Liu et al., 2011), loss of CIC through mutational inactivation and copy number loss may be an important driver of ODG formation, although its mechanism of function remains unknown.

3.7 Figures and figure legends.

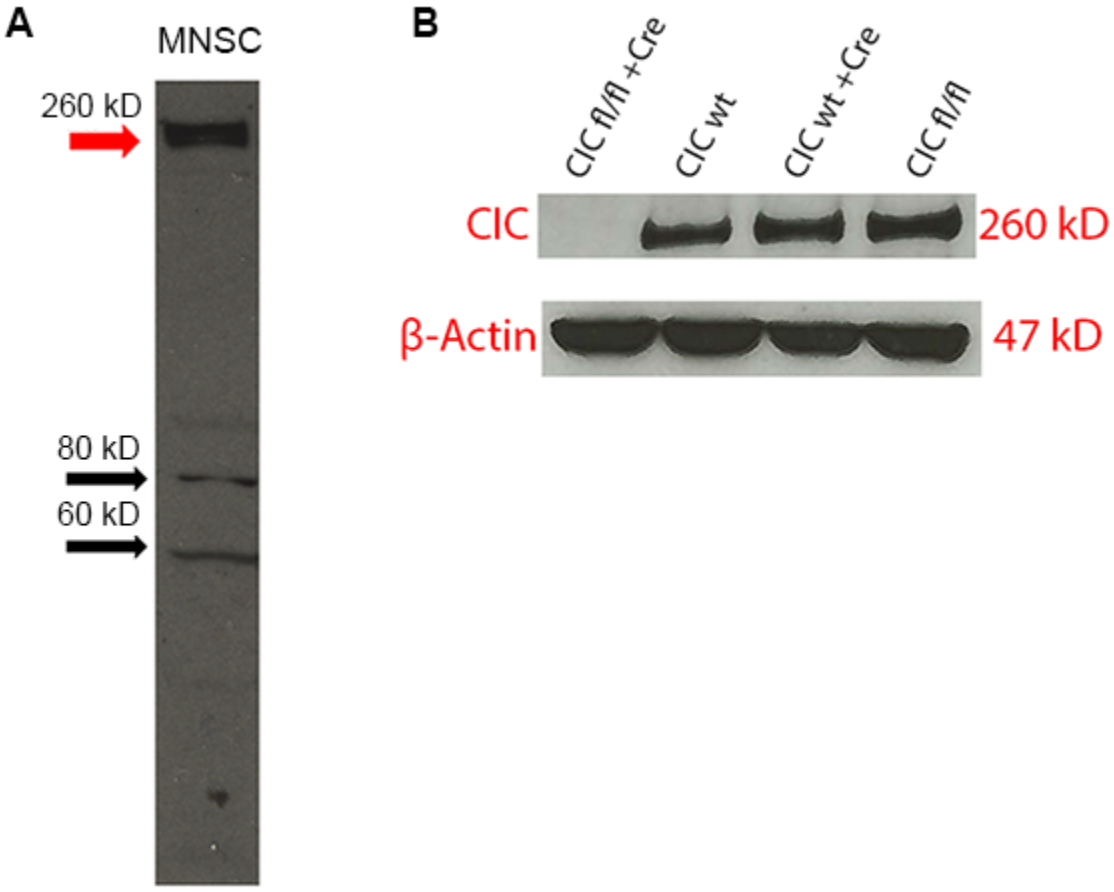

Figure 3.1. Validation of CIC antibody specificity.

A. Western blot analysis of cultured mouse neural stem cells (MNSC) shows that Thermo Scientific Rabbit anti CIC antibody recognizes a band at 260kD, the predicted molecular weight of CIC. Fainter bands are seen at 80kD and 60kD which may represent degradation products or non-specific bands. B. Confirmation of CIC antibody specificity using cells derived from CIC-CKO mice with $CIC^{wt/wt}$ or $CIC^{fl/fl}$ backgrounds. Harvested cells were nucleofected with a cre recombinase plasmid to create three functionally wild-type control lines ($CIC^{wt/wt}$, $CIC^{wt/wt}$ +Cre, $CIC^{fl/fl}$), and $CIC^{fl/fl}$ +Cre, which is CIC null. Western blot analysis of CIC expression shows an absence of expression using the Thermo Scientific rabbit polyclonal anti-CIC antibody in cells in which the gene is genetically ablated (deletion of exons 2-11, with frameshift of remaining exons 12-20).

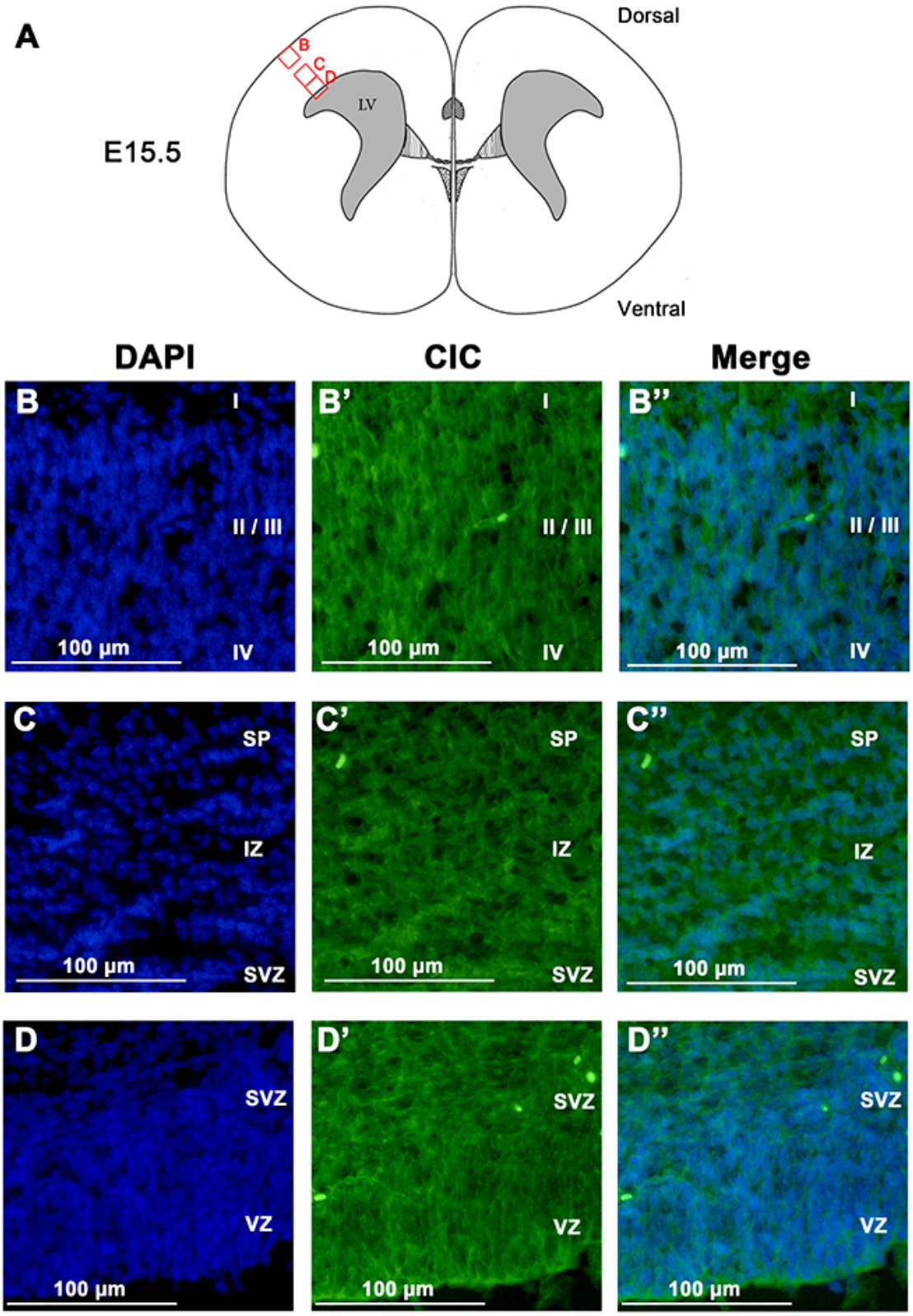
A
E15.5
Dorsal
Ventral
B
C
D
LV
DAPI
CIC
Merge
B
B'
B''
I
II / III
IV
100 μm
C
C'
C''
SP
IZ
SVZ
D
D'
D''
VZ

Figure 3.2. CIC expression in embryonic day 15 (E15) mouse neocortex.

A. Schematic showing location of images (B,C,D). B-D. Tissue harvested from E15 murine brains was immunostained for CIC (green), and counterstained with DAPI (blue). CIC expression was found to be predominantly cytoplasmic in the cortical plate (B', B''), the intermediate zone (C', C''), and the subventricular and ventricular zones (D', D''). Limited nuclear localization is seen in the cortical plate (B', B'') at this developmental stage. Cortical layer I (I), cortical layer II and III (II/III), cortical layer IV (IV), subplate (SP), intermediate zone (IZ), subventricular zone (SVZ), ventricular zone (VZ).

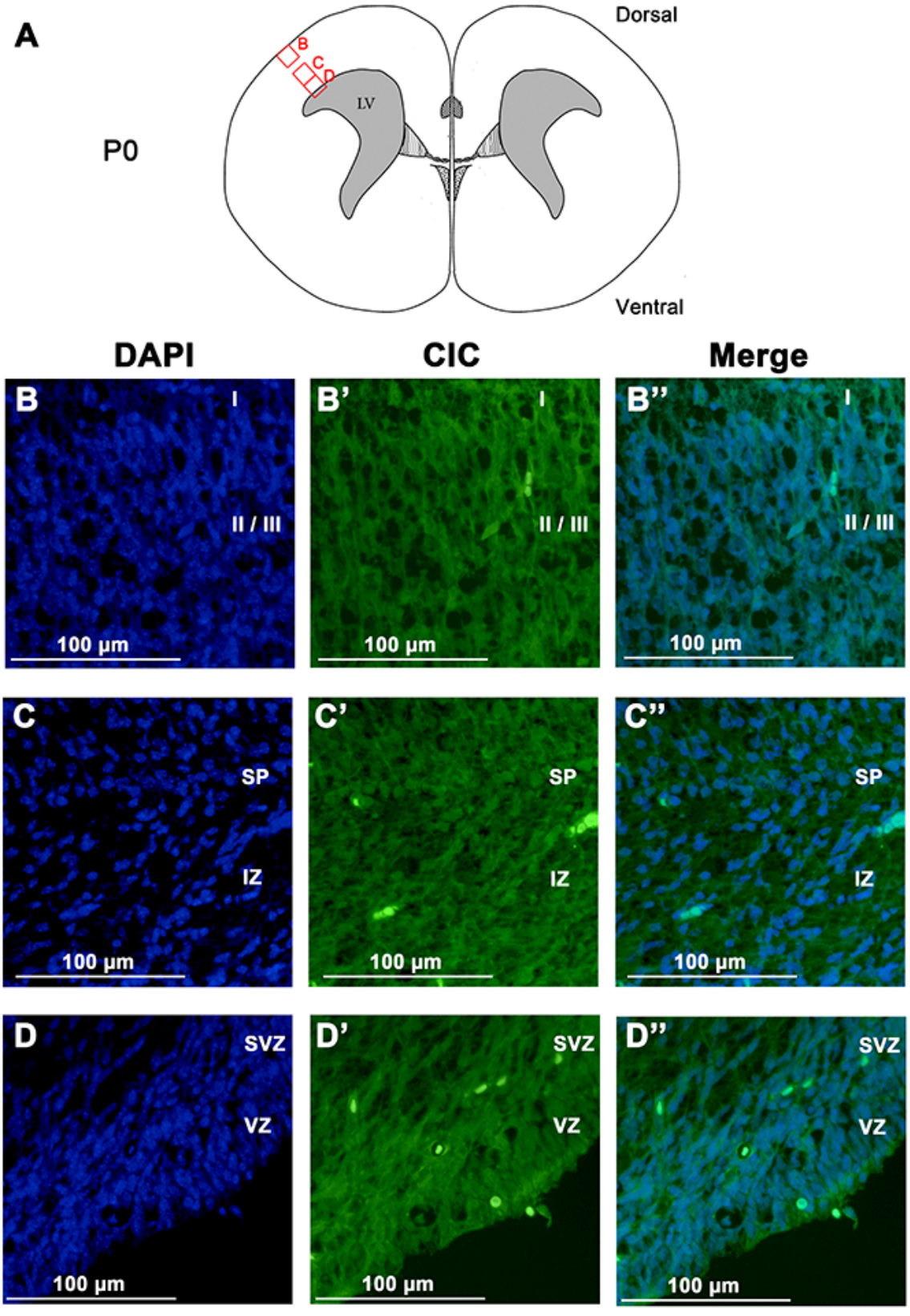
A
P0
B
C
D
LV
Dorsal
Ventral
DAPI
CIC
Merge
B
I
II / III
100 µm
B'
I
II / III
100 µm
B''
I
II / III
100 µm
C
SP
IZ
100 µm
C'
SP
IZ
100 µm
C''
SP
IZ
100 µm
D
SVZ
VZ
100 µm
D'
SVZ
VZ
100 µm
D''
SVZ
VZ
100 µm

Figure 3.3. CIC expression in postnatal day 0 (P0) mouse neocortex.

A. Schematic showing location of images (B,C,D) within the P0 murine cortex. B-D. Tissue harvested from normal P0 murine brains was immunostained for CIC (green), and counterstained with DAPI (blue). At P0, CIC expression was found to be both cytoplasmic and nuclear in the cortical plate (B', B''), the intermediate zone (C', C''), while remaining predominantly cytoplasmic in the subventricular and ventricular zones (D', D'') of the normal murine brain. Cortical layer I (I), cortical layer II and III (II/III), subplate (SP), intermediate zone (IZ), subventricular zone (SVZ), ventricular zone (VZ).

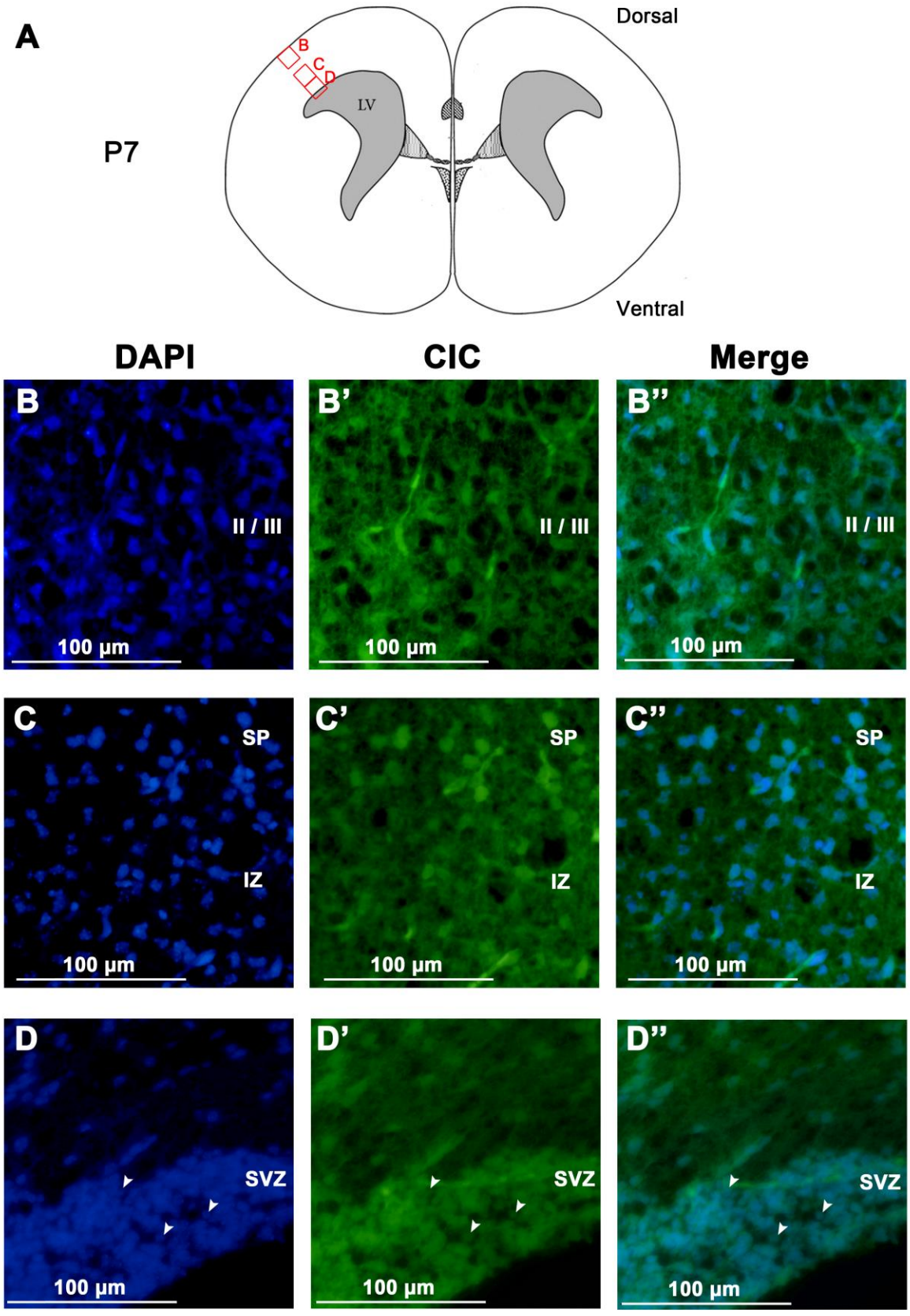
A
P7
Dorsal
Ventral
B
C
D
LV
DAPI
CIC
Merge
B
B'
B''
II / III
C
C'
C''
SP
IZ
D
D'
D''
SVZ
100 µm

Figure 3.4. CIC expression in postnatal day 7 (P7) mouse neocortex.

A. Schematic showing location of images (B,C,D) within the P7 murine cortex. B-D. Tissue harvested from normal P7 murine brains was immunostained for CIC (green), and counterstained with DAPI (blue). At P7, CIC expression was found to be predominantly nuclear in the cortical plate (B', B''), the intermediate zone (C', C''), and the subventricular zone (D', D''). However, a subpopulation of cells in the SVZ have relatively weaker nuclear CIC expression (arrowheads). Cortical layer II and III (II/III), subplate (SP), intermediate zone (IZ), subventricular zone (SVZ).

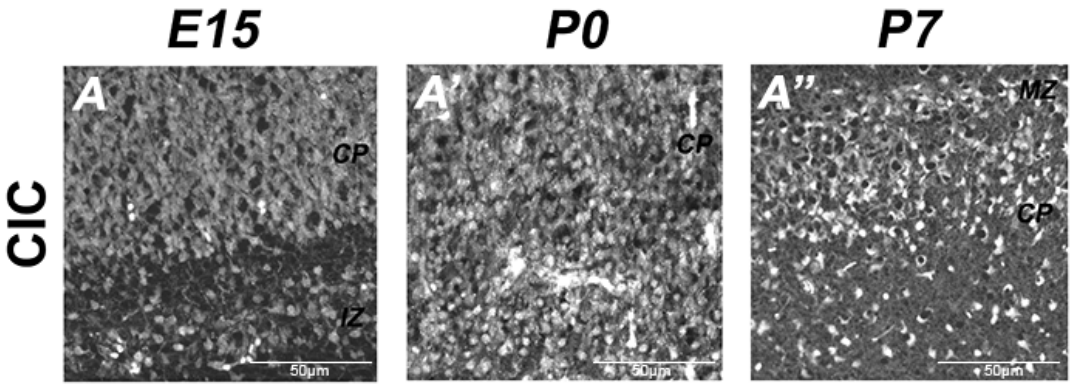
E15
P0
P7
CIC
A
A'
A''
CP
IZ
MZ
50μm

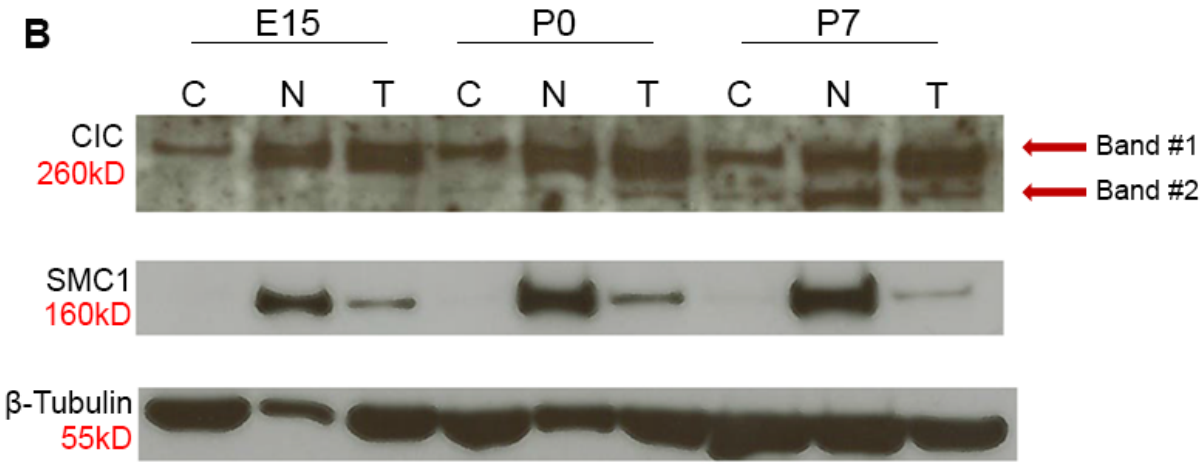
B
E15
P0
P7
C N T C N T C N T
CIC
260kD
Band #1
Band #2
SMC1
160kD
β-Tubulin
55kD

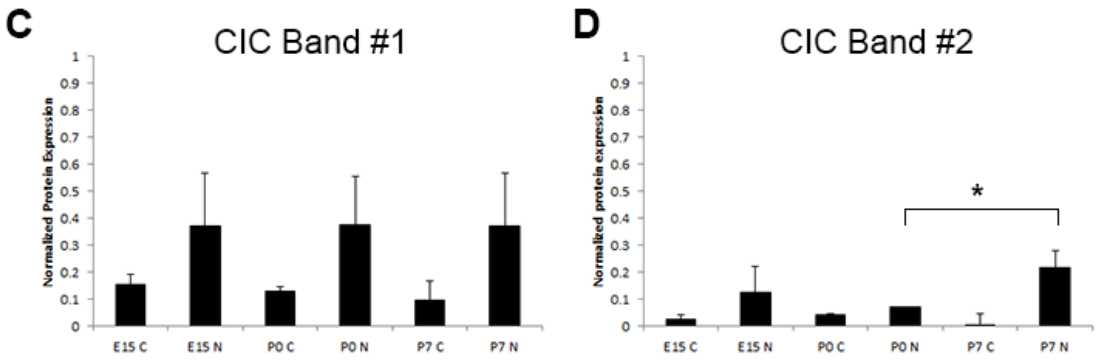
C
CIC Band #1
Normalized Protein Expression
E15 C
E15 N
P0 C
P0 N
P7 C
P7 N
D
CIC Band #2
Normalized protein expression
*

Figure 3.5. Temporal expression of CIC in the developing murine cortex.

A. Tissue harvested from embryonic day 15 (E15), postnatal day 0 (P0), and postnatal day 7 (P7) murine brains was stained using immunofluorescence with a CIC (white) antibody. CIC expression changes from being predominantly cytoplasmic at E15 (A), to increasingly nuclear in the cortex between P0 (A') and P7 (A''). B-D. Localization of CIC expression was further examined by protein fractionation to separate cytoplasmic and nuclear proteins followed by western blotting. CIC expression was measured using western blot analysis (B) and normalized to SMC1 (nuclear loading control) and β-Tubulin (cytoplasmic loading control) (C,D). Two bands were expressed; CIC band #1 is found at 260kD, the predicted molecular weight of CIC, while CIC band #2 is just below at approximately 250kD. No significant increase in nuclear localization was found with CIC band #1 (C). A significant increase in nuclear CIC expression was found in CIC band #2 between P0 and P7 ($n=3$, $p=0.0289$). Cortical plate (CP), intermediate zone (IZ), marginal zone (MZ), nuclear fraction (N), cytoplasmic fraction (C), total (both nuclear and cytoplasmic) fraction (T). *$p<0.05$.

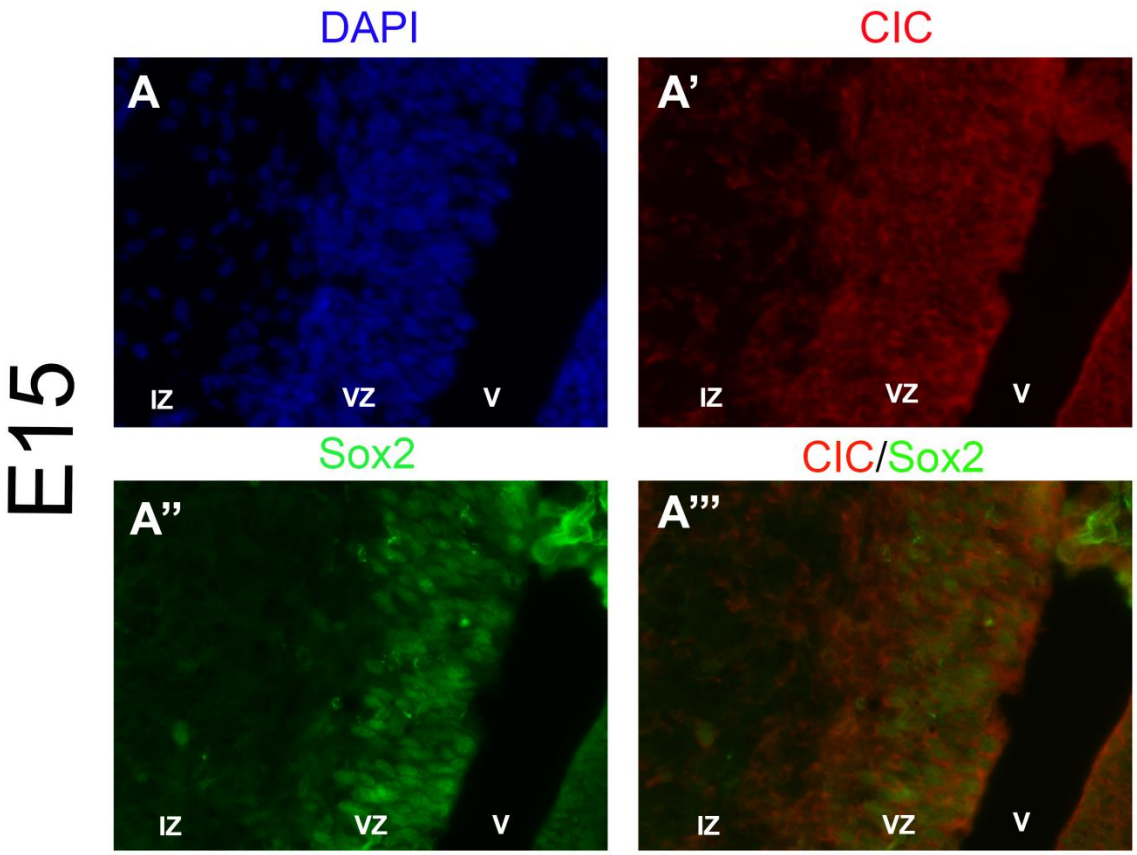

Figure 3.6. Expression of CIC with the stem cell marker Sox2.

A. Tissue harvested from normal embryonic day 15 (E15) brain was immunostained with antibodies against CIC (red) and Sox2 (green), and counterstained with DAPI (blue). CIC is expressed in Sox2+ cells (A'-A'''), but is predominantly cytoplasmic in distribution. Intermediate zone (IZ), ventricular zone (VZ), ventricle (V).

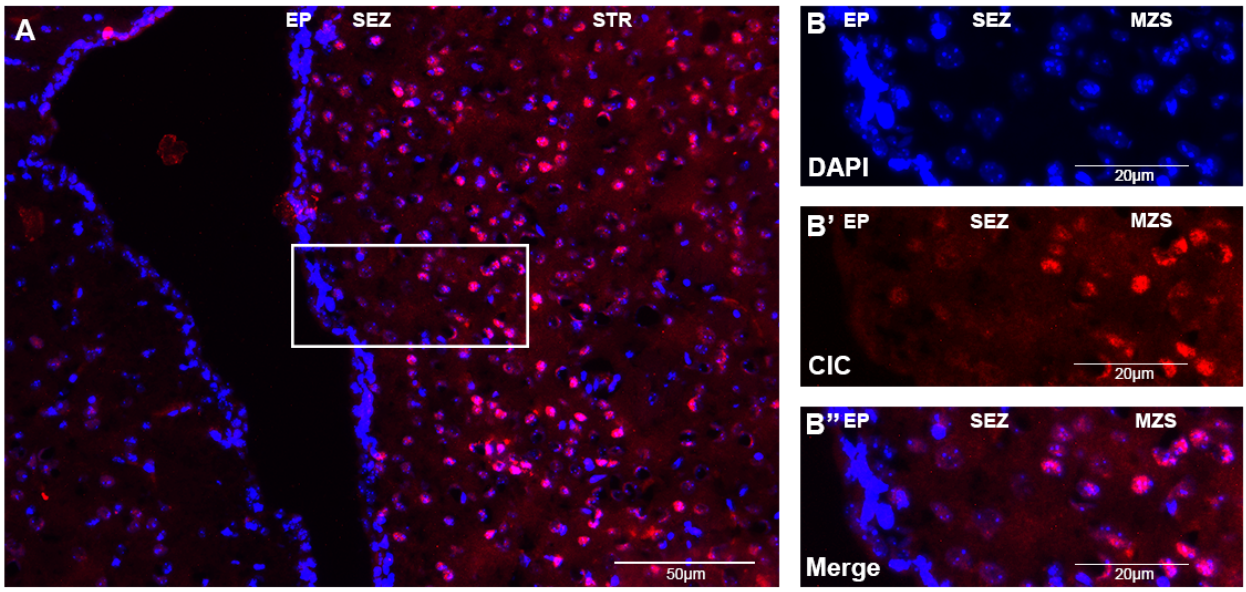

Figure 3.7. Expression of CIC in adult murine subependymal zone, an adult progenitor pool. A, B. Tissue harvested from normal adult murine brain was stained with anti-CIC antibody (red) and counterstained with DAPI (blue). A. Low magnification image for orientation. . B. Higher magnification image of the boxed region shown in panel A. CIC expression remains absent or weakly expressed in nuclei of cells in the subependymal zone (also known as the adult subventricular zone). In contrast, CIC expression is strongly nuclear in cells in the adjacent striatum. Overlay of CIC and DAPI in merged image (B``) shows positive nuclei in magenta. Ependyma (EP), subependymal zone (SEZ), striatum (STR), mantle zone of the striatum (MZS).

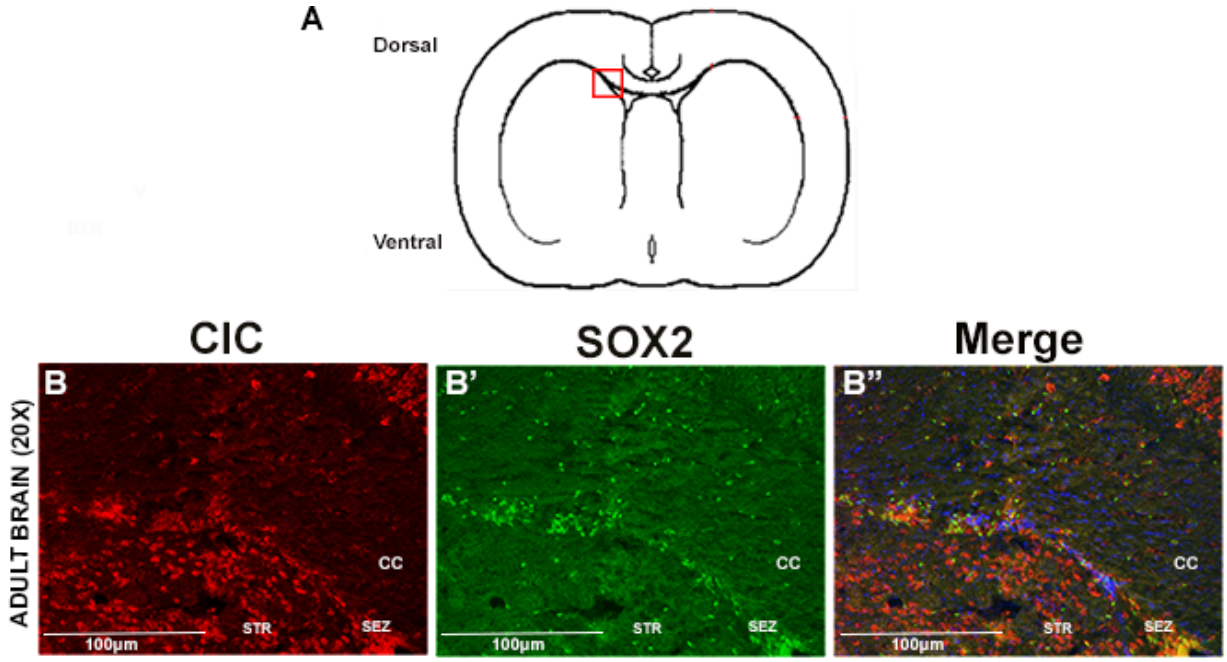

Figure 3.8. CIC and Sox2 expression in the adult murine subependymal zone.

A. Localization of images (B) within the adult murine brain. B. Tissue harvested from normal adult murine brains was stained using immunofluorescence with antibodies against CIC (red) and the stem/progenitor markerSox2 (green), and counterstained with DAPI (blue). In the subependymal zone (also known as the adult subventricular zone), CIC co-expresses with Sox2, a marker of stem/progenitor fate. The subventricular zone is considered to be an adult progenitor pool. Co-expression is shown in yellow. Striatum (STR), subependymal zone (SEZ), corpus callosum (CC).

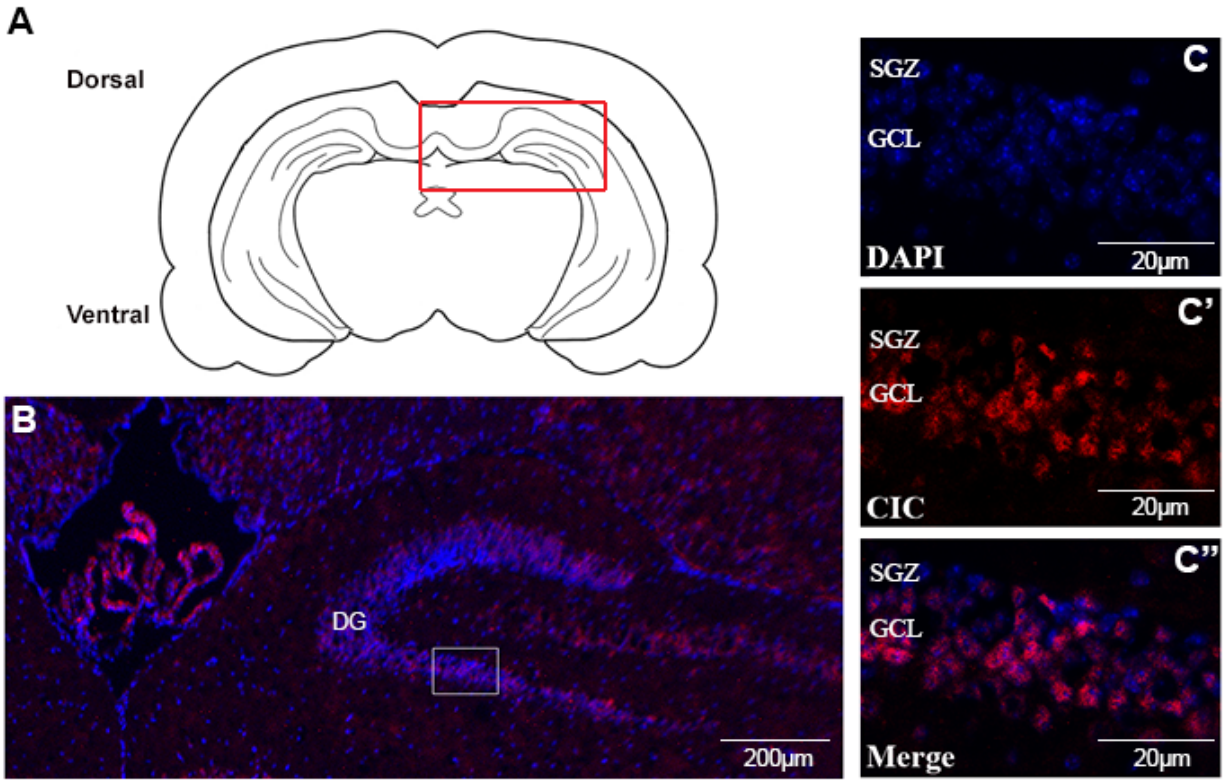

Figure 3.9. Expression of CIC in adult murine dentate gyrus, an adult progenitor pool.

A. Localization of images (B,C) within the adult murine cortex. B, C. Tissue harvested from adult murine brain was stained using immunofluorescence with antibodies against CIC (red), and counterstained with DAPI (blue). B. CIC expression and DAPI nuclear counterstain at low magnification. C-C''. Higher magnification images of the boxed region on the left. CIC expression remains predominantly cytoplasmic in the subgranular zone, the proliferative region of the dentate gryus (C''). CIC expression is increasingly nuclear in cells that have migrated away from the SGZ to occupy the granule cell layer. Overlay of CIC and DAPI shows positive nuclei in magenta. Dentate gyrus (DG), subgranular zone (SGZ), granule cell layer (GCL).

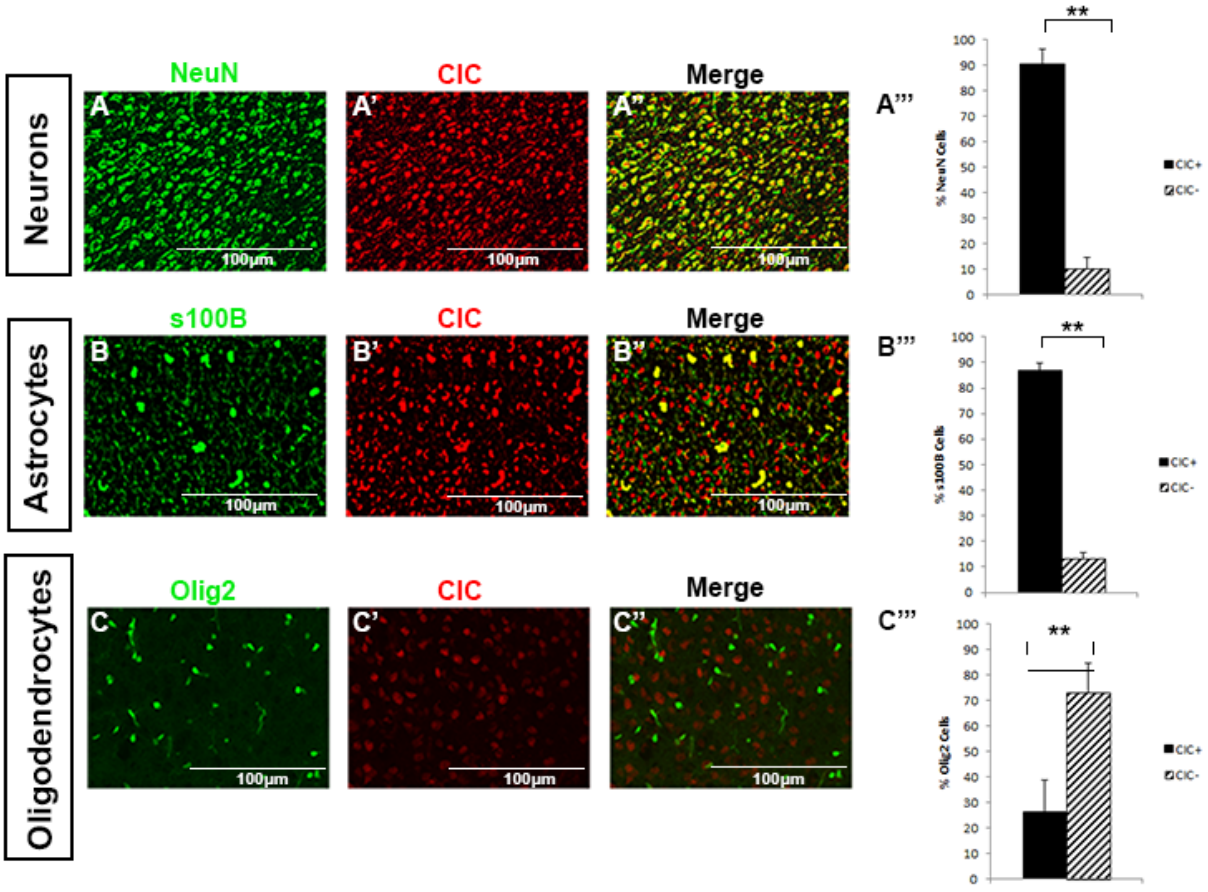
Neurons
NeuN
CIC
Merge
A
A'
A''
A'''
100µm
**
% NeuN Cells
CIC+
CIC-
Astrocytes
s100B
CIC
Merge
B
B'
B''
B'''
100µm
**
% s100B Cells
CIC+
CIC-
Oligodendrocytes
Olig2
CIC
Merge
C
C'
C''
C'''
100µm
**
% Olig2 Cells
CIC+
CIC-

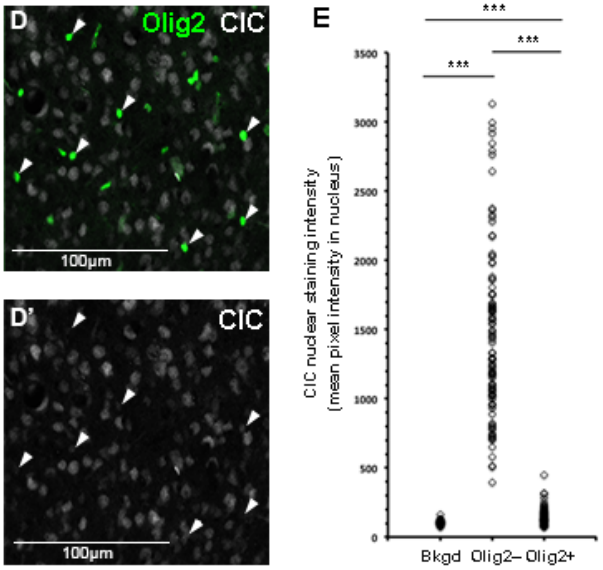
D
Olig2 CIC
100µm
D'
CIC
100µm
E
***
***
***
CIC nuclear staining intensity
(mean pixel intensity in nucleus)
Bkgd
Olig2–
Olig2+

Figure 3.10. Identity of CIC positive cells at postnatal day 7 (P7) in the normal murine brain. A-C. Tissue harvested from normal P7 murine brain was stained using immunofluorescence of CIC (red), markers of cell fate (green), and DAPI (blue) antibodies. Co-expression is shown in yellow. CIC was found to co-express with NeuN (A''), a marker of mature neuronal fate. Quantification of percentage of double-positive cells ($NeuN^+$ CIC^+ cells/$NeuN^+$ cells; A''', n=3, p=0.0041). CIC was found to co-express with s100B, a marker of astrocyte fate (B''). Quantification of percentage of double-positive cells ($s100B^+$ CIC^+/$s100B^+$ cells; B''', n=3, p=0.0014). CIC does not predominantly co-express with Olig2, a marker of oligodendrocyte cell fate (C''). Quantification of percentage of double-positive cells (Olig2+ CIC+/Olig2 positive; C''', n=3, p=0.042). D. Immunofluorescence staining of CIC (white) and Olig2 (green) was performed at P7 in normal murine brain tissue (D, D'). E. Quantification of CIC expression intensity in Olig2 positive cells versus Olig2 negative cells at postnatal day 7. **$p<0.01$, *** $p<0.001$

CHAPTER 4: CIC MODULATES PROLIFERATION, DIFFERENTIATION, AND MIGRATION IN NEURAL PROGENITORS

4.1 Introduction

CIC loss and mutations are a genetic hallmark of ODG (Bettegowda et al., 2011; Yip et al., 2012)., and I hypothesize that loss of CIC function, leading to de-repression of genes normally controlled by CIC, is important in ODG pathogenesis. In Chapter 3, I characterized the expression pattern of CIC both temporally and spatially in the murine cortex. In cortical stem/progenitor cells, CIC expression is absent or only weakly expressed in the nucleus. Among differentiated cells, nuclear CIC expression remains low or absent in oligodendrocytes but is high in neurons and astrocytes. This expression pattern would be consistent with a model in which CIC represses genes important in controlling stemness, proliferation, or oligodendroglial differentiation. Functional studies, however, are required to discern the potential role of CIC in regulating developmental processes that may be relevant to cancer.

In *Drosophila* there is evidence that CIC, downstream of RAS/MAPK pathway signaling, plays a role in repressing proliferation and also promoting differentiation in a tissue-specific manner. Loss of function mutations of CIC in fly eye disc cells show an increased representation of mutant tissue clones over normal tissue. This results in a slightly larger eye, as removing CIC accelerates the cell cycle and causes an increase in proliferation (Tseng et al., 2007). CIC has also been found to restrict proliferation by interacting with RBF1 to promoting G1 cell cycle arrest in dividing precursor cells (Krivy et al., 2013). Loss of function studies in *Drosophila* have revealed that CIC also functions as a tissue-specific repressor of cell fate. In early stages of *Drosophila* development, CIC represses appendage-producing fates in follicle cells, as mutant

CIC clones cause ectopic appendage material in the embryo (Atkey et al., 2006). In the developing wing pouch, CIC represses vein specific genes in intervein regions, in which it is highly expressed in the nucleus of cells. EGFR decreases CIC protein levels in vein nuclei, antagonising CIC repressor activity and allowing for production of vein tissue in appropriate regions (Roch et al., 2002).

To gain insight into the functional role(s) of CIC in the mammalian brain and its potential role in ODG, I took a loss-of-function approach in cortical progenitors *in vitro* and *in vivo*, and studied whether CIC plays a role in cell growth, proliferation, and differentiation.

4.2 Approaches to CIC loss of function studies

In order to identify a suitable reagent for CIC loss-of-function, I first tested the efficacy of CIC knockdown using 5 independent CIC shRNAs. CIC shRNAs or non-targeting (NT) control shRNAs were transiently transfected into p53 null mouse neural stem cells (chosen for these preliminary studies for their robust growth in culture and my experience that they have increased transfection efficiency compared to wild-type MNSC). The sequences of the CIC shRNAs and NT shRNA are detailed in Chapter 2; CIC shRNAs 1 through 5 target Exons 4, 9, 17, 5, and the 3'UTR, respectively. All CIC shRNAs tested showed at least partial knockdown of CIC *in vitro* when compared to untreated, empty vector, and non-targeting controls (ranging from approximately 60 to 85% reduction in CIC protein at approximately 2 weeks post-transfection) (Figure 4.1 A, B). The shRNA that was found to be the most effective, (CIC shRNA#4, which resulted in approximately 85% reduction in CIC protein) was then used for further functional studies *in vitro*.

I also tested whether CIC shRNA#4 could be used to manipulate CIC levels in neural progenitor cells *in vivo*. With the collaboration of Rajiv Dixit, a research associate in the Chan lab, CIC and NT shRNA constructs were introduced into ventricular zone cortical stem/progenitors via *in utero* electroporation (Figure 4.2). This technique involves injecting plasmid DNA into the ventricles of embryonic mice, drawing the DNA into the adjacent VZ cells using directional electrical pulses, then examining the targeted cells within the tissue at a subsequent timepoint (Figure 2.1). For my validation experiments, E14 embryos were electroporated with either of NT or CIC shRNA and co-electroporated with pCIG2 plasmid (containing enhanced green fluorescent protein, eGFP) to label and track electroporated cells. To determine whether the method would be suitable for my experiments, animals were sacrificed at E18, and I performed co-immunofluorescence staining for GFP (to indicate NT or CIC shRNA electroporated cells) and CIC (Figure 4.2A-A’’’, B-B’’’). I then quantified the percentage of GFP+cells that were positive for CIC. In E14->E18 electroporations, CIC shRNA #4 decreased the percentage of cells positive for CIC in the electroporated population compared to NT shRNA by 68% (76.80±3.69 % of GFP+ cells are CIC + in NT shRNA vs 24.24±7.97% in CIC shRNA, n=2, p=0.023, Figure 4.2C). The results indicated that CIC shRNA#4 could be used to reduce expression of CIC in vivo. This method was then used to study differences in proliferation and cell fate *in vivo*.

The recent creation of a CIC conditional knockout mouse line in the Chan lab also allowed me to investigate possible alterations in progenitors under more complete absence of CIC. Although expansion of the CIC-CKO mouse strain is ongoing, and crosses with cre-driver strains are still in progress, I took advantage of the existing CIC-CKO mice to isolate neural stem cells for *in vitro* CIC LOF experiments. To do so, cell lines were created by harvesting cells from

mice with either $CIC^{wt/wt}$ or $CIC^{fl/fl}$ backgrounds. Cells from each background were nucleofected using a piggyBAC transposon carrying either Cre-IRES-GFP or GFP alone, resulting in four cell lines: $CIC^{wt/wt}$, $CIC^{wt/wt}$ +Cre, and $CIC^{fl/fl}$, which are all predicted to be functionally wild-type, and $CIC^{fl/fl}$ +Cre, which is CIC null (Figure 2.2A,B). Western blot analysis of these cell lines found that CIC expression was ablated both at the RNA level, as measured using qRT-PCR with primers spanning three exons of the CIC gene, exons 1-2 (Figure 4.3B), exons 6-7 (Figure 4.3B'), and exons 11-12 (Figure 4.3B'') in the $CIC^{fl/fl}$ +Cre cell line, and at the protein level as detected by western blot analysis (Figure 4.3A). Furthermore, CIC expression was re-analysed over the course of the experiments detailed below, and remained absent throughout. In the experiments below, $CIC^{fl/fl}$ +Cre cells are hereafter referred to as CIC-null cells whereas $CIC^{wt/wt}$ +Cre cells are referred to as CIC-control cells.

4.3 CIC ablation alters proliferation

Given that gliomas are uncontrolled proliferations of abnormal glial progenitor-like cells, and that removal of CIC increases proliferation in the context of the *Drosophila* eye disc (Krivy et al., 2013; Tseng et al., 2007), it was reasonable to speculate that one role of CIC in neural progenitors could be regulation of proliferation. To determine whether CIC loss may regulate proliferation in neural stem/progenitor cells, I examined cell viability and number *in vitro* in the CIC-null ($CIC^{fl/fl}$ +Cre) and CIC-control ($CIC^{wt/wt}$ +Cre) cells. CIC-null and CIC-control mouse neural stem cells were plated at 2000 cells per well and grown for 48 hours in MNSC proliferation media (MNSC media with added growth factors EGF and FGF) (Figure 4.4). 48 hours post plating, an Alamar Blue cell assay revealed a 19% increase in viability of CIC-null cells when compared to the CIC-control cells (Figure 4.5A; $1.44x10^4 \pm 283.4$ fluorescence

intensity units (FIU) in $CIC^{wt/wt}$ +Cre cells vs $1.71x10^4 \pm 266.4$ in $CIC^{fl/fl}$ +Cre cells, n=3, p=0.00612). As the Alamar Blue assay measures metabolism of a substrate by viable cells and, as such, is only a surrogate measurement of cell number, I also performed Trypan Blue counts to determine live cell number 48 hours after seeding with 1.0×10^6 cells per flask (Figure 4.5B). Both CIC-null and CIC-control cells proliferated, as indicated by increasing live cell numbers from the time of initial plating. However, there was a >2-fold increase in live CIC-null cells after 48 hours compared to CIC-control cells (Figure 4.5B; $1.88x10^6 \pm 7.73x10^5$ live CIC-control cells vs $3.96x10^6 \pm 2.28x10^5$ live CIC-null cells, n=3, p=0.00165). These results show that, under proliferation-promoting conditions, CIC loss leads to increased cell viable cell numbers, consistent with a role for CIC as a negative regulator of proliferation.

The MNSC media used in the experiments above contained EGF and FGF, two growth factors that are necessary to maintain and propagate cells in a more stem/progenitor like state (Chojnacki and Weiss, 2008; Reynolds and Weiss, 1992). During cortical development, stem cells obtain both positional and temporal information particular to specific mitogenic niches (Hitoshi et al., 2002; Qian et al., 2000). In the VZ, where proliferation is promoted, stem cells respond differently to varying concentrations of growth factors at different stages of development; in the early embryo, low FGF expression influences proliferation and neuron production (Qian et al., 1997), while EGF expression has no effect (Tropepe et al., 1999), whereas, in the late embryo, FGF and EGF expression both influence proliferation (Burrows et al., 1997; Gritti et al., 1999). Removing EGF and FGF from the MNSC media allows for conditions in which RAS/MAPK pathways are decreased within the culture in order to mimic conditions outside the proliferative niche, and possibly unmasking effects of CIC loss. CIC-control and CIC-null cells were plated at 2000 cells/well (for Alamar Blue analysis) or 1.0×10^6

cells/flask (for Trypan Blue analysis) and grown for 48 hours in normal MNSC media without added EGF and FGF (Figure 4.4). Cells were then measured for viability and cell number using Alamar Blue and Trypan Blue, respectively (Figure 4.6). No significant change in substrate reduction was found on Alamar Blue assays in CIC-null cells in these growth conditions when compared to CIC-control cells (Figure 4.6A; $3.92x10^3$±86.8 FIU in CIC-control cells vs $4.15x10^3$±90.9 in CIC-null cells, n=3). However, Trypan Blue measurements of live cell number showed a 2-fold increase in remaining cell number in the CIC-null cells when compared to CIC-control cells after 48 hours (Figure 4.6B; $3.47x10^5$±$1.39x10^5$ live CIC-control cells vs $6.81x10^5$±$1.25x10^5$ live CIC-null cells, n=3, p=0.0139). These results show that in the absence of exogenous growth factors EGF and FGF, CIC-null cells still maintain an increased cell number compared to CIC-control cells. However, it remains to be determined whether the increase in CIC-null cell number seen under these growth conditions is a result of increased proliferation or decreased cell death or both.

To further examine whether CIC-null cells continue to have an increased viability and cell number under differentiating conditions, CIC-control and CIC-null cells were plated at 2000 cells/well (for Alamar Blue) or $1.0x10^6$ cells/flask (for Trypan Blue) and grown for 48 hours in media with 1% fetal bovine serum (FBS) (Figure 4.4). Removal of growth factors (EGF, FGF) and addition of low-serum containing media is a known technique for undirected, nonspecific differentiation of neurospheres (Louis et al., 2013). Cells were measured for viability and cell number using Alamar Blue and Trypan Blue, respectively (Figure 4.6). Alamar Blue assay showed a 28% increase in the reduction of the assay substrate in the CIC null cells under these growth condition when compared to the CIC-control cells (Figure 4.6A; 7161.7±230.9 FIU in CIC-control cells vs 9197.1±212.6 FIU in CIC-null cells, n=3, p=0.050). However, no significant

change in live cell number was found in CIC-null cells grown in 1% serum when compared to CIC-control cells (Figure 4.6B; $2.63x10^5 \pm 2.75x10^5$ live CIC-control cells vs $2.72x10^5 \pm 2.65x10^5$ live CIC-null cells, n=3, p=0.738). Thus, under serum differentiating conditions, CIC-null cells appear to show altered (increased) metabolic activity compared to control cells, but they do not have an increased live cell number.

To further study proliferation *in vivo, in utero* electroporations were conducted at E14 and allowed to develop until E16 (Figure 4.7). Mice were electroporated with either NT or CIC shRNA, and co-electroporated with pCIG2 plasmid containing enhanced green fluorescent protein (eGFP) to label and track electroporated cells. BrdU labeling was performed 30 minutes prior to sacrifice. Embryos were harvested at E16, and co-immunofluorescence staining was performed on NT and CIC shRNA electroporated brains using GFP (to indicate NT or CIC shRNA electroporated cells) and BrdU antibodies. Electroporation of CIC shRNA into cortical progenitors significantly increased the proliferative index 48 hours post-electroporation when compared to NT shRNA controls (Figure 4.7B; 32.7±8.58% of GFP cells label with BrdU in NT shRNA, 53.03±10.58% in CIC shRNA, n=4, p=0.0368) when examining electroporated cells in all layers. Further analysis of proliferation by cortical layer showed significantly more GFP-labelled cells in both the ventricular (Figure 4.7C; 32.3±1.79% of GFP cells label with BrdU in NT shRNA vs. 49.8±1.89% in CIC shRNA, n=3, p=0.00359) and intermediate zones (Figure 4.7C; 8.6±4.32% of GFP cells label with BrdU in NT shRNA vs 13.1±1.47% in CIC shRNA, n=3, p=0.0178). Thus, these results confirm my *in vitro* findings that CIC loss results in increased proliferation of neural stem/progenitor cells, supporting the notion that CIC may repress proliferation in murine brain development.

One special consideration related to proliferation is the potential of cells to self-renew (either by symmetric proliferative division or asymmetric division) to maintain a stem/progenitor population, rather than differentiating to stop replenishing the stem/progenitor pool. To further investigate whether CIC loss affects self-renewal, I performed a clonogenic sphere forming assay on CIC-null versus CIC-control mouse neural stem cells. CIC-null or -control cells were plated at 1000 cells/well in MNSC proliferation media (containing EGF and FGF) and grown for 48 hours (Figure 4.8). In this assay, the presence of a sphere after plating the disaggregated cells at low density is interpreted as though the initial cell had the ability to self-renew (although some re-aggregation of cells cannot be excluded). Thus, after plating a set number of cells, the resulting sphere number is an indicator of how many cells in the initial population had self-renewed to produce a clone of cells. Sphere volume, in contrast, would be influenced by other aspects of proliferation such as cell cycle kinetics (the rate of cycling), or the type of divisions taking place (whether symmetric or asymmetric). Assuming that cell clusters were roughly spherical in 3 dimensions, sphere volume was calculated by measuring the diameter of spheres and using the equation $V=4/3\pi r^3$ to calculate volume in μm^3. After plating the same number of cells, CIC-control and CIC-null mouse neural stem cell lines both produced a similar number of spheres per well (Figure 4.8C; 8.8±.7 spheres/well in CIC-null versus 9.85±2.3 spheres/well in CIC-control vs, n=3, p=0.0967), however the volume of CIC-null spheres was increased by >2-fold compared to controls (Figure 4.8D; $7.91x10^5 \pm 2.17x10^5$ μm^3 versus $3.02x10^4 \pm 8.16x10^3$ μm^3, respectively; n=3, $p=2.01x10^{-8}$). Together, the findings that CIC ablation results in an increased cell number and increased sphere size, suggest that CIC may not be regulating the ability of cells to self-renew, but might be influencing the mode of cell division used (i.e. symmetric versus

asymmetric division) during self-renewal or altering the length of the cell cycle in proliferating cells.

4.4 CIC influences cell type specification

CIC is known to play a tissue-specific role in repressing differentiation in *Drosophila* development (Atkey et al., 2006; Roch et al., 2002). I hypothesized that CIC may show a similar function in mammalian cortical development, and used the above models (*in vivo* and *in vitro*) to look for changes in cell fate specification after CIC loss.

Preliminary *in vitro* analysis of cell fate was performed by transfecting p53 -/- MNSC with five CIC pLKOs targeting different regions of the gene, including Exon 4 (CIC 1), Exon 9 (CIC 2), Exon 17 (CIC 3), Exon 5 (CIC 4), and the 3' UTR (CIC 5) (Figure 4.9). Expression of Tuj1, an early neuronal marker, was decreased in p53-null cells transfected with CIC shRNA when compared to controls (Figure 4.9A,B, n=1). Conversely, increased expression of GFAP, an astrocyte marker, was found in p53 null cells transfected with CIC shRNA when compared to controls (Figure 4.9C,D, n=1). Thus, loss of CIC decreased expression of neuronal markers, and increases expression of glial markers in my preliminary data.

To further investigate the possibility that CIC regulates cell type specification, I performed western blotting on lysates from CIC-null and -control mouse neural stem cells (where CIC-null cells have complete ablation of CIC rather than a partial knockdown as seen with my shRNAs) grown in MNSC proliferation media. Membranes were probed with antibodies against a panel of markers including Tuj1 (early neuronal marker), NeuN (mature neuronal marker), PDGFRa (early oligodendrocyte marker), Olig2 (early through mature oligodendrocytic lineage marker), GFAP (astrocyte marker), Sox9 (stem/glioblast marker), and Sox2 (stem

marker) (Figure 4.10A, B). Of these, Tuj1 expression was significantly decreased in CIC-null cells compared to CIC-control cells (Figure 4.10B; fold change of 0.25 from CIC-control cells to CIC-null cells, n=3, p=0.0413). PDGFRa expression was also decreased in CIC-null cells compared to controls (Figure 4.10B; fold change of 0.50 from CIC-control cells to CIC-null cells, n=3, p=0.0341). Expression levels of the other five markers (Sox2, Sox9, NeuN, GFAP, and Olig2) did not show any significant changes between CIC-control mouse neural stem cells and CIC-null cell lines, at least in the growth condition tested (MNSC proliferation media).

The effect of CIC knockdown on cell fate specification was further studied *in vivo* using CIC shRNA *in utero* electroporation experiments. Electroporations were conducted at E14 and allowed to develop until E16 or E18. Embryos were electroporated with either NT or CIC shRNA, and co-electroporated with pCIG2 track electroporated cells. Samples were harvested and analyzed by immunofluorescence for expression of GFP (to indicate NT or CIC shRNA electroporated cells) and Sox9 or NeuN. Because my *in vitro* western blot data above suggested that CIC could be influencing a neuronal-glial fate choice by which its absence decreased the neuronal population (at least as measured by Tuj1), I examined the electroporated cells for expression of Sox9 to mark stem cells and glioblasts and NeuN to mark neurons.

Sox9 is normally expressed both in VZ stem/progenitor cells as well as cells in the glioblast stage; when they are restricted to glial fate but can become either astrocytes or oligodendrocytes (Scott et al., 2010; Wegner and Stolt, 2005). In vivo, these two Sox9+ phenotypes can be distinguished based on location; the stem population are Sox9+, but still reside in the VZ, whereas glioblasts are also Sox9+, but have lost their apical contacts and have moved into the SVZ/IZ. I examined Sox9 expression in embryos that were electroporated with NT shRNA (Figure 4.11A-A'') or CIC shRNA (Figure 4.11B-B'') at E14 and allowed to

develop to E16. Although CIC shRNA electroporation did not change the overall percentage of GFP cells that were Sox9+ compared to NT shRNA (Figure 4.11C; 12.09±2.75% of GFP cells labeled with Sox9 in NT shRNA vs 13.40±1.04% in CIC shRNA, n=3, p=0.484), differences emerged when examining specific zones for the percentage of double-positive ($Sox9^{+}GFP^{+}/GFP^{+}$) cells. In the VZ, the percentage of Sox9+GFP+ cells was similar in CIC shRNA and NT shRNA conditions (Figure 4.11D; 91.30±22.07% of GFP cells labeled with Sox9 in NT shRNA vs 79.18±5.67% in CIC shRNA, n=3, p=0.381). In the IZ, however, CIC shRNA samples had greater percentage of GFP cells that were positive for Sox9 compared to NT controls (Figure 4.11D; 2.14±1.97% of GFP cells labeled with Sox9 in NT shRNA vs 8.42±2.95% in CIC shRNA, n=3, p=0.0375). These data are consistent with an increased number of glioblasts in the IZ, providing in vivo evidence supporting the notion that CIC loss in progenitors may bias cells towards glial fates. An alternate (and not mutually exclusive possibility) is that CIC loss affects cells migration, a possibility discussed further below.

To study whether CIC loss alters the production of neurons in vivo, embryos were electroporated with NT shRNA (Figure 4.12A-A'') or CIC shRNA (Figure 4.12B-B'') at E14 and allowed to develop to E18, then examined for expression of GFP and NeuN. Four days post-electroporation, CIC shRNA electroporation did not change the overall percentage of GFP-labelled cells expressing NeuN when compared to NT controls (Figure 4.12C; 85.04±3.37% GFP cells label with NeuN in NT shRNA vs 83.84±3.09% in CIC shRNA, n=3, p=0.725). However, more CIC shRNA cells expressing NeuN were present in the ventricular (Figure 4.12D; 2.16±0.375% of GFP cells label with NeuN in NT shRNA vs 8.15±0.383% in CIC shRNA, n=3, $p=1.57x10^{-5}$) and intermediate zones (Figure 4.12D; 25.1±4.26% of GFP cells label with NeuN in NT shRNA vs 40.43±8.88% in CIC shRNA, n=3, p=0.0364), and fewer reached their

expected destination in the CP (Figure 4.12D; 72.7±3.99% of GFP cells label with NeuN in NT shRNA vs 51.41±8.61% in CIC shRNA, n=3, p=0.0117). Whether or not NeuN stained cells eventually migrate to their proper location is unknown; addressing this question would require following the electroporated mice over longer periods of time. However, while this data shows that CIC ablation does not influence the total number of neuronal cells (at least as determined by NeuN expression), it does change the localization of these cells within the layers of the murine cortex. Of note, NeuN was used as the neuronal marker instead of Tuj1 in the in vivo studies because of its antibody staining qualities and greater ease of quantitation. My *in vitro* data, however, suggest that Tuj1 may have been more likely to reveal differences. In the future, it may be useful to also quantitate neurons using Tuj1 as well as distinct neuronal subtype and layer-specific markers.

In sum, the above data has shown that *in vitro*, CIC loss-of-function markedly decreased the expression of neuronal marker Tuj1, and promotes glial fates. As well, *in vivo* CIC loss-of-function increases the number of Sox9+ cells outside the VZ (consistent with an increase in glioblast number). Although no increase or decrease of neuronal cell number was found *in vivo* as measured by NeuN and GFP, possible factors in the apparent discrepancy could be the extent of knockdown or the population of cells examined or the choice of marker used.

4.5 CIC and migration

As stated above, CIC shRNA electroporation *in vivo* into cortical progenitors led to a perturbation of neuronal cell localization, causing more neurons to be found in the VZ and IZ, and fewer in the CP of the murine brain (Figure 4.12). The distribution of those in the CP was also atypical, and not as tightly confined to the upper cortical layers as is seen in the NT shRNA

conditions and as would be expected for the timing of the electroporations in these experiments (E14–>E18). To further study this phenomenon, embryos were electroporated with NT shRNA (Figure 4.13A) or CIC shRNA (Figure 4.13B) at E14 and allowed to develop to E18. Analysis of cellular localization found that there were significantly more GFP-labelled cells in the ventricular (Figure 4.13C; 4.47±1.29% of total GFP cells in NT shRNA vs 9.11±0.787 in CIC shRNA, n=3, p=0.040) and intermediate zones (Figure 4.13C; 19.18±6.32% of total GFP cells in NT shRNA vs 36.31±6.23% in CIC shRNA, n=3, $p=4.60x10^{-4}$) and significantly fewer GFP-labelled cells in the cortical plate (Figure 4.13C; 75.89±5.78% of total GFP cells in NT shRNA vs 54.58±6.67% in CIC shRNA, n=3, p=0.0028) in the CIC knockdown samples when compared to NT controls. As migration is often found to be deregulated in cancer (Chambers et al., 2002), this observation may be important to help explain how loss of CIC assists in ODG formation, although further studies specifically designed to measure migration must be conducted to confirm these results.

4.5 Conclusion

The above data have shown that genetic ablation of CIC *in vitro* results in an increased cell number, viability, and sphere volume when compared to controls. *In vivo*, a transient transfection of CIC shRNA shows an increase in proliferation in both the VZ and IZ 48 hours post-electroporation. Together, these data indicate that CIC plays a role in repressing proliferation and cell growth in murine brain development, similar to its role in *Drosophila*. Western blot analysis of markers of cell fate found that CIC knockout leads to a decreased expression of Tuj1, an early neuronal marker, and PDGFRa, an early oligodendrocyte marker, in cells grown under normal growth conditions. As well, a transient knockdown of CIC *in vivo* showed an increase in glioblasts in the IZ of the murine brain. CIC shRNA electroporation

studies did not show a difference in total number of neurons when compared to controls, however these cells were found to be mislocalized within the forebrain. Discrepancies in the *in vivo* and *in vitro* results may be explained by the differences in the remaining CIC expression *in vivo* compared to *in vitro*. It is possible that the transient knockdown of CIC *in vivo* is not enough to effect cell fate specification of all cell types in this system, and thus we may see results *in vitro* with a complete knockout of CIC that are not possible with the *in vivo* model system used in the above experiments. Future studies can be completed using the CIC-CKO mice in order to understand the role of CIC in determining cell fate. Finally, I found that CIC shRNA electroporation *in vivo* leads to significant abnormal cellular localization four days post-electroporation when compared to controls. Taken together, these findings allow us to make a general conclusion, which implicates CIC as playing an important role in murine brain development, as well as ODG formation.

4.6 Figures and figure legends.

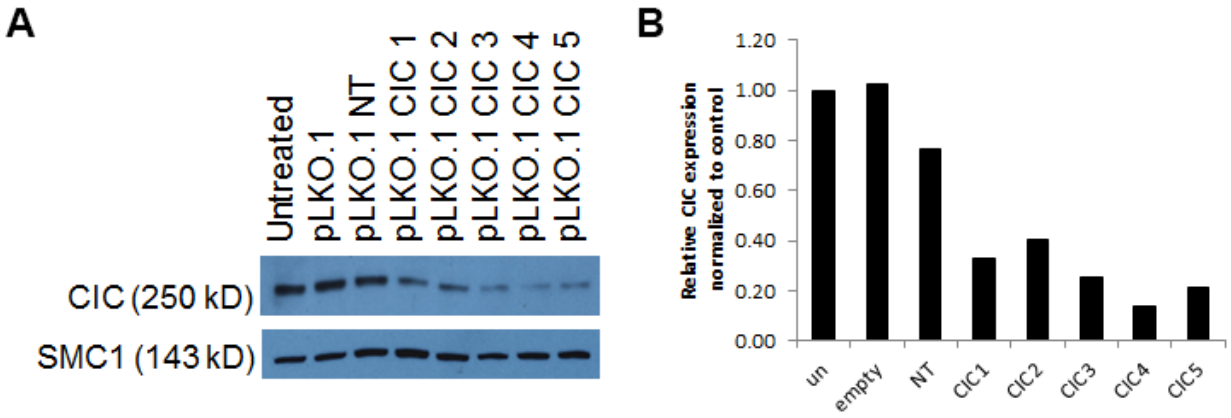

Figure 4.1. CIC shRNA knockdown in p53 -/- mouse neural stem cells (MNSC).

A,B. Western blot analysis of CIC expression after preliminary transfection in p53 null MNSC with five CIC pLKOs targeting different regions of the gene, including Exon 4 (CIC 1), Exon 9 (CIC 2), Exon 17 (CIC 3), Exon 5 (CIC 4), and the 3' UTR (CIC 5). Expression of CIC is reduced with transfection of each CIC shRNA when compared to untreated, empty vector (pLKO.1), and non-targeting controls (pLKO.1 NT) (A, n=1). Expression was normalized to the loading control, and then to the untreated control condition (B, n=1). The shRNA CIC 4 was selected for use in further experiments. (Experiment performed by Dr. Samuel Lawn, University of Calgary).

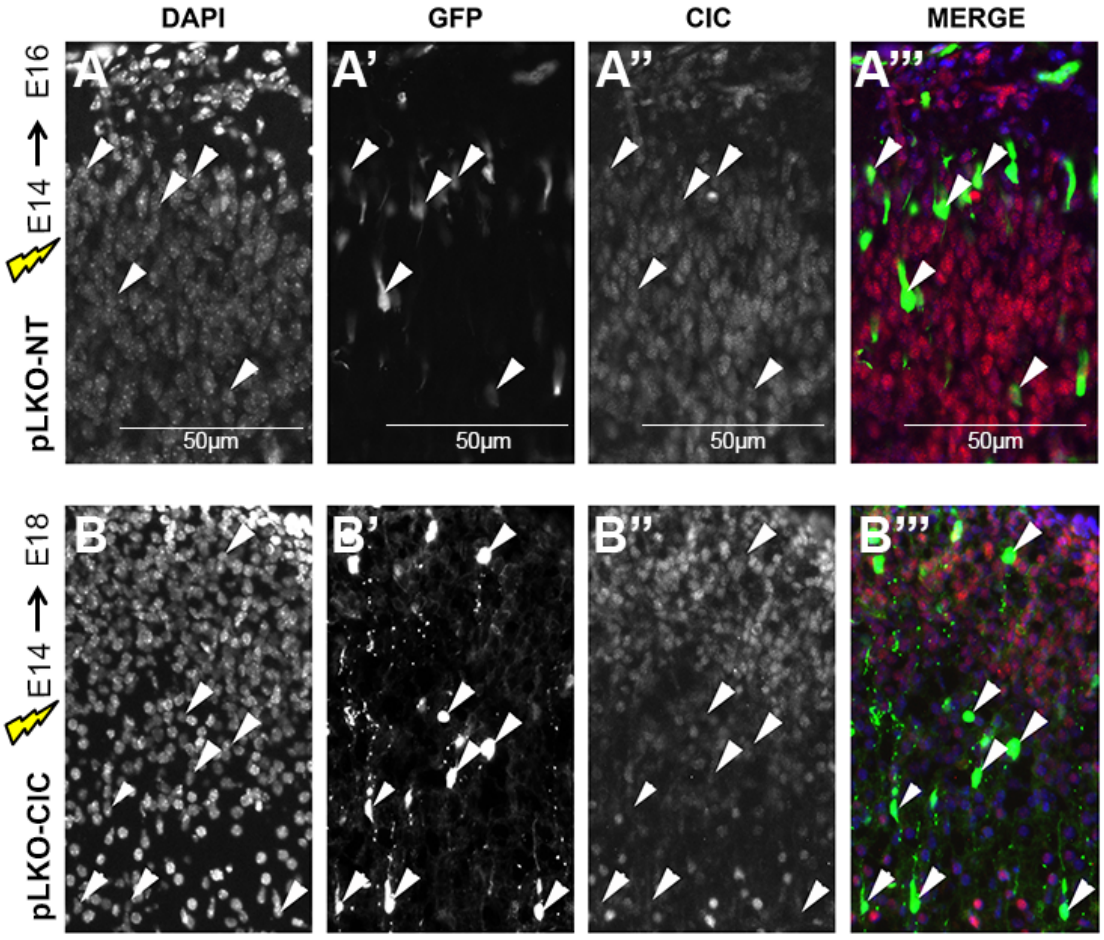
DAPI
GFP
CIC
MERGE
A
A'
A''
A'''
E16
E14
pLKO-NT
50µm
B
B'
B''
B'''
E18
E14
pLKO-CIC
50µm

C

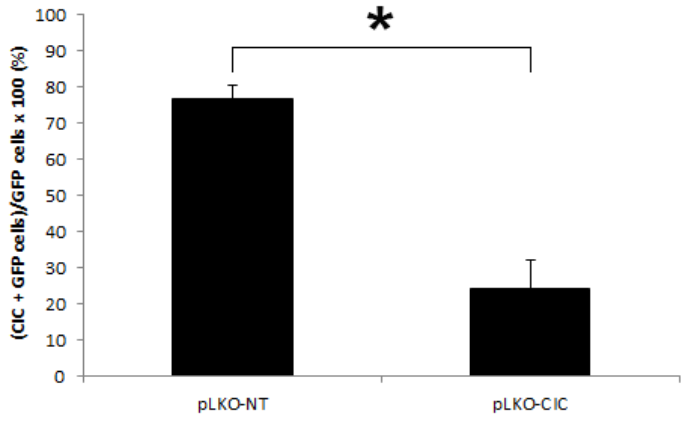
*
(CIC + GFP cells)/GFP cells x 100 (%)
100
90
80
70
60
50
40
30
20
10
0
pLKO-NT
pLKO-CIC

Figure 4.2. CIC shRNA knockdown validation *in vivo* using *in utero* electroporation.

A-C. *In utero* electroporations were conducted at embryonic day 14 and allowed to develop until embryonic day 18. Mice were electroporated with either non-targeting (NT) or CIC shRNA, and co-electroporated with pCIG2 plasmid containing enhanced green fluorescent protein (eGFP) to label and track electroporated cells. Tissues were harvested at E18, and co-immunofluorescence staining was performed on NT (A-A'') and CIC (B-B'') shRNA samples using GFP (to indicate NT or CIC shRNA electroporated cells) and CIC antibodies. Arrows indicate GFP-labelled cells that are CIC positive or negative. Quantification of the percentage of double-labeled cells was conducted to determine the extent of CIC knockdown (GFP^+ CIC^+ cells/GFP^+ cells; C, n=2, p=0.014). *$p<0.05$.

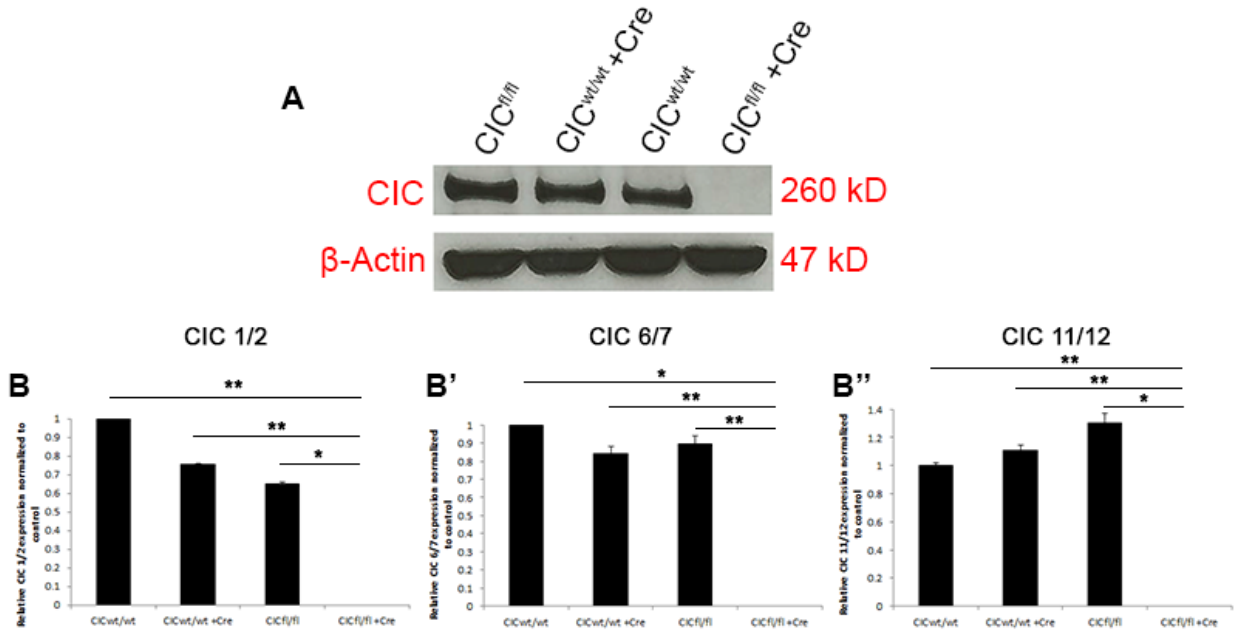

Figure 4.3. Validation of CIC inactivation in CIC knockout cells.

A,B. Expression analysis was performed on cell lines created from CIC-CKO mice. Cells are cultured from mice with a $CIC^{wt/wt}$ background and a $CIC^{fl/fl}$ background and nucleofected using a piggyBAC transposon carrying either Cre-IRES-GFP (+Cre-GFP) or GFP alone (+GFP). Of the resulting cell lines, $CIC^{wt/wt}$, $CIC^{wt/wt}$ +Cre, and $CIC^{fl/fl}$ are all predicted to be functionally wild-type and serve as controls, and $CIC^{fl/fl}$ +Cre, is CIC null. CIC expression was found to be lost at both the protein level, using western blot analysis (A) and at the RNA level, using qRT-PCR (B-B'', n=3). qRT-PCR was performed with primers that span three different exons of the gene, including Exon 1-2 (B), 6-7 (B'), and 11-12 (B''). *$p<0.05$, **$p<0.01$.

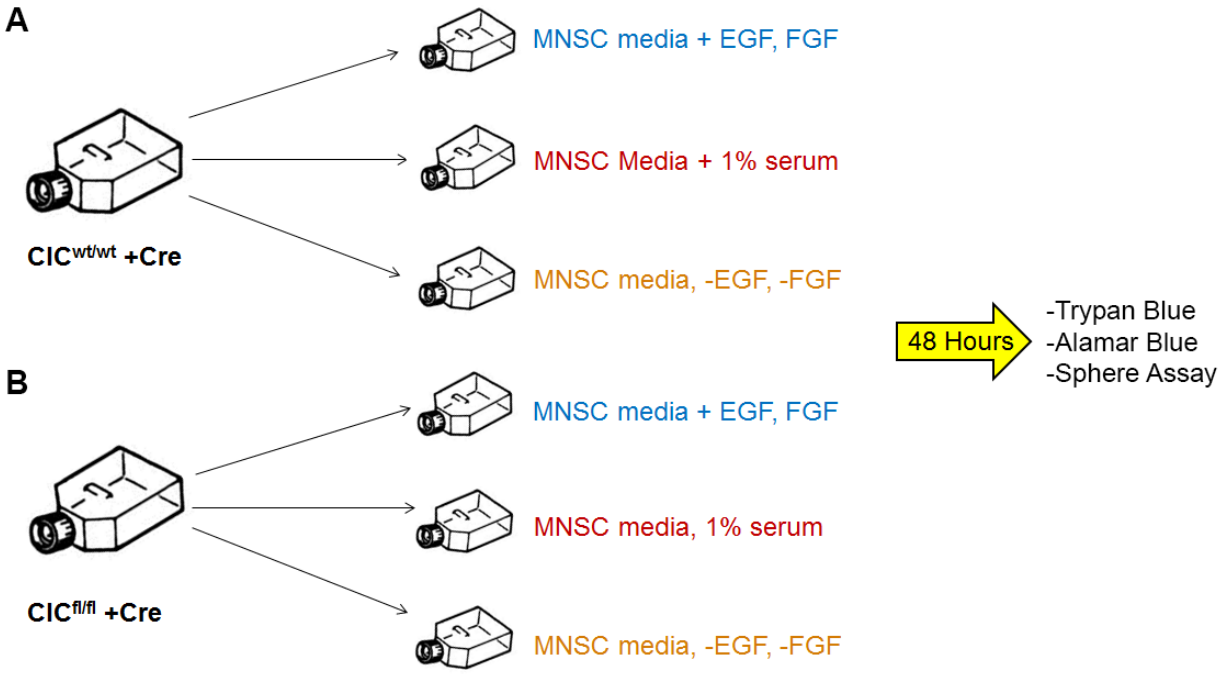

Figure 4.4. Schematic of *in vitro* CIC-KO cell line experiments.

$CIC^{wt/wt}$ +Cre cells (A) and $CIC^{fl/fl}$ +Cre cells (B) were grown for 48 hours under three conditions: 1) normal mouse neural stem cell (MNSC) media with added growth factors (EGF, FGF, and heparin), 2) MNSC media without added growth factors (EGF, FGF, and heparin), but with added 1% serum, and 3) MNSC media without added EGF, FGF, heparin, or serum. Cells were plated at $1.0x10^6$ cells per flask, and allowed to grow in culture for 48 hours after which they were analyzed using measures of cell number (Trypan Blue). To measure viability, cells were plated in at 5000 cells/well, and allowed to grow for 48 hours, after which they were analyzed using Alamar Blue. Sphere volume was measured using a Sphere Assay, in which the cells were plated at 1000 cells/well and allowed to grow in culture for 48 hours.

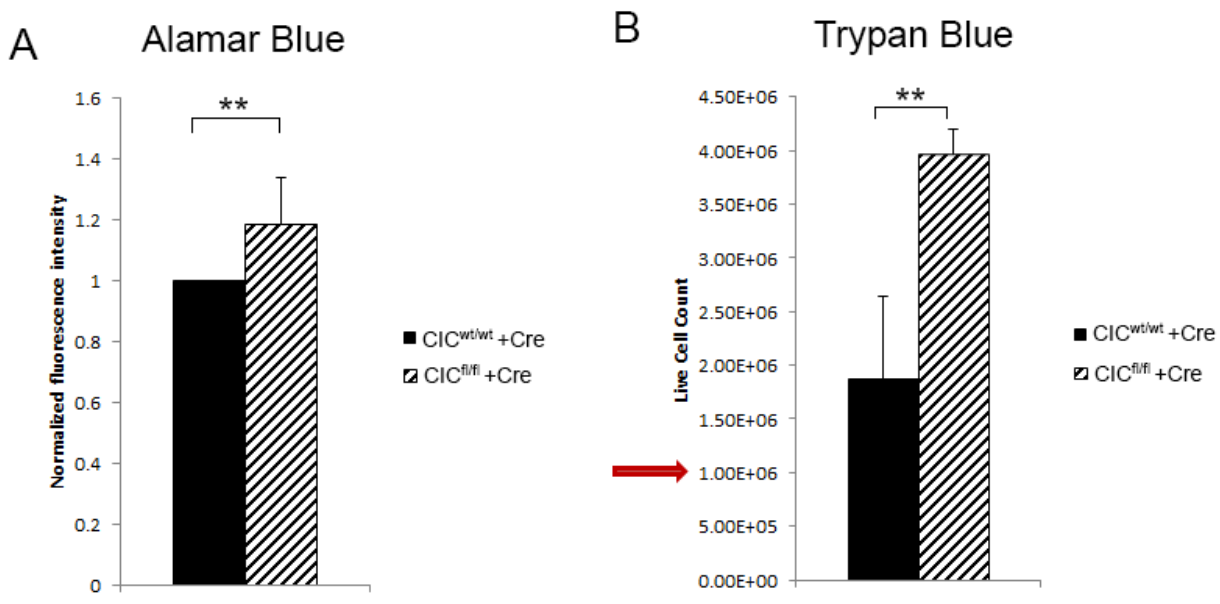

Figure 4.5. Cell viability and number measurements for CIC knockout cells grown in normal mouse neural stem cell (MSNC) proliferation media.

A,B. $CIC^{wt/wt}$ +Cre and $CIC^{fl/fl}$ +Cre cells were plated at 2000 cells/well (Alamar Blue) or $1.0x10^6$ cells per flask (Trypan Blue) and grown for 48 hours in normal MNSC media with added growth factors (EGF, FGF, and heparin). Alamar Blue measurements of cell viability, as indicated by a ability to reduce assay substrate, (A) showed a significant increase in viability in the CIC null, $CIC^{fl/fl}$ +Cre cells when compared to the control $CIC^{wt/wt}$ +Cre cells (A, n=3, p=0.00612). Trypan Blue measurements of live cell number (B) showed a significant increase in cell number in the $CIC^{fl/fl}$ +Cre cells after 48 hours when compared to the control $CIC^{wt/wt}$ +Cre cells (B, n=3, p=0.00165). **p<0.01.

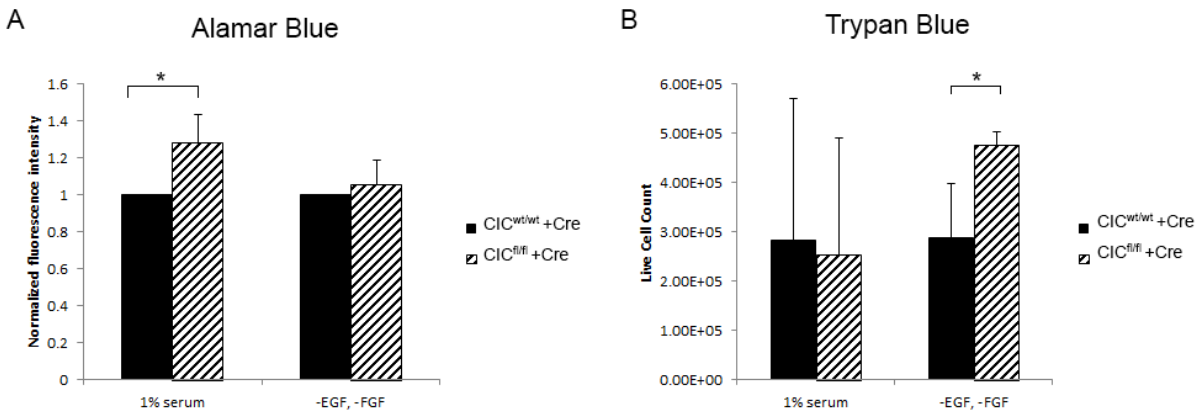

Figure 4.6. Cell viability and number measurements for CIC knockout cells grown in differentiation media or without added growth factors.

A,B. $CIC^{wt/wt}$ +Cre and $CIC^{fl/fl}$ +Cre cells were plated at 2000 cells/well (Alamar Blue), or $1.0x10^6$ cells per flask (Trypan Blue) and grown for 48 hours under two conditions: in normal mouse neural stem cell (MNSC) differentiation media (with 1% serum), and in normal MNSC media without added growth factors (w/o EGF, FGF). Alamar Blue measurements of cell viability (A) showed a significant increase in viability in the CIC null, $CIC^{fl/fl}$ +Cre cells under the 1% serum condition when compared to the control $CIC^{wt/wt}$ +Cre cells (A, n=3, p=0.050). No significant change in viability was found in $CIC^{fl/fl}$ +Cre cells in the no added growth factor condition when compared to controls (A, n=3). Trypan Blue measurements of live cell number (B) showed a significant increase in cell number in the $CIC^{fl/fl}$ +Cre cells grown in the no added growth factor condition when compared to $CIC^{wt/wt}$ +Cre cells (B, n=3, p=0.0139). No significant change in cell number was found in $CIC^{fl/fl}$ +Cre cells grown under the 1% serum condition when compared to controls (B, n=3). *$p<0.05$.

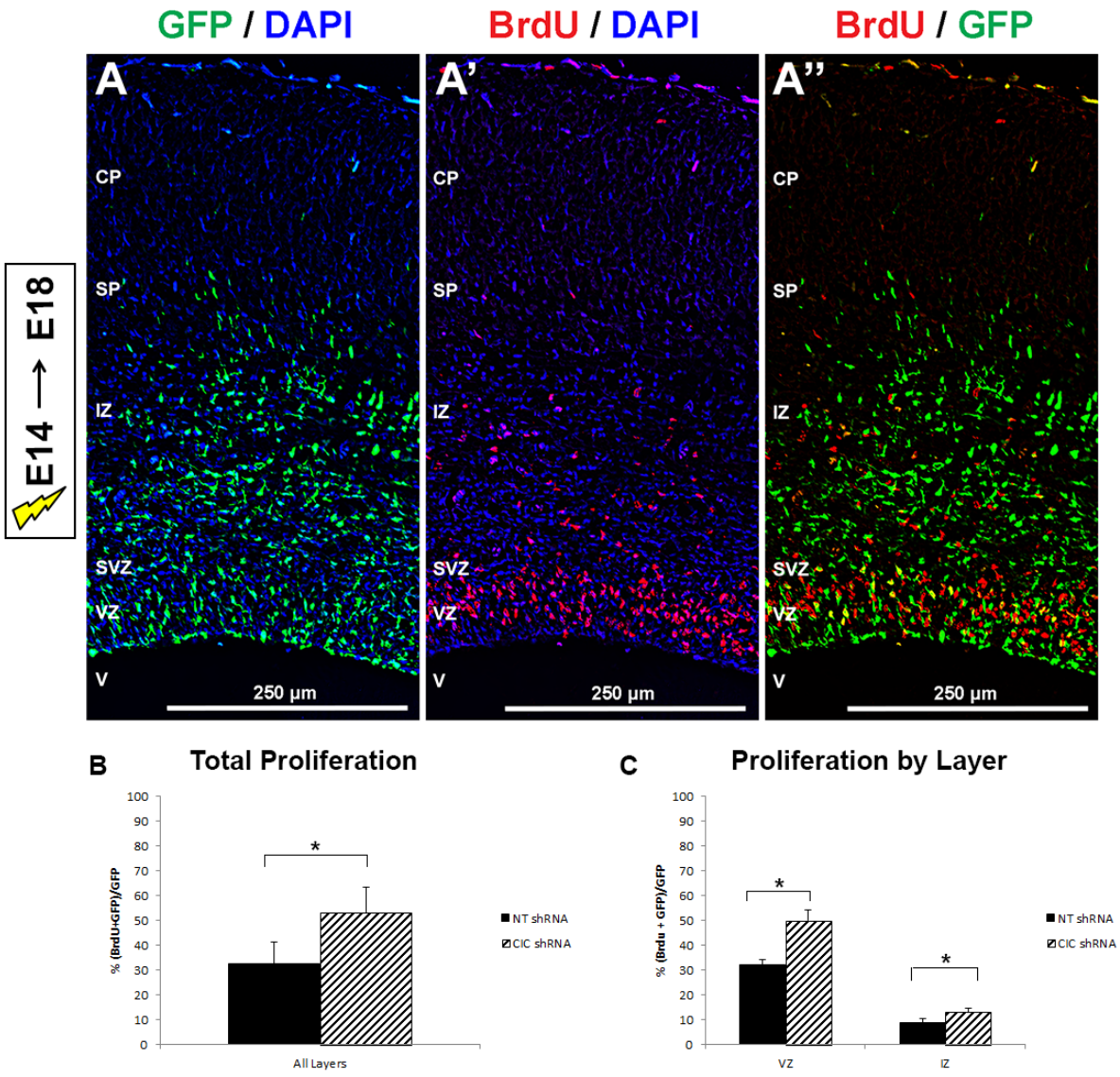
GFP / DAPI
BrdU / DAPI
BrdU / GFP
E14 → E18
A
A'
A''
CP
SP
IZ
SVZ
VZ
V
250 µm
B
Total Proliferation
% (BrdU+GFP)/GFP
All Layers
NT shRNA
CIC shRNA
C
Proliferation by Layer
% (Brdu + GFP)/GFP
VZ
IZ

Figure 4.7. BrdU incorporation analysis *in vivo* 48 hours post electroporation.

A-C. *In utero* electroporations were conducted at embryonic day 14 and allowed to develop until embryonic day 16. Mice were electroporated with either non-targeting (NT) or CIC shRNA, and co-electroporated with pCIG2 plasmid containing enhanced green fluorescent protein (eGFP) to label and track electroporated cells. BrdU labeling was performed 30 minutes prior to sacrifice. Embryos were harvested at E16, and co-immunofluorescence staining was performed on NT and CIC shRNA samples using GFP (to indicate NT or CIC shRNA electroporated cells) and BrdU antibodies. Representative image of BrdU (A, red) and GFP (A', green) immunofluorescence staining. Co-expression is shown in yellow (A''). Quantification of the total percentage of double-labeled cells (GFP+ BrdU+ cells/GFP+ cells) showed an increased proliferation in CIC shRNA samples when compared to control NT shRNA (B, n=4, p=0.0368). Quantification of the percentage of double-labeled cells (GFP+ BrdU+ cells/GFP+ cells) per cortical layer showed an increased proliferation in both the ventricular zone (C, n=3, p=0.00359) and the intermediate zone (C, n=3, p=0.0178). *$p<0.05$. Cortical plate (CP), subplate (SP), intermediate zone (IZ), subventricular zone (SVZ), ventricular zone (VZ), ventricle (V).

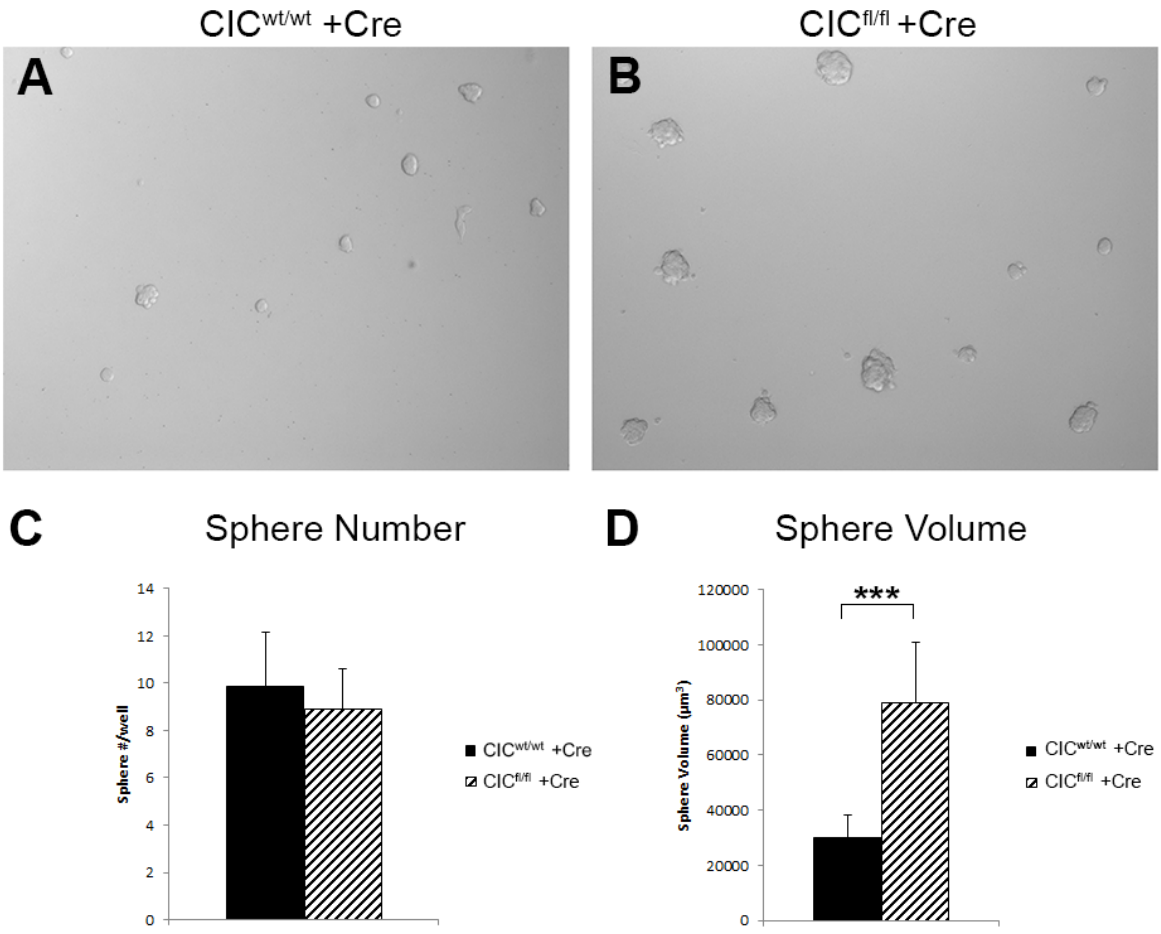
ClC$^{wt/wt}$ +Cre
ClC$^{fl/fl}$ +Cre
A
B
C
Sphere Number
Sphere #/well
14
12
10
8
6
4
2
0
ClC$^{wt/wt}$ +Cre
ClC$^{fl/fl}$ +Cre
D
Sphere Volume
Sphere Volume (μm^3)
120000
100000
80000
60000
40000
20000
0
***
ClC$^{wt/wt}$ +Cre
ClC$^{fl/fl}$ +Cre

Figure 4.8. Sphere assay analysis of CIC knockout cells grown in normal MNSC proliferation media.

A-D. $CIC^{wt/wt}$ +Cre and $CIC^{fl/fl}$ +Cre cells were plated at 1000 cells/well in normal MNSC media with added growth factors (EGF, FGF, and heparin) and grown for 48 hours. Bright field images (10X magnification) of $CIC^{wt/wt}$ +Cre spheres/clusters (A) and $CIC^{fl/fl}$ +Cre spheres/clusters (B) after 48 hours of growth. Measurement of the number of spheres/clusters per well after 48 hours did not show a significant difference in number between the $CIC^{wt/wt}$ +Cre and $CIC^{fl/fl}$ +Cre cell lines (C, n=3). Measurement of average sphere/cluster volume after 48 hours showed a significant increase in the volume of $CIC^{fl/fl}$ +Cre spheres/clusters when compared to the $CIC^{wt/wt}$ +Cre spheres/clusters (D, n=3, $p=2.01x10^{-8}$). ***$p<1.0x10^{-6}$.

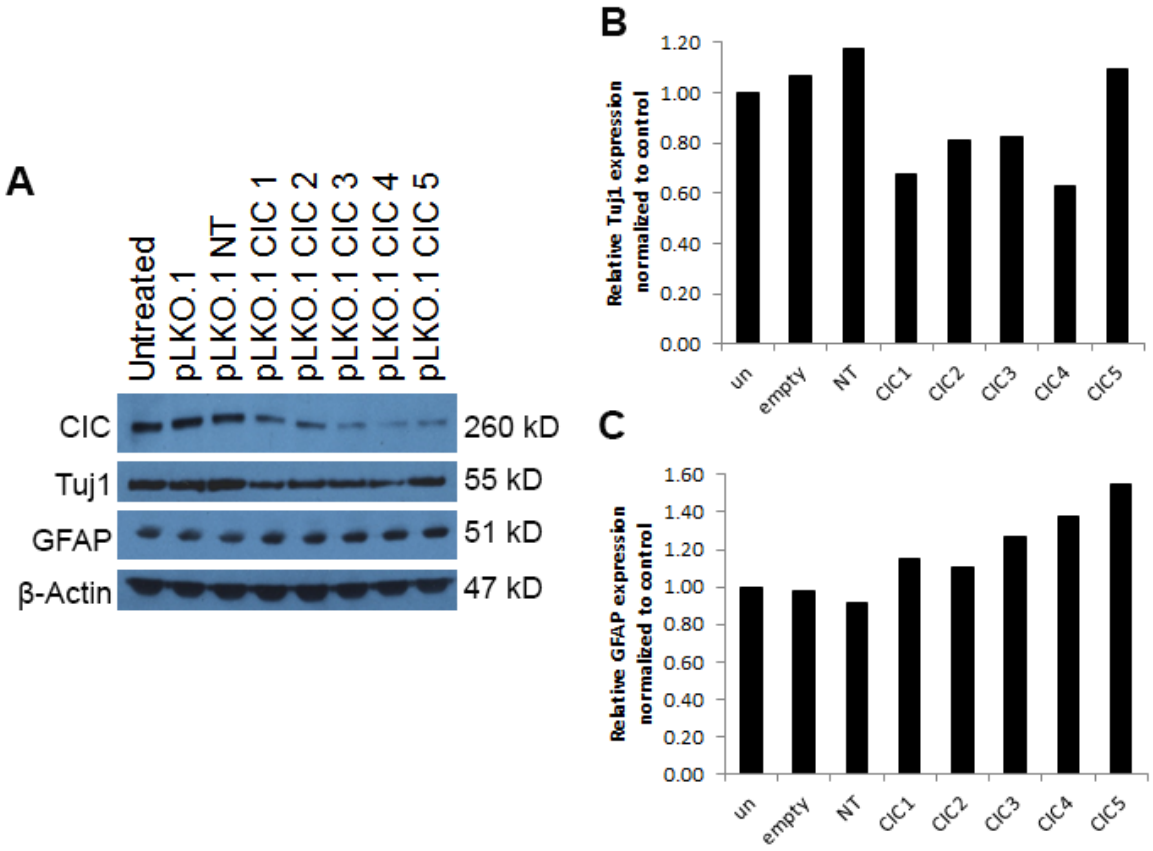

Figure 4.9. Preliminary analysis of cell fate in cultured p53 -/- MNSC transfected with CIC shRNA.

A-C. Western blot analysis of cell fate markers after preliminary transfection in p53 null MNSC with five CIC pLKO targeting different regions of the gene, including Exon 4 (CIC 1), Exon 9 (CIC 2), Exon 17 (CIC 3), Exon 5 (CIC 4), and the 3' UTR (CIC 5). Expression of Tuj1, an early neuronal marker, was decreased in p53 null cells transfected with CIC shRNA when compared to controls (A, B, n=1). Expression of GFAP, an astrocyte marker, was increased in p53 null cells transfected with CIC shRNA when compared to controls (A, C, n=1). Expression was normalized to the loading control (β-Actin) and then to the untreated control condition. (Experiment performed by Dr. Samuel Lawn, University of Calgary).

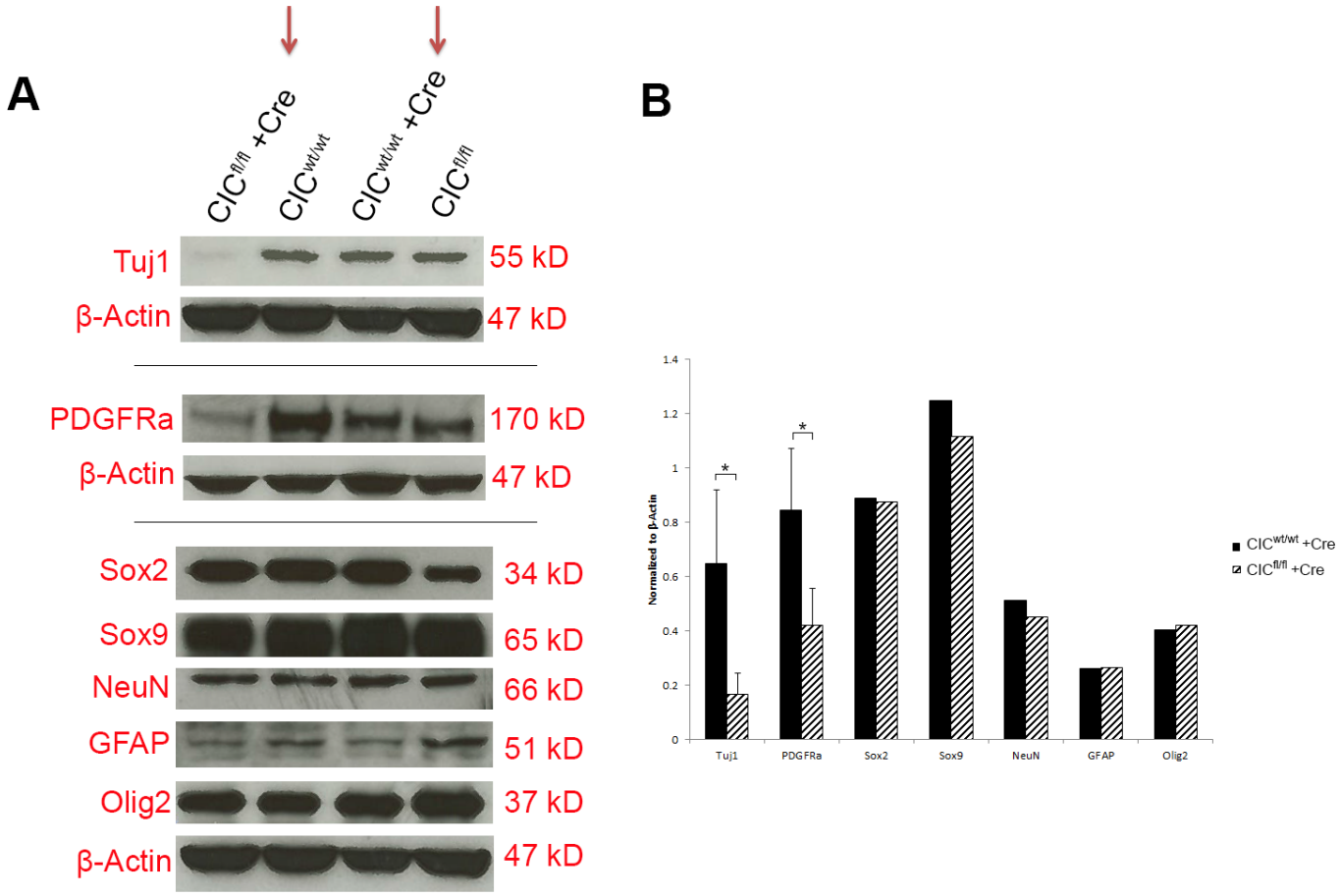
A
B
CIC fl/fl +Cre
CIC wt/wt
CIC wt/wt +Cre
CIC fl/fl
Tuj1
55 kD
β-Actin
47 kD
PDGFRa
170 kD
β-Actin
47 kD
Sox2
34 kD
Sox9
65 kD
NeuN
66 kD
GFAP
51 kD
Olig2
37 kD
β-Actin
47 kD
Normalized to β-Actin
1.4
1.2
1
0.8
0.6
0.4
0.2
0
Tuj1
PDGFRa
Sox2
Sox9
NeuN
GFAP
Olig2
CIC wt/wt +Cre
CIC fl/fl +Cre

Figure 4.10. Effect of CIC loss on cell type specification.

A, B. Western blot was performed on $CIC^{wt/wt}$ +Cre and $CIC^{fl/fl}$ +Cre cells grown in normal mouse neural stem cell media with added growth factors (EGF, FGF, and heparin). Antibodies for markers of cell fate, including Tuj1 (an early neuronal marker), PDGFRa (an early oligodendrocyte marker), Sox2 (a stem/progenitor marker), Sox9 (a stem/glioblast marker), NeuN (a mature neuronal marker), GFAP (an astrocyte marker), and Olig2 (an oligodendrocyte maker) were analyzed. Expression of Tuj1 in $CIC^{fl/fl}$ +Cre cells was found to be decreased when compared to control $CIC^{wt/wt}$ +Cre cells (B; n=3, p=0.0413). PDGFRa expression was also decreased in $CIC^{fl/fl}$ +Cre cells (B; n=3, p=0.0341). Expression levels of the other five markers (Sox2, Sox9, NeuN, GFAP, and Olig2) did not significantly change between $CIC^{fl/fl}$ +Cre and $CIC^{wt/wt}$ +Cre cell lines (B). *$p<0.05$.

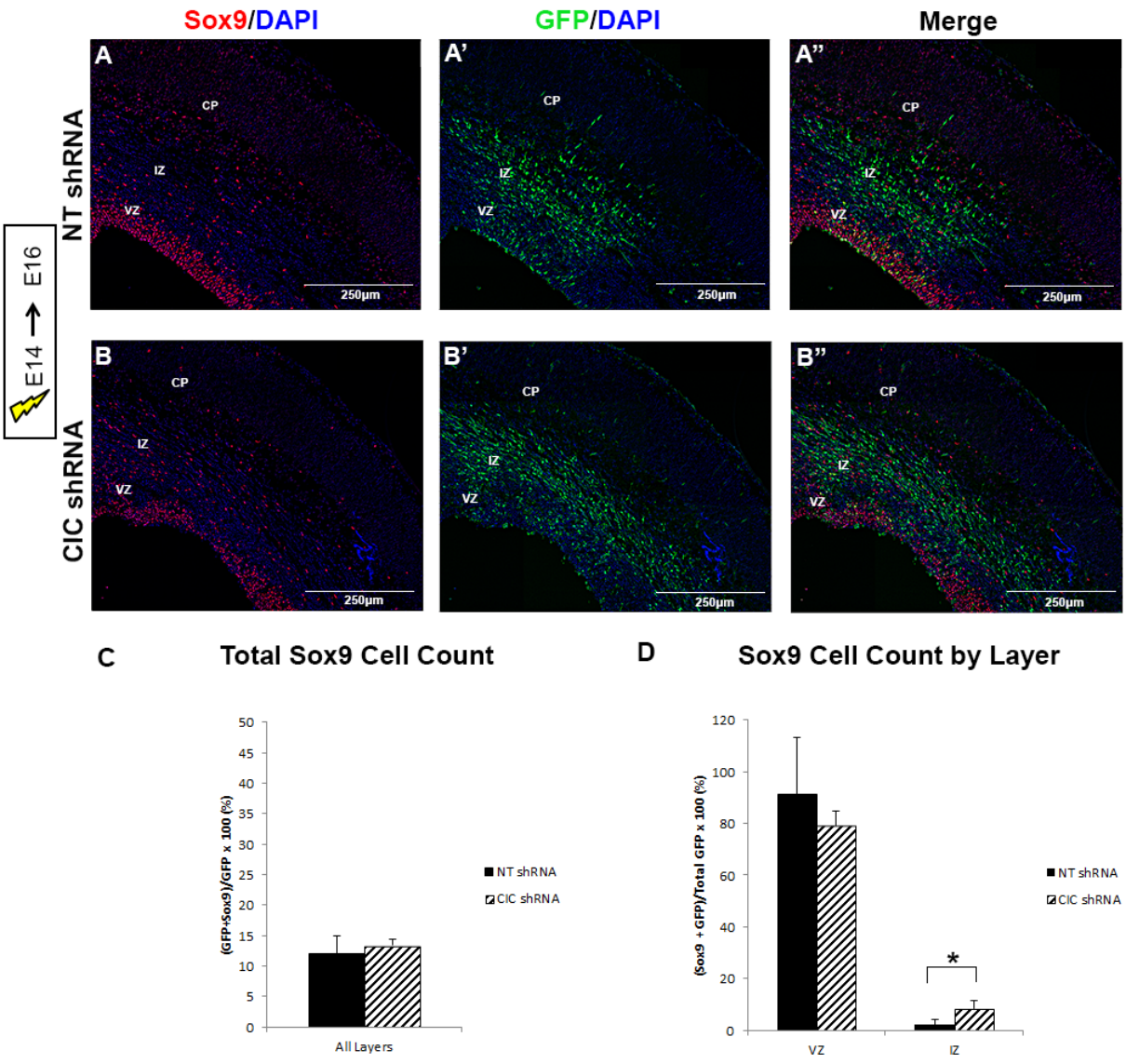
Sox9/DAPI
GFP/DAPI
Merge
NT shRNA
CIC shRNA
E14 → E16
A
A'
A''
B
B'
B''
CP
IZ
VZ
250μm
C
Total Sox9 Cell Count
(GFP+Sox9)/GFP x 100 (%)
All Layers
NT shRNA
CIC shRNA
D
Sox9 Cell Count by Layer
(Sox9 +GFP)/Total GFP x 100 (%)
VZ
IZ
*

Figure 4.11. CIC knockdown in progenitors leads to a change in glial cell fate.

A-D. *In utero* electroporations were conducted at embryonic day 14 and allowed to develop until embryonic day 16. Mice were electroporated with either non-targeting (NT) or CIC shRNA, and co-electroporated with pCIG2 plasmid containing enhanced green fluorescent protein (eGFP) to label and track electroporated cells. Embryos were harvested at E16, and co-immunofluorescence staining was performed on NT and CIC shRNA samples using GFP (to indicate NT or CIC shRNA electroporated cells) and Sox9 (a stem and glioblast marker) antibodies. Representative images of NT shRNA (A, A', A'') and CIC shRNA (B, B', B'') electroporated mice co-immunostained for GFP (A, B, green) and Sox9 (A', B', red). Co-expression is shown in yellow (A'', B''). Quantification of the total percentage of double-labeled cells (GFP^+ $Sox9^+$ cells/GFP^+ cells) did not show an increase in glial cell number in CIC shRNA samples when compared to control NT shRNA (C, n=3). Quantification of the percentage of double-labeled cells (GFP^+ $Sox9^+$ cells/GFP^+ cells) per cortical layer did not show an increase in glial cell number in the ventricular zone (D, n=3), did show an increase in glial cell number in the intermediate zone of CIC shRNA samples (D, n=3, p=0.0375) when compared to NT controls. *$p<0.05$. Cortical plate (CP), intermediate zone (IZ), ventricular zone (VZ).

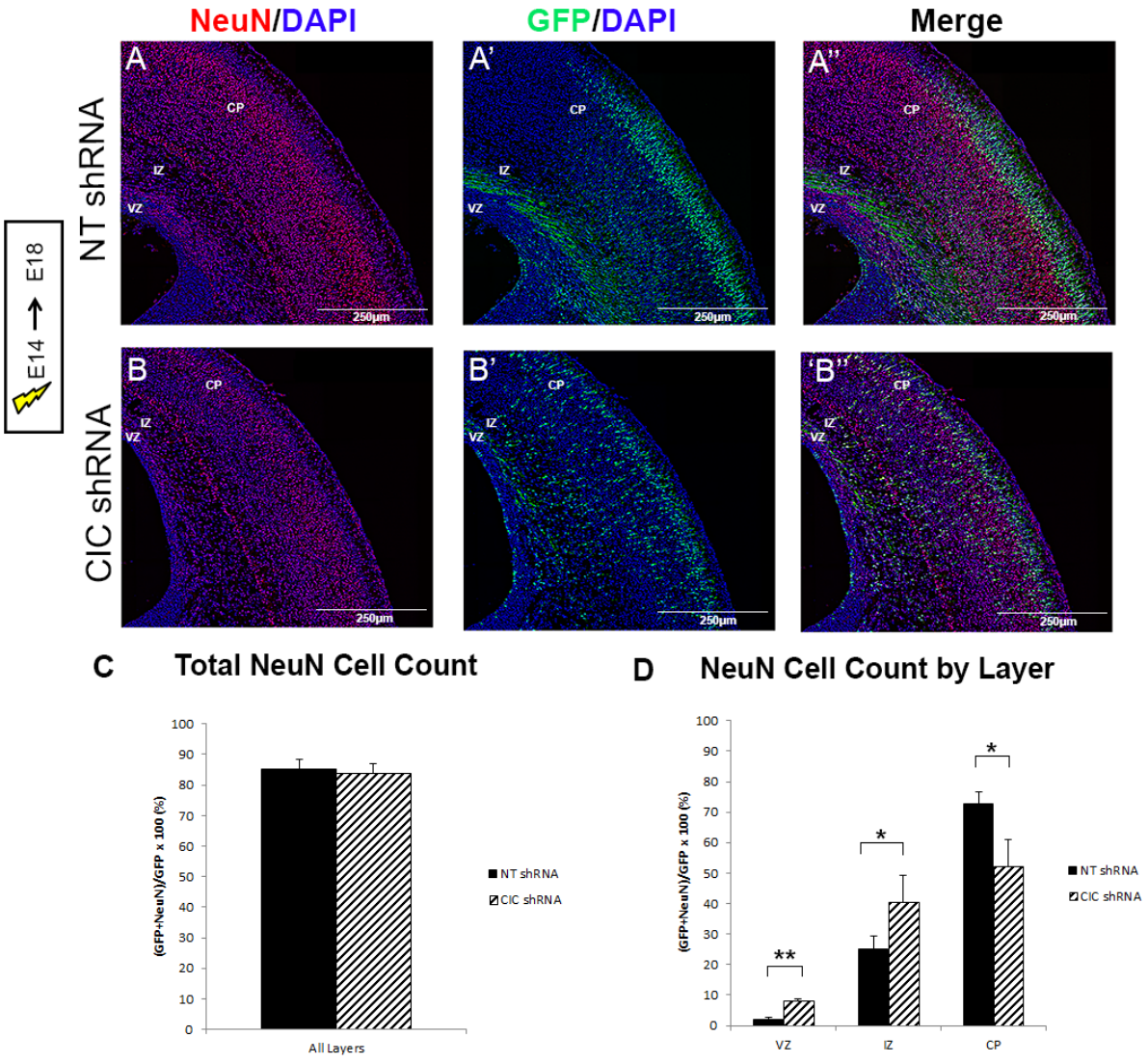
NeuN/DAPI
GFP/DAPI
Merge
E14 → E18
NT shRNA
CIC shRNA
A
A'
A''
B
B'
B''
CP
IZ
VZ
250μm
C
Total NeuN Cell Count
(GFP+NeuN)/GFP x 100 (%)
All Layers
NT shRNA
CIC shRNA
D
NeuN Cell Count by Layer
VZ
IZ
CP
*
**

Figure 4.12. CIC knockdown in progenitors leads to a change in neuronal cell localization. A-D. *In utero* electroporations were conducted at embryonic day 14 and allowed to develop until embryonic day 18. Mice were electroporated with either non-targeting (NT) or CIC shRNA, and co-electroporated with pCIG2 plasmid containing enhanced green fluorescent protein (eGFP) to label and track electroporated cells. Embryos were harvested at E18, and co-immunofluorescence staining was performed on NT and CIC shRNA samples using GFP (to indicate NT or CIC shRNA electroporated cells) and NeuN (a mature neuronal marker) antibodies. Representative images of NT shRNA (A, A', A'') and CIC shRNA (B, B', B'') electroporated mice co-immunostained for GFP (A, B, green) and NeuN (A', B', red). Co-expression is shown in yellow (A'', B''). Quantification of the total percentage of double-labeled cells (GFP^+ $NeuN^+$ cells/GFP^+ cells) did not show an increase in neuronal cell number in CIC shRNA samples when compared to control NT shRNA (C, n=3). Quantification of the percentage of double-labeled cells (GFP^+ $NeuN^+$ cells/GFP^+ cells) per cortical layer showed an increase in neuronal cell number in both the ventricular zone (D, n=3, $p=1.57x10^{-5}$) and the intermediate zone (D, n=3, p=0.0364), and a decreased in neuronal cell number in the cortical plate (D, n=3, p=0.0117) in CIC shRNA samples when compared to NT shRNA controls. *p<0.05, **p<0.01 Cortical plate (CP), intermediate zone (IZ), ventricular zone (VZ).

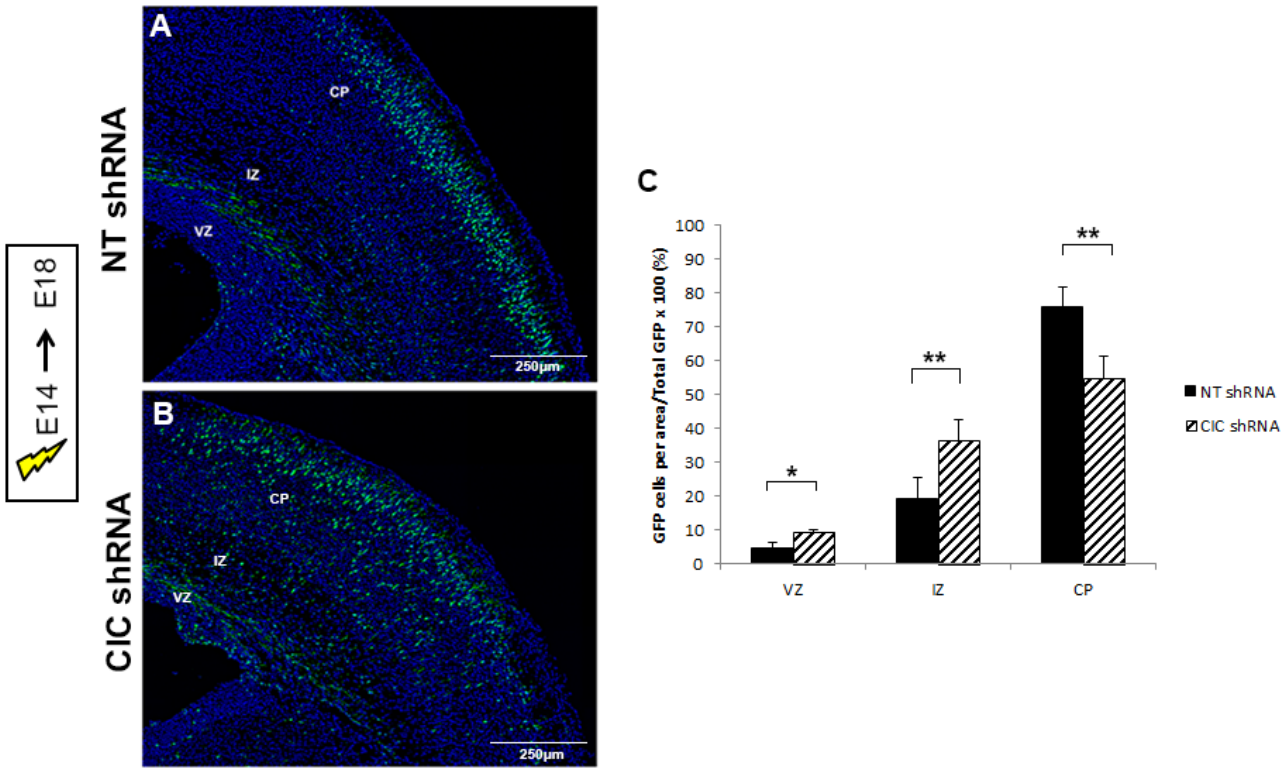
E14 → E18
NT shRNA
CIC shRNA
A
B
CP
IZ
VZ
250μm
C
GFP cells per area/Total GFP x 100 (%)
100
90
80
70
60
50
40
30
20
10
0
*
**
**
VZ
IZ
CP
NT shRNA
CIC shRNA

Figure 4.13. CIC knockdown in progenitors results in cellular mislocalization.

A-C. *In utero* electroporations were conducted at embryonic day 14 and allowed to develop until embryonic day 18. Mice were electroporated with either non-targeting (NT) or CIC shRNA, and co-electroporated with pCIG2 plasmid containing enhanced green fluorescent protein (eGFP) to label and track electroporated cells. Embryos were harvested at E18, and immunofluorescence staining was performed on NT and CIC shRNA samples using GFP (to indicate NT or CIC shRNA electroporated cells). Representative images of NT shRNA (A) and CIC shRNA (B) electroporated mice co-immunostained for GFP (A, B, green) and DAPI (A, B, blue). Quantification of the percentage of GFP-labeled cells (GFP+ cells per area/total GFP+ cells) per cortical layer showed an increase in GFP-labeled cells in both the ventricular zone (C, n=3, $p=0.040$) and the intermediate zone (D, n=3, $p=4.60x10^{-4}$), and a decreased in GFP-labeled cells in the cortical plate (D, n=3, $p=0.0028$) in CIC shRNA samples when compared to NT shRNA controls. *$p<0.05$, **$p<0.01$ Cortical plate (CP), intermediate zone (IZ), ventricular zone (VZ).

CHAPTER 5: DISCUSSION

5.1 Summary of Findings

Although ODG are generally responsive to treatment, the majority of these tumors will eventually recur and lead to patient death (Peterson and Cairncross, 1996). The discovery of novel mutations using next generation sequencing has opened avenues of research that may be exploited in the future for patient care. One newly identified ODG-associated gene is CIC, which encodes for a protein known to have transcriptional repressor functions that are relieved downstream of active RTK signaling. To gain insight into the potential role of CIC in ODG, I studied the expression and function of CIC in the murine cerebral cortex. I found that although CIC was widely expressed at the protein and RNA levels in the cortex, its subcellular distribution changed over time (increasingly nuclear over time) and there are differences with in nuclear versus cytoplasmic localization among different cell types (weak or absent nuclear positivity in stem/progenitor cells and oligodendrocytes, and strong nuclear positivity in neurons and astrocytes) suggests that CIC might influence the proliferation or developmental potential of cells. The nuclear versus cytoplasmic differences among cell types and stages raised the possibility that derepression of CIC in stem or progenitor cells may be permissive for proliferation of progenitors, or differentiation into oligodendrocytes. In functional studies, I then found that CIC knockdown or loss increased stem/progenitor cell proliferation but had a variable effect on cell type specification depending on the system used for study (*in vitro* knockout versus *in vivo* transient knockdown). These results, and their potential implications for ODG tumorigenesis, are discussed below.

5.2 CIC temporal-spatial expression in the cortex

In Chapter 3, I found that CIC was widely expressed at both the protein and RNA level in immature proliferative zones as well as mature tissue (Figures 3.2-3.4, 3.6-3.9). In the embryonic VZ, and adult SEZ and DG subgranular zone, CIC was weakly expressed, and when present was predominantly cytoplasmic (Figures 3.6, 3.7, 3.9, respectively). When cell-type specific staining was conducted, CIC was found to co-express with markers of progenitor cells (Sox2), but was predominantly cytoplasmic, at E15 (Figure 3.6). As cells matured, CIC became increasingly nuclear in localization both in neurons and in astrocytes. In the cortical plate and cortex, CIC expression was found in both the nucleus and cytoplasm of cells at E15, P0, and P7; however expression becomes increasingly nuclear between P0 and P7 (Figures 3.2-3.5). Co-expression of CIC with markers of neuronal (NeuN) and astrocyte (S100B) cell fates was found. In contrast, CIC was not co-expressed with markers of oligodendrocyte (Olig2) cell fate (Figure 3.10).

My data on CIC expression at E15, P0, P7, and adult is consistent with that reported in existing brain atlases and in the literature, which describe CIC to be expressed throughout the murine brain at similar ages. CIC was found to be present in the olfactory bulbs and the cerebellum of mice (Lee et al., 2002). This study however, did not look at the cerebral cortex, the region of the brain I am most interested in, as most ODGs arise in this area (Mork et al., 1985; Peterson and Cairncross, 1996). As well, the authors did not look at the time points in development I am interested in studying and did not remark on the subcellular distribution over developmental stages. My analyses of CIC expression in the brain are more detailed than those reported both with respect to the cell types expressing CIC and its subcellular distribution in cells, and thus add to the overall body of knowledge of CIC in the brain. Neurogenesis in mouse brain development extends from approximately E10 to E17, while gliogenesis begins around

E17. Astrocyte production peaks post-birth, and mature oligodendrocyte populations are found postnatally, around P7 (Miller and Gauthier, 2007). Throughout early development, progenitor cell populations are continually dividing asymmetrically in order to produce cells of the same potency, for self-renewal, or cells that may further differentiate into specialized cell types (Huttner and Kosodo, 2005). As CIC is present in the brain at these times, it may have the ability to influence progenitor proliferation and differentiation.

A study of murine brain development found that the behavior of multipotent cortical progenitors changes temporally *in vivo*, generating neurons first, then glia (McCarthy et al., 2001). This timing is integral to normal development, as it allows neuronal circuitry to be established prior to positioning of glial cells within the circuit. The switch from neurogenesis to gliogenesis is a complicated interplay of both extrinsic and intrinsic factors is required to promote neurogenesis while supressing gliogenesis, and vice versa (Sauvageot and Stiles, 2002; Shen et al., 2006). Among the factors controlling the switch, environmental signals resulting from RTK-pathway activation can act to regulate the competence of precursor cells by promoting neurogenesis and blocking astrocyte formation during this period (Barnabé-Heider et al., 2005; Liu et al., 2006; Ménard et al., 2002). CIC, as a component downstream of MAPK signalling, thus may be a key intermediary regulating this switch.

In my work, CIC was found to be predominantly expressed in the cytoplasm of cells stained for progenitor markers (Sox2), although some nuclear expression was recognized (Figure 3.6). As progenitors are cells which have yet to be differentiated into mature cell types, the presence of CIC in these cells suggests that it may be influencing cell fate or proliferation. CIC is expressed at a time and place in which it has the ability to do so, although whether or not it does indeed function in this role remains to be studied. Over the developmental time course

experiments, I noticed that CIC expression moved from more cytoplasmic at earlier stages, to increasingly nuclear at later stages of maturation (Figures 3.2-3.5).

Previous literature in *Drosophila* has shown that CIC functions as a repressor of genes downstream of RTK pathways (Ajuria et al., 2011; Astigarraga et al., 2007), and that it must bind in the nucleus of cells in order to function. Although I have shown that CIC moves to the nucleus of cells as they go from progenitor state to more mature cell types (Figure 3.6), further experiments would be necessary to confirm that the gene is indeed active in the nucleus during murine development. My data shows that CIC also co-expresses in the nucleus of more mature cell types, including neurons (NeuN) and astrocytes (S100B) (Figure 3.10). However, CIC did not predominantly co-express in the nucleus of cells staining for Olig2, a marker of oligodendrocyte cells (Figure 3.10). My findings are consistent with a model in which CIC may function as a repressor of oligodendrocyte cell fate in cells that are destined to be neurons or astrocytes (hence its co-expression with NeuN and S100B). Conversely, CIC function would be de-repressed in cells destined to be oligodendrocytes, and the protein is shuttled out into the cytoplasm of these cells.

Since CIC expression changes over time as progenitors become more mature, and it is expressed in the nucleus of neurons and astrocytes, but not oligodendrocytes, it may be that CIC plays a role within the neurogenic to gliogenic switch. Specifically, CIC could be repressing oligodendrocyte production not only during neurogenesis, but also after the gliogenic switch, throughout the early astrocyte formation. CIC de-repression (whether by mutation or by increasing RAS/MAPK signalling in cells) might then be either permissive or instructive for oligodendrocyte specification or maturation during the later stages of gliogenesis.

5.3 Functional roles of CIC in the cortex

CIC was first discovered in *Drosophila*, and found to function largely as a repressor of cell growth, proliferation, and differentiation in this model (Atkey et al., 2006; Herranz et al., 2012; Krivy et al., 2013; Roch et al., 2002; Tseng et al., 2007). In *Drosophila*, repression of proliferation seems to be a general function of CIC in diverse developmental tissues. On the other hand, control over differentiation may be tissue specific; CIC represses differentiation of wing vein tissue in the developing wing pouch (Tseng et al., 2007), but does not affect cell fate in the eye disc (Roch et al., 2002). To date, little has been described in the literature about the role(s) of CIC in the mammalian brain. Although a CIC genetrap knockout mouse was created in one study, the effects of CIC loss on my organ of interest, the brain, were not reported (Lee et al., 2011). Functional studies looking at CIC in mouse models have focused on the role of CIC in spinocerebellar ataxin 1 (SCA1), a neurodegenerative disease which causes degeneration of white matter tracts. In the genetrap mouse, CIC loss caused lung alveolarization defects and postnatal death prior to weaning age, yet the effects on the brain, if any, were not discussed (Lee et al., 2011). Thus, my work adds new knowledge about the function of CIC in the mammalian brain.

In Chapter 4, I conducted LOF studies to begin to determine the role of CIC in murine brain development. Using two techniques, it was discovered that knocking down CIC results in an increase in cell number, viability, and sphere volume *in vitro* (Figures 4.5 and 4.8 respectively), and an increase in proliferation *in vivo* (Figure 4.7). CIC knockout cells grown in differentiation media (1% serum) were found to have increased cell viability compared to controls (Figure 4.6). As well, CIC-null cells grown in media that does not promote proliferation (without added EGF and FGF) were found to have an increased live cell count compared to CIC-

control cells (Figure 4.6). CIC loss decreased expression of markers of early neuronal (Tuj1) and oligodendrocytic (PDGFRa) markers *in vitro* (Figure 4.10). An increased expression of Sox9, a glioblast marker, was seen in vivo (Figure 4.11), however no change in expression of NeuN, a mature neuronal marker, was found (Figure 4.12). Finally, CIC shRNA electroporation produced a perturbation in localization when compared to controls, with more cells remaining in the ventricular and intermediate zones, and less reaching the cortical plate, suggesting a role for CIC in regulating migration (Figure 4.13).

5.3.1 CIC is a negative regulator of proliferation in neural stem/progenitor cells

In Chapter 4, I found that *in vitro*, CIC-null cells have an increased cell number, viability, and sphere volume compared to controls (Figures 4.5 and 4.8 respectively). Similar results were found *in vivo*, where CIC shRNA knockdown leads to an increased in proliferation via BrdU incorporation. Significantly more cells were found to be proliferating in both the ventricular zone and intermediate zone 48 hours post-electroporation (Figure 4.7). My data implies that CIC plays an important role in murine brain development by restricting cell growth and proliferation in progenitors. My findings are consistent with previous research in *Drosophila* wherein flies with loss of function mutations in eye disc cells have an increased representation of mutant clones over normal clones (Tseng et al., 2007). The mutant Capicua clones also show a higher proliferative rate and accelerated cell cycle (Tseng et al., 2007). More recently, CIC was found to interact with RBF1 in *Drosophila* eye development to restrict proliferation by promoting G1 cell cycle arrest in dividing precursors (Krivy et al., 2013). These studies confirm my results and open up a potential avenue of study in murine CIC function. As I did not analyze cell cycle kinetics in my system, in future studies it would be important to perform cell cycle analyses

using flow cytometry and other techniques such as FUCCI (Newman and Zhang, 2008), in order to determine whether CIC effects either the number or proportion of cells that are cycling, the length of the cell cycle in those cells, or both. Furthermore, my results suggest that CIC may modulate the propensity of stem/progenitor cells to undergo symmetric versus asymmetric cell division, a possibility that is discussed in more detail below.

5.3.2 CIC may influence progenitor cells away from neuronal cell fates

Using western blot analysis, I found that CIC-null cells show a decreased expression of an early neuronal and oligodendrocyte markers (Tuj1 and PDGFRa, respectively), when grown under normal stem cell conditions (Figure 4.10). Using CIC shRNA transient knockdown *in vivo*, I found evidence of increased glioblasts in the intermediate zone of the brain (Figure 4.11), however, I did not see an increase or decrease in neuronal cell counts (Figure 4.12). Thus, loss of CIC may bias cells away from neuronal fates, and towards glial fates. There is some evidence from *Drosophila* that CIC has a role in repressing differentiation throughout development. For example, mutating Capicua in follicle cells of embryonic flies results in the ectopic expression of appendage material (Atkey et al., 2006). Ectopic and abundant vein tissue is also seen in the developing wing disc when looking at embryos with complete loss of function of CIC (Roch et al., 2002). These studies promote the idea that CIC plays a role in repressing differentiation in a tissue-specific manner.

In the cultured CIC-null cells, I saw a decrease in PDGFRa expression, which can be considered an early oligodendrocyte marker (Ellison and de Vellis, 1994), and Tuj1 expression (an early neuronal marker), but did not see a corresponding increase in any of the other markers tested (Figure 4.10). My studies, however, were limited to a small set of late progenitor markers

as well as early and more mature cell type markers. Further study of other types of markers could better elucidate changes in cell lineage or differentiation. For example, it is possible that there is an increased expression of earlier progenitor markers, such as FABP7 (Young et al., 2013) or Musashi-1 (MSI1) (Okano et al., 2002). These markers are expressed prior to cells being fate-committed. As well, it may be that in culture, the identity of the cell population is changing from dorsal to ventral stem/progenitor cells when CIC is lost, which could be tested by looking markers such as DLX1/2 (Petryniak et al., 2007) or NGN1/2 (Gowan et al., 2001). Finally, there are a proportion of cells in each culture at various stages of specification. Since there are a larger number of cells in the knockout cultures, it may be more difficult to see specific changes in any of these proportions when using the western blot technique. To address this, cell by cell analysis could be conducted using immunofluorescence staining to precisely determine cell specification. As well, short-term lineage tracing experiments could also be used to address this issue.

My *in vivo* shRNA knockdown of CIC did not result in a significant increase or decrease in neuronal cell fates (Figure 4.12). However, the ability of transient transfections of shRNA to affect cell type specification must be considered, whether due to the timing/duration of knockdown or the degree of knockdown itself. It is possible that a more complete removal of CIC over a prolonged period, as seen in the *Drosophila* studies discussed above, is necessary to see any distinct changes in neuronal cell fate *in vivo*. As well, while this data shows that CIC ablation does not influence the total number of neuronal cells (determined by NeuN expression), it does change the localization of $NeuN^+$ cells within the cortical layers. NeuN was chosen as the neuronal marker *in vivo* due to the antibody staining qualities and ease of quantitation. My *in vitro* data, however, suggest that Tuj1 may have been more likely to reveal differences in neuronal cell count. Thus, in the future it may be necessary to quantitate neurons using Tuj1

staining, as well as distinct neuronal subtype and layer-specific markers. Finally, my *in vivo* functional analyses were restricted to a narrow window temporally and spatially in the embryonic cortex. It may be that CIC is influencing an earlier or later progenitor cell fate instead of a neuronal fate, which I was unable to study with the *in vivo* model.

When comparing the *in vitro* and *in vivo* results, it is important to note that differences between techniques and environmental factors could also play a role in the results. My *in vivo* knockdown technique using *in utero* electroporation is a transient transfection, whereas the *in vitro* knockout approach resulted in complete CIC loss that was maintained throughout the duration of the experiments. A long-term, consistent knockout of CIC may be necessary to see distinct changes in cell type specification, perhaps explaining the disparity in my results. As well, the influences of the microenvironment and its constituents cannot be discounted, as it is distinctly different in my two studies. Directly comparing cells in the developing mouse brain, with all its corresponding influences, to growing cells in a tissue culture environment may be a difficult. Finally, cell type expression was analyzed in two distinct manners between these experiments, as I used immunofluorescence staining *in vivo*, and western blotting *in vitro*.

5.3.3 CIC loss alters progenitor cells' migration

I have shown evidence *in vivo* that transient knockdown of CIC leads to perturbation of cellular localization compared to controls. Significantly more cells remained in the VZ and IZ, and significantly fewer reached the CP 48 hours after electroporation of CIC shRNA (Figure 4.13). Previous literature has shown that CIC knockdown via siRNA in the Sbcl2 melanoma cell line causes an increase in migration compared to control cells transfected with non-targeting siRNA (Dissanayake et al., 2011). However, the effect of CIC on migration has yet to be studied

in murine cortical development, making this a novel result that should be investigated more thoroughly in the future. In this respect, my finding that CIC knockdown cells failed to reach their appropriate destinations (at least in the time period studied) is intriguing. Whether the result is a reflection of lack of migration or of movement that occurs in an undirected/haphazard fashion is unclear. Time-lapse studies and other focused migration specific assays could be useful in the future to discern the mechanism of action of CIC in migration.

There are two major types of migration in the developing brain; radial, in which neural cells move from ventricular regions to the pial surface, and tangential, which allows neural cells to move into different compartments parallel to the brain surface (Rakic, 1990). Cells migrate along radial glial fibers, which form scaffolds that can restrain lateral movement of migrating neural cells in order to determine laminar structures like the neocortex (Rakic, 1972). Migratory processes are believed to be driven by both cell-intrinsic processes as well as external regulators. For example, Notch is an intracellular regulatory of migration; increased Notch expression alters migrating neuron morphology to a structure which favors migration (Hashimoto-Torii et al., 2008). Chemokines are an example of external regulators of migration. Stromal-cell derived factor 1 (SCD1) increases neuroblast motility by upregulating EGFR (Asensio and Campbell, 1999). Although my results in this area are preliminary, CIC may be a novel intrinsic regulator of migration in the developing mouse brain.

In future studies of this phenomenon, it would be interesting to determine whether this change in migration is also seen in the CIC knockout mice, in my *in vitro* cultured knockout cell system, or in hybrid systems such as plating CIC knockout cells on ex vivo slice cultures. As well, further study of cellular localization in the *in vivo* model could be undertaken in order to determine what cell types are found in the different cortical layers of the developing mouse brain

when CIC is removed, and whether there is significant layer-specific disruption. Layer specific markers such as Satb2 (Alcamo et al., 2008), Cux1 (Nieto et al., 2004), and Tbr1/2 (Englund et al., 2005) are potential candidates for assessment. Finally, it would be interesting to continue to follow the electroporated embryos further in development, in order to assess whether the cells that are aberrantly located in the ventricular and intermediate zones of the brain at E18 eventually migrate to appropriate cortical layers. Although it is difficult to follow electroporated animals postnatally, a foster system, involving placing electroporated pups within a litter of non-electroporated animals, could potentially be used to do so.

5.4 Potential role of CIC in ODG tumorigenesis

Mutations of CIC in ODG are associated with 1p19q co-deletion (Chan et al., 2014; Yip et al., 2012). As CIC is located on chromosome 19q of the human genome, tumors which show CIC mutations have also lost a second copy of the gene when 19q is deleted. Thus, it can be inferred that CIC loss and mutation plays a role in ODG formation. To begin, my data shows that complete knockout of CIC *in vitro* results in a significant increase in cell number, viability, and sphere volume (Figures 4.5 and 4.8 respectively). Interestingly, although there is a large increase in sphere volume in CIC-null cells, sphere number remains the same when compared to controls, at least at the early time point at which the assays were performed (48 hours). This implies that CIC knockout cells may be more prone to dividing symmetrically instead of asymmetrically, resulting in an increased size and cell number, while retaining a similar sphere count.

In normal development, stem/progenitor cells can undergo both symmetric and asymmetric division. There are two types of symmetric division; symmetric proliferative division allows for an increase in progenitor number, producing two identical daughter cells from one

original progenitor, while symmetric differentiative division produces two identical differentiated cells (Huttner and Kosodo, 2005; Knoblich, 2010; Wodarz and Huttner, 2003). Asymmetric division allows progenitors to self-renew while also producing cells that differentiate into other lineages (Knoblich, 2010; Kosodo et al., 2004). In relation to tumorigenesis, previous work in *Drosophila* has suggested that asymmetric cell division is lost when cells move from a progenitor to a precancerous state (Caussinus and Gonzalez, 2005). Oncogenes have been found to increase symmetric proliferative divisions in hematopoietic progenitors (Wu et al., 2007). In gliomagenesis, OPCs, which are thought to be a cell of origin for ODG (Lindberg et al., 2009; Persson et al., 2010), are found to undergo self-renewal instead of differentiating when subjected to defects in asymmetrical division (Sugiarto et al., 2011). This study concluded that the transformation from OPC to malignant cell can occur due to changes from asymmetric to symmetric division.

To further implicate CIC as playing a role in ODG formation, I found that CIC was expressed in early stem/progenitor cells (Figure 3.6), as well as in regions of the adult murine brain, the SEZ (Figure 3.7). and the DG (Figure 3.9), which are capable of neurogenesis, and thus cell division (Eriksson et al., 1998; Lois and Alvarez-Buylla, 1993). The SEZ in particular has been shown to produce a small population of NG2+ oligodendrocyte precursors, the presumed cell of origin for ODG (Menn et al., 2006). As well, electroporation of CIC shRNA was shown to increase the number of glioblasts in vivo (Figure 4.11), which have the potential to differentiate into either astrocytes or oligodendrocytes. Thus, loss of CIC may bias progenitors in the SEZ and/or the DG to undergo symmetric division, producing a large population of cells that may differentiate into glioblasts, and possibly promoting a malignant state. Further experiments using paired cell assays would shed further light on this possibility.

It remains to be seen whether CIC loss alone eventually lead to tumorigenesis of ODG-like lesions. Based on our knowledge that human ODGs harbour IDH1/2 mutations, we expect that CIC loss alone would be insufficient and that additional hits are necessary. It will also be important, in future experiments, to follow the knockout animals for extended periods of time and also in the context of concurrent IDH mutation in order to answer these questions.

5.5 Possible mechanisms of CIC action in the cortex

The Ras/MAPK pathway is a signal transduction pathway which activates genes for cell important for development (Molina and Adjei, 2006). Functions of this pathway include cell growth, proliferation, migration, and differentiation. These functions can be context dependent, as growth factors which activate this pathway can promote either progenitor proliferation or differentiation (Lukaszewicz et al., 2002). I found that CIC loss results in an increased proliferation *in vivo* (Figure 4.7), and an increased cell number and viability *in vitro* (Figure 4.5), but the molecular mechanisms underpinning my findings remain unclear. ETS transcription factors have been found to be activated by Ras, leading to cell proliferation (Yordy and Muise-Helmericks, 2000). As CIC has previously been shown to repress ETV (Ets translocation variant) transcription factors (Kawamura-Saito et al., 2006), it may be involved in repressing proliferation downstream of the murine RTK pathway. When CIC is de-repressed by ERK, ETS is allowed to function, leading to proliferation. Thus, loss or mutation of CIC could result in an increase in proliferation. Definitive experiments to determine which ETVs might be mediating my effects have not been performed, and it is unknown whether ETVs mediate all CIC responses or only some.

I show that transient knockdown of CIC is enough to cause cellular perturbation *in vivo* compared to controls (Figure 4.13). The implication of these results is that CIC represses a second function which is activated by the Ras pathway, migration. Ets translocation variant 1 (ETV1) is regulated by posttranslational modification through the MAPK pathway (Janknecht, 1996), and has previously been shown to stimulate migration and invasion in prostate cancer (Hermans et al., 2008). CIC was found to repress ETV functions *in vitro* (Kawamura-Saito et al., 2006), and thus may be interacting with these transcription factors to influence migration during murine development.

Finally, I found that CIC loss results in a decrease in expression of early neuronal (Tuj1) and early oligodendrocyte (PDGFRa) markers in vitro, as well as an increase in glioblast (Sox9) cells in vivo. Previous literature in *Drosophila* has also shown that CIC can repress cell fate downstream of RTK pathways (Roch et al., 2002). Ras pathways are also implicated in differentiation; for example, ETV1 has been shown to be required for regulation of the identity of cerebellar granule cells (Abe et al., 2011). Thus it seems that many of the functions which are promoted by Ras activation are repressed by CIC.

Does CIC regulate all Ras/MAPK effects, or just a specific subset of responses? In *Drosophila*, CIC is thought to be a general response element for Ras/MAPK signalling pathways. This conclusion derives from the observation that common octomeric elements, which are used by RTK pathways to control expression of downstream genes, are binding sites for the HMG-box of the Capicua gene (Astigarraga et al., 2007). Other literature argues that CIC may be more of a general sensor of RTK signalling, rather than the regulator of every Ras/MAPK effect (Jimenez et al., 2012). Whether or not all of the functions of CIC are associated with RTK signalling remains to be determined both in *Drosophila* and mouse models of development.

5.6 Future Directions

Many studies remain to be completed beyond the scope of this thesis work, in order to better understand the function of CIC. Although I have shown that CIC effects cell growth, proliferation, migration, and differentiation in murine models, I have yet to determine what targets downstream of CIC are mediating these effects in its absence. Candidates for study include ETV1/4/5, protein coding genes which are known targets of CIC. It would be of interest to determine whether the changes seen *in vitro* and *in vivo* are mediated through these pathways. This could be studied using the *in vitro* CIC-CKO cells, and manipulating the expression of the ETVs to determine if the effects of CIC knockout remain.

Identifying other downstream targets of CIC repression, and whether or not these targets are direct or indirect effectors of CIC would add to the knowledge of the function of this gene. Downstream effectors could be analyzed to discover tumor promoting genes that CIC may be repressing. As one copy of CIC is lost, and the other likely mutated in oligodendroglioma, it is important to note what downstream effectors may be de-repressed due to loss of CIC function. To do so, an unbiased, genome-wide transcriptional analysis could be undertaken to look for expression changes with and without CIC loss. Pathway enrichment or network analyses could then be performed in order to look for enrichment and to gain insight into potential new functions or mechanisms of action. Although these types of experiments would identify possible targets of CIC, chromatin immunoprecipitation (ChIP) would be necessary to determine whether those targets might be direct or indirect. Understanding the targets of CIC could also lead to discovery of potential candidates for novel therapeutics in the future.

5.7 Concluding remarks

In conclusion, I have shown that CIC, a gene commonly mutated in oligodendroglioma, is expressed in an appropriate time and place to be able to influence progenitor fate and proliferation in the developing mouse brain. CIC loss results in increased proliferation *in vitro* and *in vivo*, perturbed migration *in vivo*, and biases cells away from a neuronal fate *in vitro.* Overall, my results support the notion that CIC is important in murine neurodevelopment, and that loss of the gene may be a driver of ODG tumor formation through multiple mechanisms.

REFERENCES

Abe, H., Okazawa, M., and Nakanishi, S. (2011). The Etv1/Er81 transcription factor orchestrates activity-dependent gene regulation in the terminal maturation program of cerebellar granule cells. Proc. Natl. Acad. Sci. *108*, 12497–12502.

Ajuria, L., Nieva, C., Winkler, C., Kuo, D., Samper, N., Andreu, M.J., Helman, A., Gonzalez-Crespo, S., Paroush, Z., Courey, A.J., et al. (2011). Capicua DNA-binding sites are general response elements for RTK signaling in Drosophila. Development *138*, 915–924.

Alcamo, E.A., Chirivella, L., Dautzenberg, M., Dobreva, G., Fariñas, I., Grosschedl, R., and McConnell, S.K. (2008). Satb2 Regulates Callosal Projection Neuron Identity in the Developing Cerebral Cortex. Neuron *57*, 364–377.

Alvarez-Buylla, A., Garcia-Verdugo, J.M., and Tramontin, A.D. (2001). A unified hypothesis on the lineage of neural stem cells. Nat. Rev. Neurosci. *2*, 287–293.

Angevine, J.B., and Sidman, R.L. (1961). Autoradiographic Study of Cell Migration during Histogenesis of Cerebral Cortex in the Mouse. Nature *192*, 766–768.

Asensio, V.C., and Campbell, I.L. (1999). Chemokines in the CNS: plurifunctional mediators in diverse states. Trends Neurosci. *22*, 504–512.

Astigarraga, S., Grossman, R., Diaz-Delfin, J., Caelles, C., Paroush, Z., and Jimenez, G. (2007). A MAPK docking site is critical for downregulation of Capicua by Torso and EGFR RTK signaling. EMBO J *26*, 668–677.

Atkey, M.R., Lachance, J.-F.B., Walczak, M., Rebello, T., and Nilson, L.A. (2006). Capicua regulates follicle cell fate in the Drosophila ovary through repression of mirror. Development *133*, 2115–2123.

Barnabé-Heider, F., Wasylnka, J.A., Fernandes, K.J.L., Porsche, C., Sendtner, M., Kaplan, D.R., and Miller, F.D. (2005). Evidence that Embryonic Neurons Regulate the Onset of Cortical Gliogenesis via Cardiotrophin-1. Neuron *48*, 253–265.

Baumann, N., and Pham-Dinh, D. (2001). Biology of oligodendrocyte and myelin in the mammalian central nervous system. Physiol Rev *81*, 871–927.

Bennett, M.R., Rizvi, T.A., Karyala, S., McKinnon, R.D., and Ratner, N. (2003). Aberrant growth and differentiation of oligodendrocyte progenitors in neurofibromatosis type 1 mutants. J Neurosci *23*, 7207–7217.

Bertrand, N., Castro, D.S., and Guillemot, F. (2002). Proneural genes and the specification of neural cell types. Nat Rev Neurosci *3*, 517–530.

Bettegowda, C., Agrawal, N., Jiao, Y., Sausen, M., Wood, L.D., Hruban, R.H., Rodriguez, F.J., Cahill, D.P., McLendon, R., Riggins, G., et al. (2011). Mutations in CIC and FUBP1 contribute to human oligodendroglioma. Science *333*, 1453–1455.

Bignami, A., Eng, L.F., Dahl, D., and Uyeda, C.T. (1972). Localization of the glial fibrillary acidic protein in astrocytes by immunofluorescence. Brain Res. *43*, 429–435.

Bonni, A., Sun, Y., Nadal-Vicens, M., Bhatt, A., Frank, D.A., Rozovsky, I., Stahl, N., Yancopoulos, G.D., and Greenberg, M.E. (1997). Regulation of gliogenesis in the central nervous system by the JAK-STAT signaling pathway. Science *278*, 477–483.

Brill, M.S., Ninkovic, J., Winpenny, E., Hodge, R.D., Ozen, I., Yang, R., Lepier, A., Gascon, S., Erdelyi, F., Szabo, G., et al. (2009). Adult generation of glutamatergic olfactory bulb interneurons. Nat Neurosci *12*, 1524–1533.

Britz, O., Mattar, P., Nguyen, L., Langevin, L.M., Zimmer, C., Alam, S., Guillemot, F., and Schuurmans, C. (2006). A role for proneural genes in the maturation of cortical progenitor cells. Cereb Cortex *16 Suppl 1*, i138–51.

Burrows, R.C., Wancio, D., Levitt, P., and Lillien, L. (1997). Response Diversity and the Timing of Progenitor Cell Maturation Are Regulated by Developmental Changes in EGFR Expression in the Cortex. Neuron *19*, 251–267.

Cairncross, G., and Jenkins, R. (2008). Gliomas with 1p/19q codeletion: a.k.a. oligodendroglioma. Cancer J *14*, 352–357.

Cairncross, J.G., Ueki, K., Zlatescu, M.C., Lisle, D.K., Finkelstein, D.M., Hammond, R.R., Silver, J.S., Stark, P.C., Macdonald, D.R., Ino, Y., et al. (1998). Specific genetic predictors of chemotherapeutic response and survival in patients with anaplastic oligodendrogliomas. J. Natl. Cancer Inst. *90*, 1473–1479.

Cameron, H.A., Woolley, C.S., McEwen, B.S., and Gould, E. (1993). Differentiation of newly born neurons and glia in the dentate gyrus of the adult rat. Neuroscience *56*, 337–344.

Casarosa, S., Fode, C., and Guillemot, F. (1999). Mash1 regulates neurogenesis in the ventral telencephalon. Development *126*, 525–534.

Castro, D.S., Martynoga, B., Parras, C., Ramesh, V., Pacary, E., Johnston, C., Drechsel, D., Lebel-Potter, M., Garcia, L.G., Hunt, C., et al. (2011). A novel function of the proneural factor Ascl1 in progenitor proliferation identified by genome-wide characterization of its targets. Genes Dev *25*, 930–945.

Caussinus, E., and Gonzalez, C. (2005). Induction of tumor growth by altered stem-cell asymmetric division in Drosophila melanogaster. Nat. Genet. *37*, 1125–1129.

Chambers, A.F., Groom, A.C., and MacDonald, I.C. (2002). Metastasis: Dissemination and growth of cancer cells in metastatic sites. Nat. Rev. Cancer *2*, 563–572.

Chan, A.K.-Y., Pang, J.C.-S., Chung, N.Y.-F., Li, K.K.-W., Poon, W.S., Chan, D.T.-M., Shi, Z., Chen, L., Zhou, L., and Ng, H.-K. (2014). Loss of CIC and FUBP1 expressions are potential markers of shorter time to recurrence in oligodendroglial tumors. Mod. Pathol. Off. J. U. S. Can. Acad. Pathol. Inc *27*, 332–342.

Chojnacki, A., and Weiss, S. (2008). Production of neurons, astrocytes and oligodendrocytes from mammalian CNS stem cells. Nat. Protoc. *3*, 935–940.

Colasante, G., and Sessa, A. (2010). Last But Not Least: Cortical Interneurons from Caudal Ganglionic Eminence. J. Neurosci. *30*, 7449–7450.

Crespo-Barreto, J., Fryer, J.D., Shaw, C.A., Orr, H.T., and Zoghbi, H.Y. (2010). Partial loss of ataxin-1 function contributes to transcriptional dysregulation in spinocerebellar ataxia type 1 pathogenesis. PLoS Genet *6*, e1001021.

Dissanayake, K., Toth, R., Blakey, J., Olsson, O., Campbell, D.G., Prescott, A.R., and MacKintosh, C. (2011). ERK/p90(RSK)/14-3-3 signalling has an impact on expression of PEA3 Ets transcription factors via the transcriptional repressor capicua. Biochem J *433*, 515–525.

Dixit, R., Lu, F., Cantrup, R., Gruenig, N., Langevin, L.M., Kurrasch, D.M., and Schuurmans, C. (2011). Efficient gene delivery into multiple CNS territories using in utero electroporation. J Vis Exp.

Doetsch, F., Garcia-Verdugo, J.M., and Alvarez-Buylla, A. (1997). Cellular composition and three-dimensional organization of the subventricular germinal zone in the adult mammalian brain. J Neurosci *17*, 5046–5061.

Duffy, J.B., and Perrimon, N. (1994). The Torso Pathway in Drosophila: Lessons on Receptor Tyrosine Kinase Signaling and Pattern Formation. Dev. Biol. *166*, 380–395.

Ellison, J.A., and de Vellis, J. (1994). Platelet-derived growth factor receptor is expressed by cells in the early oligodendrocyte lineage. J. Neurosci. Res. *37*, 116–128.

Englund, C., Fink, A., Lau, C., Pham, D., Daza, R.A.M., Bulfone, A., Kowalczyk, T., and Hevner, R.F. (2005). Pax6, Tbr2, and Tbr1 Are Expressed Sequentially by Radial Glia, Intermediate Progenitor Cells, and Postmitotic Neurons in Developing Neocortex. J. Neurosci. *25*, 247–251.

Ericson, J., Rashbass, P., Schedl, A., Brenner-Morton, S., Kawakami, A., van Heyningen, V., Jessell, T.M., and Briscoe, J. (1997). Pax6 Controls Progenitor Cell Identity and Neuronal Fate in Response to Graded Shh Signaling. Cell *90*, 169–180.

Eriksson, P.S., Perfilieva, E., Bjork-Eriksson, T., Alborn, A.M., Nordborg, C., Peterson, D.A., and Gage, F.H. (1998). Neurogenesis in the adult human hippocampus. Nat Med *4*, 1313–1317.

Fishell, G. (1995). Striatal Precursors Adopt Cortical Identities in Response to Local Cues (Vol 121, Pg 803, 1995). Development *121*, U4–&.

Fishell, G., and Kriegstein, A.R. (2003). Neurons from radial glia: the consequences of asymmetric inheritance. Curr. Opin. Neurobiol. *13*, 34–41.

Fryer, J.D., Yu, P., Kang, H., Mandel-Brehm, C., Carter, A.N., Crespo-Barreto, J., Gao, Y., Flora, A., Shaw, C., Orr, H.T., et al. (2011). Exercise and genetic rescue of SCA1 via the transcriptional repressor Capicua. Science *334*, 690–693.

Fukuda, S., Kondo, T., Takebayashi, H., and Taga, T. (2004). Negative regulatory effect of an oligodendrocytic bHLH factor OLIG2 on the astrocytic differentiation pathway. Cell Death Differ *11*, 196–202.

Furriols, M., and Casanova, J. (2003). In and out of Torso RTK signalling. EMBO J *22*, 1947–1952.

Geha, S., Pallud, J., Junier, M.P., Devaux, B., Leonard, N., Chassoux, F., Chneiweiss, H., Daumas-Duport, C., and Varlet, P. (2010). NG2+/Olig2+Cells are the Major Cycle-Related Cell Population of the Adult Human Normal Brain. Brain Pathol. *20*, 399–411.

Ghandour, M.S., Langley, O.K., Labourdette, G., Vincendon, G., and Gombos, G. (1981). Specific and Artefactual Cellular Localizations of S100 Protein: An Astrocyte Marker in Rat Cerebellum. Dev. Neurosci. *4*, 66–78.

Gowan, K., Helms, A.W., Hunsaker, T.L., Collisson, T., Ebert, P.J., Odom, R., and Johnson, J.E. (2001). Crossinhibitory Activities of Ngn1 and Math1 Allow Specification of Distinct Dorsal Interneurons. Neuron *31*, 219–232.

Graham, C., Chilton-MacNeill, S., Zielenska, M., and Somers, G.R. (2012). The CIC-DUX4 fusion transcript is present in a subgroup of pediatric primitive round cell sarcomas. Hum Pathol *43*, 180–189.

Graham, V., Khudyakov, J., Ellis, P., and Pevny, L. (2003). SOX2 Functions to Maintain Neural Progenitor Identity. Neuron *39*, 749–765.

Grimm, O., Zini, V.S., Kim, Y., Casanova, J., Shvartsman, S.Y., and Wieschaus, E. (2012). Torso RTK controls Capicua degradation by changing its subcellular localization. Development *139*, 3962–3968.

Gritti, A., Frölichsthal-Schoeller, P., Galli, R., Parati, E.A., Cova, L., Pagano, S.F., Bjornson, C.R., and Vescovi, A.L. (1999). Epidermal and Fibroblast Growth Factors Behave as Mitogenic Regulators for a Single Multipotent Stem Cell-Like Population from the Subventricular Region of the Adult Mouse Forebrain. J. Neurosci. *19*, 3287–3297.

Guardiola-Diaz, H.M., Ishii, A., and Bansal, R. (2012). Erk1/2 MAPK and mTOR signaling sequentially regulates progression through distinct stages of oligodendrocyte differentiation. Glia *60*, 476–486.

Hashimoto-Torii, K., Torii, M., Sarkisian, M.R., Bartley, C.M., Shen, J., Radtke, F., Gridley, T., Šestan, N., and Rakic, P. (2008). Interaction between Reelin and Notch Signaling Regulates Neuronal Migration in the Cerebral Cortex. Neuron *60*, 273–284.

Hermans, K.G., Korput, H.A. van der, Marion, R. van, Wijngaart, D.J. van de, Made, A.Z. der, Dits, N.F., Boormans, J.L., Kwast, T.H. van der, Dekken, H. van, Bangma, C.H., et al. (2008). Truncated ETV1, Fused to Novel Tissue-Specific Genes, and Full-Length ETV1 in Prostate Cancer. Cancer Res. *68*, 7541–7549.

Herranz, H., Hong, X., and Cohen, S.M. (2012). Mutual repression by bantam miRNA and Capicua links the EGFR/MAPK and Hippo pathways in growth control. Curr Biol *22*, 651–657.

Hitoshi, S., Tropepe, V., Ekker, M., and Kooy, D. van der (2002). Neural stem cell lineages are regionally specified, but not committed, within distinct compartments of the developing brain. Development *129*, 233–244.

Huttner, W.B., and Kosodo, Y. (2005). Symmetric versus asymmetric cell division during neurogenesis in the developing vertebrate central nervous system. Curr. Opin. Cell Biol. *17*, 648–657.

Janknecht, R. (1996). Analysis of the ERK-stimulated ETS transcription factor ER81. Mol. Cell. Biol. *16*, 1550–1556.

Jiao, Y., Killela, P.J., Reitman, Z.J., Rasheed, A.B., Heaphy, C.M., de Wilde, R.F., Rodriguez, F.J., Rosemberg, S., Oba-Shinjo, S.M., Marie, S.K., et al. (2012). Frequent ATRX, CIC, and FUBP1 mutations refine the classification of malignant gliomas. Oncotarget *3*, 709–722.

Jimenez, G., Guichet, A., Ephrussi, A., and Casanova, J. (2000). Relief of gene repression by torso RTK signaling: role of capicua in Drosophila terminal and dorsoventral patterning. Genes Dev *14*, 224–231.

Jimenez, G., Shvartsman, S.Y., and Paroush, Z. (2012). The Capicua repressor - a general sensor of RTK signaling in development and disease. J Cell Sci *125*, 1383–1391.

Kawamura-Saito, M., Yamazaki, Y., Kaneko, K., Kawaguchi, N., Kanda, H., Mukai, H., Gotoh, T., Motoi, T., Fukayama, M., Aburatani, H., et al. (2006). Fusion between CIC and DUX4 up-regulates PEA3 family genes in Ewing-like sarcomas with t(4;19)(q35;q13) translocation. Hum Mol Genet *15*, 2125–2137.

Kleihues, P., Soylemezoglu, F., Schäuble, B., Scheithauer, B.W., and Burger, P.C. (1995). Histopathology, classification, and grading of gliomas. Glia *15*, 211–221.

Knoblich, J.A. (2010). Asymmetric cell division: recent developments and their implications for tumour biology. Nat. Rev. Mol. Cell Biol. *11*, 849–860.

Kopan, R., and Ilagan, M.X. (2009). The canonical Notch signaling pathway: unfolding the activation mechanism. Cell *137*, 216–233.

Kosodo, Y., Röper, K., Haubensak, W., Marzesco, A.-M., Corbeil, D., and Huttner, W.B. (2004). Asymmetric distribution of the apical plasma membrane during neurogenic divisions of mammalian neuroepithelial cells. EMBO J. *23*, 2314–2324.

Kreutzberg, G.W. (1996). Microglia: a sensor for pathological events in the CNS. Trends Neurosci. *19*, 312–318.

Krivy, K., Bradley-Gill, M.-R., and Moon, N.-S. (2013). Capicua regulates proliferation and survival of RB-deficient cells in Drosophila. Biol. Open *2*, 183–190.

Krushel, L.A., Johnston, J.G., Fishell, G., Tibshirani, R., and Vanderkooy, D. (1993). Spatially Localized Neuronal Cell Lineages in the Developing Mammalian Forebrain. Neuroscience *53*, 1035–1047.

Lam, Y.C., Bowman, A.B., Jafar-Nejad, P., Lim, J., Richman, R., Fryer, J.D., Hyun, E.D., Duvick, L.A., Orr, H.T., Botas, J., et al. (2006). ATAXIN-1 interacts with the repressor Capicua in its native complex to cause SCA1 neuropathology. Cell *127*, 1335–1347.

Lee, C.J., Chan, W.I., Cheung, M., Cheng, Y.C., Appleby, V.J., Orme, A.T., and Scotting, P.J. (2002). CIC, a member of a novel subfamily of the HMG-box superfamily, is transiently expressed in developing granule neurons. Brain Res Mol Brain Res *106*, 151–156.

Lee, J.S., Padmanabhan, A., Shin, J., Zhu, S., Guo, F., Kanki, J.P., Epstein, J.A., and Look, A.T. (2010). Oligodendrocyte progenitor cell numbers and migration are regulated by the zebrafish orthologs of the NF1 tumor suppressor gene. Hum Mol Genet *19*, 4643–4653.

Lee, Y., Fryer, J.D., Kang, H., Crespo-Barreto, J., Bowman, A.B., Gao, Y., Kahle, J.J., Hong, J.S., Kheradmand, F., Orr, H.T., et al. (2011). ATXN1 protein family and CIC regulate extracellular matrix remodeling and lung alveolarization. Dev Cell *21*, 746–757.

Levy, D.E., and Darnell, J.E., Jr. (2002). Stats: transcriptional control and biological impact. Nat Rev Mol Cell Biol *3*, 651–662.

Li, S., Mattar, P., Zinyk, D., Singh, K., Chaturvedi, C.-P., Kovach, C., Dixit, R., Kurrasch, D.M., Ma, Y.-C., Chan, J.A., et al. (2012). GSK3 Temporally Regulates Neurogenin 2 Proneural Activity in the Neocortex. J. Neurosci. *32*, 7791–7805.

Li, S., Mattar, P., Dixit, R., Lawn, S.O., Wilkinson, G., Kinch, C., Eisenstat, D., Kurrasch, D.M., Chan, J.A., and Schuurmans, C. (2014). RAS/ERK Signaling Controls Proneural Genetic Programs in Cortical Development and Gliomagenesis. J. Neurosci. *34*, 2169–2190.

Lim, B., Samper, N., Lu, H., Rushlow, C., Jiménez, G., and Shvartsman, S.Y. (2013). Kinetics of gene derepression by ERK signaling. Proc. Natl. Acad. Sci. U. S. A. *110*, 10330–10335.

Lindberg, N., Kastemar, M., Olofsson, T., Smits, A., and Uhrbom, L. (2009). Oligodendrocyte progenitor cells can act as cell of origin for experimental glioma. Oncogene *28*, 2266–2275.

Liu, C., Sage, J.C., Miller, M.R., Verhaak, R.G.W., Hippenmeyer, S., Vogel, H., Foreman, O., Bronson, R.T., Nishiyama, A., Luo, L., et al. (2011). Mosaic Analysis with Double Markers Reveals Tumor Cell of Origin in Glioma. Cell *146*, 209–221.

Liu, L., Cundiff, P., Abel, G., Wang, Y., Faigle, R., Sakagami, H., Xu, M., and Xia, Z. (2006). Extracellular signal-regulated kinase (ERK) 5 is necessary and sufficient to specify cortical neuronal fate. Proc. Natl. Acad. Sci. *103*, 9697–9702.

Livneh, E., Glazer, L., Segal, D., Schlessinger, J., and Shilo, B.-Z. (1985). The Drosophila EGF receptor gene homolog: Conservation of both hormone binding and kinase domains. Cell *40*, 599–607.

Lois, C., and Alvarez-Buylla, A. (1993). Proliferating subventricular zone cells in the adult mammalian forebrain can differentiate into neurons and glia. Proc Natl Acad Sci U A *90*, 2074–2077.

Louis, S.A., Mak, C.K.H., and Reynolds, B.A. (2013). Methods to Culture, Differentiate, and Characterize Neural Stem Cells from the Adult and Embryonic Mouse Central Nervous System. In Basic Cell Culture Protocols, C.D. Helgason, and C.L. Miller, eds. (Humana Press), pp. 479–506.

Lu, Q.R., Sun, T., Zhu, Z., Ma, N., Garcia, M., Stiles, C.D., and Rowitch, D.H. (2002). Common developmental requirement for Olig function indicates a motor neuron/oligodendrocyte connection. Cell *109*, 75–86.

Lukaszewicz, A., Savatier, P., Cortay, V., Kennedy, H., and Dehay, C. (2002). Contrasting effects of basic fibroblast growth factor and neurotrophin 3 on cell cycle kinetics of mouse cortical stem cells. J Neurosci *22*, 6610–6622.

Lwin, Z., Gan, H.K., and Mason, W.P. (2009). Low-grade oligodendroglioma: current treatments and future hopes. Expert Rev Anticancer Ther *9*, 1651–1661.

Malatesta, P., Hartfuss, E., and Gotz, M. (2000). Isolation of radial glial cells by fluorescent-activated cell sorting reveals a neuronal lineage. Development *127*, 5253–5263.

Mancall, E.L., and Brock, D.G. (2011). Gray's Clinical Neuroanatomy: The Anatomic Basis for Clinical Neuroscience (Elsevier Health Sciences).

Mattar, P., Langevin, L.M., Markham, K., Klenin, N., Shivji, S., Zinyk, D., and Schuurmans, C. (2008). Basic Helix-Loop-Helix Transcription Factors Cooperate To Specify a Cortical Projection Neuron Identity. Mol. Cell. Biol. *28*, 1456–1469.

McCarthy, M., Turnbull, D.H., Walsh, C.A., and Fishell, G. (2001). Telencephalic Neural Progenitors Appear To Be Restricted to Regional and Glial Fates before the Onset of Neurogenesis. J. Neurosci. *21*, 6772–6781.

Mcconnell, S.K., and Kaznowski, C.E. (1991). Cell-Cycle Dependence of Laminar Determination in Developing Neocortex. Science *254*, 282–285.

Ménard, C., Hein, P., Paquin, A., Savelson, A., Yang, X.M., Lederfein, D., Barnabé-Heider, F., Mir, A.A., Sterneck, E., Peterson, A.C., et al. (2002). An Essential Role for a MEK-C/EBP Pathway during Growth Factor-Regulated Cortical Neurogenesis. Neuron *36*, 597–610.

Menezes, J.R., and Luskin, M.B. (1994). Expression of neuron-specific tubulin defines a novel population in the proliferative layers of the developing telencephalon. J. Neurosci. *14*, 5399–5416.

Menn, B., Garcia-Verdugo, J.M., Yaschine, C., Gonzalez-Perez, O., Rowitch, D., and Alvarez-Buylla, A. (2006). Origin of oligodendrocytes in the subventricular zone of the adult brain. J. Neurosci. *26*, 7907–7918.

Miller, F.D., and Gauthier, A.S. (2007). Timing is everything: Making neurons versus glia in the developing cortex. Neuron *54*, 357–369.

Miyata, T., Kawaguchi, A., Okano, H., and Ogawa, M. (2001). Asymmetric inheritance of radial glial fibers by cortical neurons. Neuron *31*, 727–741.

Molina, J.R., and Adjei, A.A. (2006). The Ras/Raf/MAPK pathway. J. Thorac. Oncol. *1*, 7–9.

Molyneaux, B.J., Arlotta, P., Menezes, J.R.L., and Macklis, J.D. (2007). Neuronal subtype specification in the cerebral cortex. Nat. Rev. Neurosci. *8*, 427–437.

Mork, S.J., Lindegaard, K.F., Halvorsen, T.B., Lehmann, E.H., Solgaard, T., Hatlevoll, R., Harvei, S., and Ganz, J. (1985). Oligodendroglioma: incidence and biological behavior in a defined population. J Neurosurg *63*, 881–889.

Murre, C., McCaw, P.S., Vaessin, H., Caudy, M., Jan, L.Y., Jan, Y.N., Cabrera, C.V., Buskin, J.N., Hauschka, S.D., Lassar, A.B., et al. (1989). Interactions between heterologous helix-loop-helix proteins generate complexes that bind specifically to a common DNA sequence. Cell *58*, 537–544.

Nakashima, K., Yanagisawa, M., Arakawa, H., Kimura, N., Hisatsune, T., Kawabata, M., Miyazono, K., and Taga, T. (1999). Synergistic signaling in fetal brain by STAT3-Smad1 complex bridged by p300. Science *284*, 479–482.

Newman, R.H., and Zhang, J. (2008). Fucci: Street Lights on the Road to Mitosis. Chem. Biol. *15*, 97–98.

Nieto, M., Monuki, E.S., Tang, H., Imitola, J., Haubst, N., Khoury, S.J., Cunningham, J., Gotz, M., and Walsh, C.A. (2004). Expression of Cux-1 and Cux-2 in the subventricular zone and upper layers II–IV of the cerebral cortex. J. Comp. Neurol. *479*, 168–180.

Novitch, B.G., Chen, A.I., and Jessell, T.M. (2001). Coordinate regulation of motor neuron subtype identity and pan-neuronal properties by the bHLH repressor Olig2. Neuron *31*, 773–789.

Okano, H., Imai, T., and Okabe, M. (2002). Musashi: a translational regulator of cell fate. J. Cell Sci. *115*, 1355–1359.

Parnavelas, J.G. (2000). The origin and migration of cortical neurones: new vistas. Trends Neurosci. *23*, 126–131.

Parras, C.M., Hunt, C., Sugimori, M., Nakafuku, M., Rowitch, D., and Guillemot, F. (2007). The proneural gene Mash1 specifies an early population of telencephalic oligodendrocytes. J Neurosci *27*, 4233–4242.

Persson, A.I., Petritsch, C., Swartling, F.J., Itsara, M., Sim, F.J., Auvergne, R., Goldenberg, D.D., Vandenberg, S.R., Nguyen, K.N., Yakovenko, S., et al. (2010). Non-stem cell origin for oligodendroglioma. Cancer Cell *18*, 669–682.

Peterson, K., and Cairncross, J.G. (1996). Oligodendroglioma. Cancer Invest. *14*, 243–251.

Petryniak, M.A., Potter, G.B., Rowitch, D.H., and Rubenstein, J.L.R. (2007). Dlx1 and Dlx2 control neuronal versus oligodendroglial cell fate acquisition in the developing forebrain. Neuron *55*, 417–433.

Qian, X., Davis, A.A., Goderie, S.K., and Temple, S. (1997). FGF2 Concentration Regulates the Generation of Neurons and Glia from Multipotent Cortical Stem Cells. Neuron *18*, 81–93.

Qian, X., Shen, Q., Goderie, S.K., He, W., Capela, A., Davis, A.A., and Temple, S. (2000). Timing of CNS Cell Generation: A Programmed Sequence of Neuron and Glial Cell Production from Isolated Murine Cortical Stem Cells. Neuron *28*, 69–80.

Rakic, P. (1972). Mode of cell migration to the superficial layers of fetal monkey neocortex. J. Comp. Neurol. *145*, 61–83.

Rakic, P. (1988). Specification of cerebral cortical areas. Science *241*, 170–176.

Rakic, P. (1990). Principles of neural cell migration. Experientia *46*, 882–891.

Ray, R.P., and Schüpbach, T. (1996). Intercellular signaling and the polarization of body axes during Drosophila oogenesis. Genes Dev. *10*, 1711–1723.

Reifenberger, J., Reifenberger, G., Liu, L., James, C.D., Wechsler, W., and Collins, V.P. (1994). Molecular genetic analysis of oligodendroglial tumors shows preferential allelic deletions on 19q and 1p. Am. J. Pathol. *145*, 1175–1190.

Reynolds, B.A., and Weiss, S. (1992). Generation of neurons and astrocytes from isolated cells of the adult mammalian central nervous system. Science *255*, 1707–1710.

Richardson, W.D., Kessaris, N., and Pringle, N. (2006). Oligodendrocyte wars. Nat. Rev. Neurosci. *7*, 11–18.

Roch, F., Jimenez, G., and Casanova, J. (2002). EGFR signalling inhibits Capicua-dependent repression during specification of Drosophila wing veins. Development *129*, 993–1002.

Sarnat, H.B., Nochlin, D., and Born, D.E. (1998). Neuronal nuclear antigen (NeuN): a marker of neuronal maturation in the early human fetal nervous system. Brain Dev. *20*, 88–94.

Sauvageot, C.M., and Stiles, C.D. (2002). Molecular mechanisms controlling cortical gliogenesis. Curr. Opin. Neurobiol. *12*, 244–249.

Scheffler, B., Walton, N.M., Lin, D.D., Goetz, A.K., Enikolopov, G., Roper, S.N., and Steindler, D.A. (2005). Phenotypic and functional characterization of adult brain neuropoiesis. Proc Natl Acad Sci U A *102*, 9353–9358.

Schuurmans, C., Armant, O., Nieto, M., Stenman, J.M., Britz, O., Klenin, N., Brown, C., Langevin, L.-M., Seibt, J., Tang, H., et al. (2004). Sequential phases of cortical specification involve Neurogenin-dependent and -independent pathways. EMBO J. *23*, 2892–2902.

Scott, C.E., Wynn, S.L., Sesay, A., Cruz, C., Cheung, M., Gaviro, M.-V.G., Booth, S., Gao, B., Cheah, K.S.E., Lovell-Badge, R., et al. (2010). SOX9 induces and maintains neural stem cells. Nat. Neurosci. *13*, 1181–1189.

Shatz, C.J. (1992). Dividing up the Neocortex. Science *258*, 237–238.

Shen, Q., Wang, Y., Dimos, J.T., Fasano, C.A., Phoenix, T.N., Lemischka, I.R., Ivanova, N.B., Stifani, S., Morrisey, E.E., and Temple, S. (2006). The timing of cortical neurogenesis is encoded within lineages of individual progenitor cells. Nat. Neurosci. *9*, 743–751.

Shimojo, H., Ohtsuka, T., and Kageyama, R. (2011). Dynamic expression of notch signaling genes in neural stem/progenitor cells. Front Neurosci *5*, 78.

Shoshan, Y., Nishiyama, A., Chang, A., Mork, S., Barnett, G.H., Cowell, J.K., Trapp, B.D., and Staugaitis, S.M. (1999). Expression of oligodendrocyte progenitor cell antigens by gliomas: implications for the histogenesis of brain tumors. Proc Natl Acad Sci U A *96*, 10361–10366.

Smart, I.H.M., Dehay, C., Giroud, P., Berland, M., and Kennedy, H. (2002). Unique morphological features of the proliferative zones and postmitotic compartments of the neural epithelium giving rise to striate and extrastriate cortex in the monkey. Cereb. Cortex *12*, 37–53.

Sprenger, F., Stevens, L.M., and Nüsslein-Volhard, C. (1989). The Drosophila gene torso encodes a putative receptor tyrosine kinase. Nature *338*, 478–483.

Stolt, C.C., Lommes, P., Sock, E., Chaboissier, M.-C., Schedl, A., and Wegner, M. (2003). The Sox9 transcription factor determines glial fate choice in the developing spinal cord. Genes Dev. *17*, 1677–1689.

Sugiarto, S., Persson, A.I., Munoz, E.G., Waldhuber, M., Lamagna, C., Andor, N., Hanecker, P., Ayers-Ringler, J., Phillips, J., Siu, J., et al. (2011). Asymmetry-Defective Oligodendrocyte Progenitors Are Glioma Precursors. Cancer Cell *20*, 328–340.

Taga, T., and Fukuda, S. (2005). Role of IL-6 in the neural stem cell differentiation. Clin Rev Allergy Immunol *28*, 249–256.

Takebayashi, H., Yoshida, S., Sugimori, M., Kosako, H., Kominami, R., Nakafuku, M., and Nabeshima, Y. (2000). Dynamic expression of basic helix-loop-helix Olig family members: implication of Olig2 in neuron and oligodendrocyte differentiation and identification of a new member, Olig3. Mech Dev *99*, 143–148.

Tekki-Kessaris, N., Woodruff, R., Hall, A.C., Gaffield, W., Kimura, S., Stiles, C.D., Rowitch, D.H., and Richardson, W.D. (2001). Hedgehog-dependent oligodendrocyte lineage specification in the telencephalon. Development *128*, 2545–2554.

Tropepe, V., Sibilia, M., Ciruna, B.G., Rossant, J., Wagner, E.F., and van der Kooy, D. (1999). Distinct Neural Stem Cells Proliferate in Response to EGF and FGF in the Developing Mouse Telencephalon. Dev. Biol. *208*, 166–188.

Tseng, A.S., Tapon, N., Kanda, H., Cigizoglu, S., Edelmann, L., Pellock, B., White, K., and Hariharan, I.K. (2007). Capicua regulates cell proliferation downstream of the receptor tyrosine kinase/ras signaling pathway. Curr Biol *17*, 728–733.

Vallstedt, A., Klos, J.M., and Ericson, J. (2005). Multiple Dorsoventral Origins of Oligodendrocyte Generation in the Spinal Cord and Hindbrain. Neuron *45*, 55–67.

Wegner, M., and Stolt, C.C. (2005). From stem cells to neurons and glia: a Soxist's view of neural development. Trends Neurosci. *28*, 583–588.

Wodarz, A., and Huttner, W.B. (2003). Asymmetric cell division during neurogenesis in Drosophila and vertebrates. Mech. Dev. *120*, 1297–1309.

Wu, M., Kwon, H.Y., Rattis, F., Blum, J., Zhao, C., Ashkenazi, R., Jackson, T.L., Gaiano, N., Oliver, T., and Reya, T. (2007). Imaging Hematopoietic Precursor Division in Real Time. Cell Stem Cell *1*, 541–554.

Yip, S., Butterfield, Y.S., Morozova, O., Chittaranjan, S., Blough, M.D., An, J., Birol, I., Chesnelong, C., Chiu, R., Chuah, E., et al. (2012). Concurrent CIC mutations, IDH mutations, and 1p/19q loss distinguish oligodendrogliomas from other cancers. J Pathol *226*, 7–16.

Yoon, K., and Gaiano, N. (2005). Notch signaling in the mammalian central nervous system: insights from mouse mutants. Nat. Neurosci. *8*, 709–715.

Yordy, J.S., and Muise-Helmericks, R.C. (2000). Signal transduction and the Ets family of transcription factors. Oncogene *19*, 6503.

Yoshimoto, M., Graham, C., Chilton-MacNeill, S., Lee, E., Shago, M., Squire, J., Zielenska, M., and Somers, G.R. (2009). Detailed cytogenetic and array analysis of pediatric primitive sarcomas reveals a recurrent CIC–DUX4 fusion gene event. Cancer Genet. Cytogenet. *195*, 1–11.

Young, J.K., Heinbockel, T., and Gondré-Lewis, M.C. (2013). Astrocyte fatty acid binding protein-7 is a marker for neurogenic niches in the rat hippocampus. Hippocampus *23*, 1476–1483.

Zhou, Q., and Anderson, D.J. (2002). The bHLH transcription factors OLIG2 and OLIG1 couple neuronal and glial subtype specification. Cell *109*, 61–73.

Zhou, Q., Wang, S., and Anderson, D.J. (2000). Identification of a novel family of oligodendrocyte lineage-specific basic helix-loop-helix transcription factors. Neuron *25*, 331–343.

Zhou, Q., Choi, G., and Anderson, D.J. (2001). The bHLH Transcription Factor Olig2 Promotes Oligodendrocyte Differentiation in Collaboration with Nkx2.2. Neuron *31*, 791–807.